BULGARIAN CHEMICAL COMMUNICATIONS

2012 Volume 44 / Number 1

Journal of the Chemical Institutes
of the Bulgarian Academy of Sciences
and of the Union of Chemists in Bulgaria

Bulgarian Chemical Communications, Volume 44, Number 1 (pp. 5 – 10) 2012

Green analytical chemistry and its perspectives in Bulgaria

E. H. Ivanova, A. K. Detcheva

Institute of General and Inorganic Chemistry, Bulgarian Academy of Sciences, 11 Acad. G. Bontchev Str., 1113 Sofia, Bulgaria

Received: March 17, 2011; accepted: April 3, 2011

The concept of green chemistry emerged in the 1990s with the aim of minimizing the environmental impact of chemical activities. The basic principles to which a chemical procedure should correspond in order to be recognized as environmentally friendly (green) are reviewed. These include reduction of reagent and solvent usage, minimization of solid, liquid and gaseous materials, produced by the processes involved, reduction of energy and water consumption. Special emphasis is put on the features of green analytical chemistry, the challenges to the introduction of green principles to analytical laboratories, the assessment of the environmental impact and the waste management. The present state and the perspectives of green analytical chemistry in Bulgaria are discussed with an emphasis on the contributions of Bulgarian researchers in this field.

Key words: green analytical chemistry, basic principles, perspectives in Bulgaria, review.

This article is dedicated to the memory of Professor Dr. Nikolay Jordanov on the occasion of his 90th anniversary.

SUSTAINABLE DEVELOPMENT AND GREEN CHEMISTRY

In 1987 the World Commission on Environment and Development defined sustainable development as a form of development that meets the needs of the present generation without compromising the ability of future generations to meet their own needs [1]. One of the major goals of sustainability is to maintain an optimal balance between increases in manufacturing output, and a clean and safe environment. In the 1990s the concept of green chemistry emerged with the aim of minimizing the environmental impact of chemical activities. In their book "Green chemistry" published in 1998 [2], P. Anastas and R. Warner defined the principles to which a chemical procedure should correspond in order to be recognized as environmentally friendly. These include reduction of reagent and solvent usage, minimization of solid, liquid and gaseous materials, produced by the processes involved, reduction of energy and water consumption. Environmentally friendly (green) chemistry has received widespread interest in the past two decades due to its ability to harness chemical innovation to meet economic and environmental goals simultaneously [3–7].

Green chemistry embodies two main components. First, it addresses the problem of efficient utilisation of raw materials and concomitant elimination of waste. Second, it deals with the health, safety and environmental issues associated with the manufacture, use and disposal or re-use of chemicals. The activities in the area of green chemistry should meet two goals [1]:

- teaching of basic aspects of environmental science at all levels of education, resulting in the production of specialists, capable of handling and solving existing and potential environmental problems;
- creating a fresh approach to typical chemical activities, leading to the environmentally more friendly use of facilities.

GREEN ANALYTICAL CHEMISTRY

An important part of the green chemistry philosophy is the need to develop and adopt green analytical techniques and procedures. Analytical chemistry takes a special place in the green chemistry concept. It is aimed to detect and quantitatively determine various substances by means of methods which often use harmful reagents. As a result, the analysis itself may become a source of pollution. Analytical chemistry is considered to be a small-scale activity, but this is not always true in the case of controlling and

* To whom all correspondence should be sent:
e-mail: eliva@svr.igic.bas.bg

© 2012 Bulgarian Academy of Sciences, Union of Chemists in Bulgaria

monitoring laboratories with a large number of runs performed. The use of instrumental methods instead of wet chemistry; the miniaturization and automation are the new trends of analytical chemistry, making this branch of chemistry more sustainable [8]. The determination of a broad spectrum of analytes at low concentrations (ppb, even ppt) in samples of complex matrix composition has been facilitated by the introduction of a new generation of highly sensitive analytical devices and by the development of new sample preparation procedures. The main features of green analytical chemistry are [9]:

- elimination or significant reduction of reagents, especially toxic substances and organic solvents from the analytical procedures;
- reduced emissions of vapors and gases, as well as liquid and solid wastes, generated in the analytical laboratories;
- reduced labor, energy and water consumption of the analytical procedures;
- reduced time between sampling and obtaining of the desired information about the sample.
- The challenges to the introduction of sustainable development (green) principles to analytical laboratories are related to:
- preferable use of direct methods of analysis;
- simplification, intensification and acceleration of the sample preparation procedures;
- miniaturization, integration and automation of the analytical systems;
- assessment of the environmental impact of the analytical procedures.

The challenges are magnified when trace analysis and particularly microtrace analysis is concerned.

Methods of analysis

The development of direct instrumental methods is a general trend in analytical chemistry resulting in time saving and waste reduction. Optimization of instrumental methods is often related to a decrease in sample volume needed for analysis. In some cases, there is a choice of direct techniques of analysis which may be defined as green processes, especially when the method is automated and uses a minimal amount of sample.

Presently, spectroscopic methods dominate the area of green analytical chemistry [10]. A special issue of *Spectroscopy letters* appeared in 2009 as an attempt to put green spectroscopy in the first line of the objectives of the spectroscopy community. The issue was dedicated to green analytical techniques in the spectrometric analysis of environmental and biological samples [11], simple alternatives for sample pretreatment and analyte determination [12], alternative solid sample pretreatment methods in green analytical atomic spectrometry [13], a.o.

The most common method of sample introduction in atomic spectrometry is via a solution despite the fact that the large volume of solvent compared to the analyte may present problems to the atom cell: decrease in temperature, increase in the time of atomization, *etc*. The use of a thermospray sample introduction system is a way to remove or considerably reduce the solvent in a solution prior to its delivery to the atom cell. This can minimize potential interferences and improve the accuracy and precision of the analysis, as well as reduce the amount of waste [14,15].

Solid sampling spectroscopy strongly contributes to the development of green analytical chemistry methodologies. Direct solid sampling methods of atomic spectrometry are particularly useful for the analysis of materials that need sophisticated and time-consuming decomposition. Only several milligrams of the sample are consumed; contamination and loss hazards are brought to the minimum, no reagents are needed and there are no wastes. A number of direct solid sampling methods of atomic spectrometry are developed and optimized for the trace and microtrace analysis in various matrices like industrial materials, plants, plastics, foods, *etc*. [16–23]. Slurry sampling is another highly efficient green approach of atomic spectrometry, applicable to the trace element analysis in solid samples by flame AAS, electrothermal AAS, total reflection X-ray fluorescence spectrometry (TXRF) and other spectroanalytical techniques [24–31].

There are several benefits of using field analysis to reduce environmental impact. Along with better efficiency and financial profile, field techniques allow for analysis and data collection to be conducted on-site. As an example the field portable X-ray fluorescence (XRF) facilities for analysis of environmental samples may be mentioned [32, 33]. Energy dispersive XRF has found application as a field analysis method for the determination of trace and microtrace element contents in a large variety of samples like objects of arts, industrial materials, as well as for *in-vivo* measurements [34–38].

Sample preparation methods

Direct methods of analysis are although preferable, but not always available, particularly in the case of microtrace analysis in samples of complex matrix composition. In these cases sample preparation procedures are unavoidable. Sample preparation has three main functions [39]: (i) digestion/dissolution of the sample; (ii) preconcentration of the analytes; and (iii) separation of the analytes from the matrix components.

The choice of a separation/preconcentration procedure depends on the particular analytical task – method of analysis, type of analytes and matrix, required level of sensitivity, accuracy and precision of the analysis, loss/contamination hazards. Some of the most popular separation/preconcentration techniques are liquid-liquid extraction, precipitation/co-precipitation and solid phase extraction. These techniques are continuously improved and new techniques are introduced by the demand for faster, more cost-effective and environmentally friendlier analytical methods. For example, a simple and efficient sample preparation procedure was proposed for the flame or electrothermal AAS determination of trace elements in nails and hair by sample solubilization with aqueous tetraalkylammonium hydroxide [40].

Both existing methods and new procedures were improved by miniaturization and integration to provide higher sample throughput and/or unattended operation using minicolumns, coiled or knotted reactors, most often in flow injection performance [41–57]. A modern way of increasing the selectivity of the separation/preconcentration process is the solid-phase extraction using molecularly imprinted or ion imprinted polymers [58–61]. The hyphenation (integration) of separation and detection, as well as the incorporation of microwave or ultrasonic treatment considerably contributes to increase the efficiency and environmental safety of the methods, *e.g.* [62–67].

ASSESSMENT OF THE ENVIRONMENTAL IMPACT AND WASTE MANAGEMENT

Nowadays, in the development of new analytical procedures, the amount and toxicity of the wastes are as important as any other analytical feature. Miniaturization and automation are explored as approaches for waste minimization. As stated in the priority order for establishing of cleaner analytical methods, if the use of toxic reagents cannot be avoided, the involved amounts should be minimized. This approach also has the advantage of reducing operational costs, including those spent on waste treatment and disposal [24]. Promoting clean methodologies in environmental remediation is the best way to address future challenges [68].

The use of organic solvents in separation and preconcentration methods is the main source of organic waste. The search for alternative solvents is an important step in making an analysis “greener” and environmentally friendlier. Moreover, alternative solvents like supercritical fluids and ionic liquids are even more attractive due to the possibility of varying their properties like solubility, polarity or volatility. Using supercritical fluids instead of organic solvents is becoming popular for most liquid-liquid extractions, especially when supercritical water or CO_2 are used as solvents [8,69]. The application of ionic liquids is intensifying in many areas of analytical chemistry, particularly in chromatography [70]. The non-volatility and good solvating properties, together with a large range of spectral transparency make them suitable solvents for spectroscopic measurements as well [8].

During the last two decades cloud point extraction has become a versatile and simple alternative to liquid-liquid extraction. In this method the organic solvents are replaced with non-ionic surfactants [71,72]. Some recent examples for the use of cloud point extraction for the preconcentration of metal ions prior to their spectrometric determination are given in [73-79].

Green analytical chemistry in Bulgaria

The analytical laboratories in Bulgaria are presently in a process of renovating their methodologies and adapting them to the European norms. This renovation is based on the green chemistry concept, recognized as one of the main tools for reducing environmental pollution. In Bulgaria, however, this process is at the initial stage. Nevertheless, some of the methods for trace element analysis by atomic spectrometry (XRF, AAS, ICP-OES, ICP-MS), published by Bulgarian scientists, are essentially green analytical methods, e.g., [44, 80–93].

Recently, two projects in the area of green analytical chemistry were funded by the National Science Fund of Bulgaria. According to the first one, the GAMA – Green Analytical Methods Academic Centre was created at the University of

Plovdiv "Paisii Hilendarski". The aim of this research centre was to unify the efforts of prominent experts and young scientists of five universities and to focus their varied expertise towards development and application of modern analytical methodologies of trace element analysis in environmental samples like soils, plants and animal tissues. This project accentuates on the possibilities of inductively coupled plasma mass spectrometry and electrothermal atomic absorption spectrometry, combined with suitable sample preparation methods by observing the principles of green chemistry. A major activity of the GAMA Centre is the teaching of university students, PhD students and specialists on the issues of green analytical chemistry.

The second project deals with the development and practical application of total reflection X-ray fluorescence spectrometry (TXRF) at the Institute of General and Inorganic Chemistry of the Bulgarian Academy of Sciences. As an exemplary green analytical method TXRF uses sample amounts at the milligram level; involves minimum sample pretreatment for the analysis of solutions, suspensions or powders; the analysis is rapid and automated, with low energy, water and gas consumption [33, 94-96]. Within the project, TXRF will be applied to the trace element analysis of bottled Bulgarian mineral, spring and table waters, to the determination of the elemental composition of archaeological glasses and the determination of major and trace components in ashes of industrial biomass. Educational activities in the field of green analytical chemistry are also foreseen.

The dissemination of the theoretical and practical results of the mentioned projects at an educational, scientific and industrial level will contribute to achieving the goals of green chemistry in Bulgaria by:

- educating specialists, capable of handling and solving environmental problems in the (micro)trace analysis of different materials;
- creating a new approach to typical chemical activities leading to environmentally friendly use of facilities in science and technology.

***Acknowledgements**: The authors thank the National Science Fund at the Ministry of Education, Youth and Science of Republic of Bulgaria for the financial support (Contracts DTK 02-5/2010 and DCVP-02/2/2009).*

REFERENCES

1 Our Common Future. The Report of the World Commission on Environment and Development "Towards Sustainable Development", Oxford University Press, Oxford, 1987.
2 P. T. Anastas, R. Warner, Green Chemistry, Theory and Practice, Oxford University Press, New York, 1998.
3 P. T. Anastas, *Crit. Rev. Anal. Chem.,* **29**, 167 (1999).
4 P. T. Anastas, T. C. Williamson (eds.), Green Chemistry: Designing Chemistry for the Environment, ACS Symp. Ser. No. 626, Am. Chem. Soc., Washington, DC, 1996.
5 P. T. Anastas, T. C. Williamson (eds.), Green Chemistry: Frontiers in Benign Chemical Synthesis and Processes, Oxford University Press, Oxford, 1998.
6 P. T. Anastas, C. A. Farris (eds.), Benign by Design: Alternative Synthetic Design for Pollution Prevention, ACS Symp. Ser. No. 577, Am. Chem. Soc., Washington, DC, 1994.
7 J. J. Breen, M. J. Dellarco (eds.), Pollution Prevention, in Industrial Processes: the Role of Process Analytical Chemistry, ACS Symp. Ser. No. 508, Am. Chem. Soc., Washington, DC, 1992.
8 M. Koel, M. Kaljurand, *Pure Appl. Chem.*, **78**, 1993 (2006).
9 M. Tobiszewski, A. Mechlinska, J. Namiesnik, *Chem. Soc. Rev.,* **39**, 2869 (2010).
10 Y. He, L. Tang, X. Wu, X. Hou, Y.-I. Lee, *Appl. Spectrosc. Rev.,* **42**, 119 (2007).
11 M. L. Cervera, M. de la Guardia, S. Dutta, A. K. Das, *Spectrosc. Lett.,* **42**, 284 (2009).
12 F. R. Rocha, L. S. Teixeira, J. A. Nobrega, *Spectrosc. Lett.,* **42**, 418 (2009).
13 A. Moreda-Pineiro, M. del Carmen Barciela-Alonso, R. Dominguez-Gonzalez, E. Pena-Vazquez, P. Herbello-Hermelo, P. Bermejo-Barrera, *Spectrosc. Lett.,* **42**, 394 (2009).
14 X. D. Wen, P. Wu, K. L. Xu, J. W. Wang, X. D. Hou, *Microchem. J.*, **91**, 193 (2009).
15 M. A. Bezerra, V. A. Lemos, J. S. Garcia, *Talanta*, **82**, 437 (2010).
16 A. Molina-Díaz, J. F. García-Reyes, B. Gilbert-López, *Trends Anal. Chem.*, **29**, 654 (2010).
17 A. Detcheva, K. H. Grobecker, *Eurasian J. Anal. Chem.*, **3**, 70 (2008).
18 A. Detcheva, P. Barth, J. Hassler, *Anal. Bioanal. Chem.*, **394**, 1485 (2009).
19 K. H. Grobecker, A. Detcheva, *Talanta*, **70**, 962 (2006).
20 A. Detcheva, K. H. Grobecker, *Trans. Univ. Kosice,* **2**, 35 (2007).
21 A. Detcheva, K. H. Grobecker, *Environ. Chem. Lett.*, **6**, 183 (2008).

22 W. Schroen, A. Detcheva, B. Dressler, K. Danzer, *Fresenius' J. Anal. Chem.,* **361**, 106 (1998).
23 J. Hassler, A. Detcheva, O. Foerster, P. Perzl, K. Florian, *Ann. Chim. Rome,* **89**, 827 (1999).
24 G. C. Brandao, G. D. Matos, S. L. Ferreira, *Microchem. J.,* **98**, 231 (2011).
25 S. Gunduz, S. Akman, M. Kahraman, *J. Hazard. Mat.,* **186**, 212 (2011).
26 S. L. Ferreira, M. Miró, E. G. da Silva, G. D. Matos, P. S. dos Reis, G. C. Brandao, W. N. dos Santos, R. G. Araujo, *Appl. Spectrosc. Rev.,* **45**. 44 (2010).
27 F. R. de Amorim, M. B. Franco, C. C. Nascentes, J. B. da Silva, *Food Anal. Meth.,* **4**, 41 (2011).
28 M. Savio, S. Cerutti, L. D. Martinez, P. Smichowski, R. A. Gil, *Talanta,* **82**,523 (2010).
29 N. Campillo, E. Muñoz-Delgado, I. López-García, Y. Baeza-Albarracín, M. Hernández-Córdoba, *Microchim. Acta,* **171**, 71 (2010).
30 M. A. Amberger, M. Höltig, J. A. Broekaert, *Spectrochim. Acta Part B,* **65**, 152 (2010).
31 A. Detcheva, G. Gentscheva, I. Havezov, E. Ivanova, *Talanta,* **58**, 489 (2002).
32 D. J. Kalnicky, R. Singhvi, *J. Hazard. Mat.*, **83**, 93 (2001).
33 H. Stosnach, *Spectrochim. Acta Part B,* **61**, 1141 (2006).
34 N. Miskolczi, R. Nagy, L. Bartha, P. Halmos, B. Fazekas, *Microchem. J.,* **88**, 14 (2008).
35 I. Ranjith Jayasekera, M. C. Freitas, M. F. Araojo, *J. Trace Elem. Med. Biol.*, **17**, 221 (2004).
36 V. Zaichick, N. Ovcharenko, S. Zaichick, *Appl. Rad. Isot.,* **50**, 283 (1999).
37 A. Pitarch, I. Queralt, *Nucl. Instr. Meth. Phys. Res. Part B*, **268**, 1682 (2010).
38 R. Cesareo, A. Castellano, G. Buccolieri, S. Quarta, M. Marabelli, P. Santopadre, M. Leole, A. Brunetti, *Nucl. Instr. Meth. Phys. Res. Part B*, **213**, 703 (2004).
39 E. Ivanova, in: Fundamentals of Chemical Analysis, R. Borissova (ed.) Vodolei Press, Sofia, 2009 (in Bulgarian).
40 D. L. Tsalev, E. I. Tserovski, A. G. Raicheva, A. I. Barzev, R. G. Georgieva, Z. K. Zaprianov, *Spectrosc. Lett.*, **26**, 331 (1993).
41 F. R. Rocha, J. A. Nóbrega, O. Fatibello-Filho, *Green Chem.*, **3**, 216 (2001).
42 A. Velasco Arjona, M. D. Luque de Castro, E. Ivanova, F. Adams, *Lab. Rob. Instr.*, **10**, 293 (1998).
43 K. Benkhedda, H. Goenaga-Infante, E. Ivanova, F. Adams, *Trends Anal. Chem.*, **21**, 332 (2002).
44 B. Dimitrova, K. Benkhedda, E. Ivanova, F. Adams, *Talanta,* **71**, 44 (2007).
45 L. S. Teixeira, F. R. Rocha, *Talanta*, **71**, 1507 (2007).
46 J. Curylo, W. Wardencki, J. Namiesnik, *Polish J. Environ. Studies,* **16**, 5 (2007).
47 A. L. Washburn, R. C. Bailey, *Analyst*, **136**, 227 (2011).
48 C. Cui, M. He, B. Hu, *J. Hazard. Mat.,* **187**, 379 (2011).
49 M. A. Jeannot, A. Przyjazny, J. M. Kokosa, *J. Chromatogr. Part A,* **1217**, 2326 (2010).
50 Q. Zhao, J. L. Anderson, *Anal. Bioanal. Chem.* (2011), in press.
51 A. Sanz-Medel (ed.), Flow Analysis with Atomic Spectrometric Detectors, Elsevier, Amsterdam, 1999.
52 Y. Gao, W. Yang, C. Zheng, X. Hou, L. Wu, *J. Anal. At. Spectrom.,* **26**, 126 (2011).
53 D. L. Tsalev, M. Sperling, B. Welz, *Talanta,* **51**, 1059 (2000).
54 B. Koleva, E. Ivanova, *Eurasian J. Anal. Chem.*, **3**, 183 (2008).
55 A. O. AlSuhaimi, T. McCreedy, *Arab. J. Chem.* **4**, 195 (2011).
56 M. C. Yebra-Biurrun, N. Carro-Mariño, *Talanta,* **83**, 425 (2010).
57 Y.-F. Huang, Y. Li, Y. Jiang, X.-P. Yan, *J. Anal. At. Spectrom.,* **25**, 1467 (2010).
58 S. Özkara, M. Andaç, V. Karakoç, R. Say, A. Denizli, *J. Appl. Polym. Sci.,* **120**, 1829 (2011).
59 I. Dakova, I. Karadjova, I. Ivanov, V. Georgieva, B. Evtimova, G. Georgiev, *Anal. Chim. Acta,* **584**, 196 (2007).
60 I. Dakova, I. Karadjova, V. Georgieva, G. Georgiev, *Talanta,* **78**, 523 (2009).
61 H. Huang, Z. Huang, X. Wang, *Asian J. Chem.* **23**, 1527 (2011).
62 M. S. Eschner, W. Welthagen, T. M. Groger, *Anal. Bioanal. Chem.*, **398**, 1435 (2010).
63 D. Z. Dan, Modern Microwave Sample Preparation Technology, Sichuan University Press, Chengdu, 2003.
64 J. L. Burguera, M. Burguera, C. Rondon, *Talanta*, **58**, 1167 (2002).
65 C. Bendicho, I. Lavilla, Encyclopedia of Separation Science: Application of Ultrasound-Assisted Metal Extractions, **9**, Academic Press, London, 2000.
66 E. Molaakbari, A. Mostafavi, D. Afzali, *J. Hazard. Mat.,* **185**, 647 (2011).
67 K. Simitchiev, E. Harizanova, V. Stefanova, V. Kmetov, N. Kovachev, A. Canals, *Asian Chem. Lett.,* **15** (2011), in print.
68 S. Dutta, A. K. Das, *Trends Anal. Chem.*, **29**, 636 (2010).
69 K. Oukebdane, F. Portet-Koltalo, N. Machour, *Talanta*, **82**, 227 (2010).
70 Y. Wang, M. L. Tian, W. T. Bi, *Intern. J. Mol. Sci.*, **10**, 2591 (2009).
71 M. J. Rosen, Surfactants and Interfacial Phenomena, Wiley, Hoboken, New Jersey, 2004.

72 A. Sanz-Medel, M. Campa, E. B. Gonzalez, M. L. Fernandez-Sanchez, *Spectrochim. Acta Part B*, **54**, 251 (1999).
73 H.C. Rezende, C.C. Nascentes, N. M. Coelho, *Microchem. J.,* **97**, 118 (2011)
74 S. Tong, Q. Jia, N. Song, W. Zhou, T. Duan, C. Bao, *Microchim. Acta,* **172**, 95 (2011).
75 J. Borkowska-Burnecka, A. Szymczycha-Madeja, W. Zyrnicki, *J. Hazard. Mat.* **182**, 477 (2010).
76 T. A. Şahin, T. Tokgöz, S. Bektaş, *J. Hazard. Mat.,* **181**, 359 (2010).
77 N. N. Meeravali, S. J. Kumar, S.-J. Jiang, *Anal. Methods,* **2**, 1101 (2010).
78 N. N. Meeravali, S.-J. Jiang, *At. Spectrosc.,* **31**, 111 (2010).
79 S. G. Silva, P. V. Oliveira, F. R. Rocha, *J. Braz. Chem. Soc.,* **21**, 234 (2010).
80 K. Simitchiev, V. Stefanova, V. Kmetov, G. Andreev, N. Kovachev, A. Canals, *J. Anal. At. Spectrom.,* **23**, 717 (2008).
81 A. Detcheva, K. H. Grobecker, *Spectrochim. Acta Part B,* **61**, 454 (2006).
82 A. Detcheva, I. Havezov, G. Gentscheva, E. Ivanova, *Ann. Chim. Rome*, **92**, 595 (2002).
83 S. Tsakovski, K. Benkhedda, E. Ivanova, F. Adams, *Anal. Chim. Acta*, **453**, 143 (2002).
84 K. Benkhedda, H. Goenaga-Infante, E. Ivanova, F. Adams, *J. Anal. At. Spectrom*., **16**, 995 (2001).
85 E. Ivanova, H. Berndt, E. Pulvermacher, *J. Anal. At. Spectrom.,* **19**, 1507 (2004).
86 G. Gentscheva, J. Jordanov, E. Ivanova, V. Petrova, L. Vladeva, *Bulg. Chem. Commun*., **37**, 69 (2005).
87 K. Simitchiev, V. Stefanova, V. Kmetov, A. Canals, *Ann. Univ. Sofia "St. Kliment Ohridski", Fac. Chim.,* **100**, 107 (2008).
88 K. Simitchiev, V. Stefanova, V. Kmetov, G. Andreev, A. Sanchez, A. Canals, *Talanta,* **77**, 889 (2008).
89 I. B. Karadjova, L. Lampugnani, A. D'Ulivo, M. Onor, D. L. Tsalev, *Anal. Bioanal. Chem.,* **388**, 801 (2007).
90 I. B. Karadjova, P. K. Petrov, I. Serafimovski, T. Stafilov, D. L. Tsalev, *Spectrochim. Acta Part B,* **62,** 258 (2007).
91 K. Tsekova, D. Todorova, S. Ganeva, *Intern. Biodeterior. Biodegrad.,* **64**, 447 (2010).
92 S. Arpadjan, I. Karadjova, L. Jordanova, *Fresenius' J. Anal. Chem.*, **367,** 207 (2000).
93 K. Tasev, I. Karadjova, S. Arpadjan, J. Cvetkovic, T. Stafilov, *Food Control*, **17**, 484 (2006).
94 M. Dargie, A. Markowicz, A. Tajani, V. Valkovic, *Fresenius' J. Anal. Chem.,* **357**, 589 (1997).
95 M. Garcia-Heras, R. Fernandez-Ruiz, J. D. Tornero, *J. Archaeol. Sci.,* **24**, 1003 (1997).
96 Collection of papers presented at the 12th Conference on TXRF Analysis and Related Methods (TXRF 2007), Trento, Italy, *Spectrochim. Acta Part B,* **63**, Special issue, (2008).

ЗЕЛЕНА АНАЛИТИЧНА ХИМИЯ И НЕЙНИТЕ ПЕРСПЕКТИВИ В БЪЛГАРИЯ

Е. Х. Иванова, А. К. Дечева

Институт по обща и неорганична химия, Българска академия на науките, ул. „Акад. Г. Бончев", бл. 11, София 1113

(Резюме)

Постъпила на 17 март 2011 г.; приета на 3 април 2011 г.

Терминът „зелена химия" е въведен през 90-те години на миналия век с цел да се минимизира влиянието на химичните дейности върху околната среда. В обзора са разгледани основните принципи, на които трябва да отговаря една химична процедура, за да бъде призната за зелена (щадяща околната среда). Тези принципи включват използване на по-малки количества реагенти и разтворители, отделяне на по-малки количества твърди, течни и газообразни продукти в резултат на използваните процеси, по-малко потребление на вода и енергия. Специално внимание е обърнато на особеностите на зелената аналитична химия, въвеждането на зелени принципи в аналитичната практика, оценката на влиянието върху околната среда и оползотворяването/обезопасяването на отпадните продукти. Разгледано е състоянието и перспективите за развитието на зелената аналитична химия в България, като е посочен приносът на българските аналитици.

Bulgarian Chemical Communications, Volume 44, Number 1(pp. 11 –19) 2012

Catalytic synthesis of diphenylmethyl ethers (DPME) using Preyssler acid $H_{14}[NaP_5W_{30}O_{110}]$ and silica-supported Preyssler catalysts

Ali Gharib [1,2]*, Nader Noroozi Pesyan[3], Manouchehr Jahangir [1], Mina Roshani [1], J. (Hans) W. Scheeren[4]

[1]*Department of Chemistry, Islamic Azad University, Mashhad, Iran*
[2]*Agricultural Researches and Services Center, Mashhad, Iran*
[3]*Department of Chemistry, Faculty of Science, Urmia University, 57159, Urmia, Iran*
[4]*Cluster for Molecular Chemistry, Department of Organic Chemistry, Radboud University Nijmegen, The Netherlands*

Received September 4, 2010; Revised March 18, 2011

A simple procedure for the preparation of diphenylmethylethers from benzhydrol and alcohols or phenols using Preyssler acid and silica-supported heteropolyacids (HPAs) catalysts is reported. The inexpensive and ecofriendly (green) synthesis offers satisfactory yields. The catalyst is easily recoverable and may be recycled and reused without loss of catalytic activity.

Keywords: Diphenylmethyl ethers, Preyssler catalyst, Heteropolyacid, Phenol

INTRODUCTION

Among solid catalysts, heteropolyacids constitute a large class of compounds that are remarkable owing to their physicochemical properties like strong Brønsted acidity, reversible transformations, activation of molecular oxygen and hydrogen peroxide, high proton mobility and solubility in polar solvents. These properties have made them popular in many fields, such as catalysis, biology, medicine, magnetism, photochemistry and material science [1]. Heteropolyacids (HPAs) are transition metal oxygen anion clusters that exhibit a wide range of well-defined molecular structures, surface charge densities, chemical and electronic properties [2]. They also display acid and redox catalytic properties [3]. Among various HPA structural classes, Keggin-type [4] HPAs have been mostly investigated as catalytic materials. The acid and redox catalytic properties of HPAs have been conventionally modified by replacing the protons with metal cations and/or by changing the heteroatom of the framework polyatoms [5,7]. HPAs are inorganic acids and strong oxidizing agents [6]. Although Keggin-type polyoxoanions and their derivatives have been widely studied and much attention has been devoted to their catalytic behavior [8], the catalytic reactions and the application of Preyssler anions have been largely overlooked [9]. The Preyssler type heteropolyacid, $H_{14}[NaP_5W_{30}O_{110}]$, is remarkable owing to its

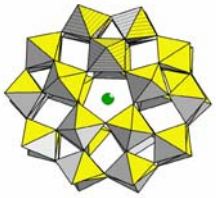

Fig. 1.

exclusive physicochemical properties such as strong Brønsted acidity, reversible transformations, solubility in polar and non-polar solvents, high hydrolytic stability and high thermal stability, all very important in catalytic processes. The structure of the Preyssler anion, $[NaP_5W_{30}O_{110}]^{14-}$, is shown in Fig. 1. The anion has an approximate D_5h symmetry and consists of a cyclic assembly of five PW_6O_{22} units; each derived from the Keggin anion, $[PW_{12}O_{40}]^{3-}$, by removal of two sets of three corner-shared WO_6 octahedra. A sodium ion is located within the polyanion on the fivefold axis and 1.25Å above the pseudo mirror plane that contains the five phosphorus atoms [10]. Preyssler polyanion as a large anion can provide many ‘‘sites’’ on the oval-shaped molecule that are likely to render the catalyst effective. Recently, we studied the catalytic activity in preparation of DPME by using various heteropolyacids as catalysts under green and mild conditions. We have already used this catalyst in the esterification of butanol, esterification of salicylic acid with aliphatic and benzylic alcohols,

*) To whom all correspondence should be sent: E-mail: : aligharib5@yahoo.com

© 2012 Bulgarian Academy of Sciences, Union of Chemists in Bulgaria

synthesis of β-butyrolactone, ε-caprolactone and 2-cumaranone, synthesis of aspirin [11-14]. DPME and DPM groups are found as part of the structure of pharmacologically active compounds [15]. There are some studies on the preparation of DPME from diphenylmethyl phosphate-trifluoroacetic acid [16], xenon difluoride [17], diphenylmethyl chloride or bromide in the presence of a base [18] or *p*-toluenesulfonic acids [19], diphenylmethyl-diazomethane [20], diphenylmethanol in the presence of concentrated sulphuric acid [21], ytterbium triflate-ferric chloride [22]. In this research, we used a Preyssler heteropolyacid and a silica-supported Preyssler catalyst in preparation of DPME from various alcohols and phenols.

EXPERIMENTAL

Materials

All chemicals were obtained from Merck and were used as received.

Instruments

IR spectra were obtained on a Buck Scientific 500 spectrometer. ^{1}H NMR spectra were recorded on a FT NMR Bruker 100 MHz Aspect 3000 spectrometer. GLC analysis was performed on a PU 4500 gas chromatograph with FID detector. The purity of the products was determined by GC analysis. The products were characterized by comparison of their spectroscopic (IR, ^{1}H NMR, GC) data with those of authentic samples. The yields were determined by GC. The mass spectra were scanned on a Varian MAT CH-7 instrument at 70 eV. Melting points were recorded on an Electrothermal type 9100 melting point apparatus without correction.

Catalyst Preparation

$H_{14}[NaP_5W_{30}O_{110}]$,($H_{14}$-$P_5$), $H_{14}[NaP_5W_{29}MoO_{110}]$, ($H_{14}$-$P_5Mo$) and $H_{14}P_5/SiO_2$ were prepared as described earlier [11-14].

Procedure for the preparation of DPME of alcohols

In a round-bottom flask, alcohol (1 mmol), diphenylmethanol (1 mmol), heteropolyacid catalyst (0.05 mmol) and solvent (5 mL) were added and the mixture was stirred as indicated in Tables 1a, 1b, 1c. After completion of the reaction, the catalyst was filtered off and washed with ethyl ether (3 ×10 mL). Then, the solution was washed with water (3 × 10 mL) and 3M NaOH (15 mL), dried over anhydrous $MgSO_4$, after which the solvent was evaporated. The pure product (DPME) was obtained by column chromatography.

Recycling of the catalyst

The filtered catalyst was washed with toluene (2 × 5 mL), dried under vacuum and then reused.

Benzhydryl phenethyl ether (1a). ^{1}H-NMR (400 MHz, δ_H , $CDCl_3$): 2.72 (t, 2H, 6Hz), 3.50 (t, 2H, 6Hz), 5.43 (s, 1H), 7.13-7.35 (m, 15H); IR (KBr) ν_{max}/cm^{-1}: 1635, 1240, 1040, 1048, 710, 842.

Dibenzhydryl ether (1b). ^{1}H-NMR (400 MHz, δ_H , $CDCl_3$): 5.40 (s, 2H), 7.21-7.39 (m, 20H); IR (KBr) ν_{max}/cm^{-1}: 1645, 1243, 1040, 1051, 720, 842.

Benzhydryl 4-methylphenyl ether (1c). ^{1}H-NMR (400 MHz, δ_H , $CDCl_3$): 2.20 (s, 3H), 5.50 (s, 1H), 6.70 (d, 2H, J=8Hz), 6.96 (d, 2H, J=8Hz), 7.17-7.36 (m, 10H); IR (KBr) ν_{max}/cm^{-1}: 1639, 1240, 1038, 1049, 719, 840.

Benzhydryl 3-methylphenyl ether (2c). ^{1}H-NMR (400 MHz, δ_H , $CDCl_3$): 2.22 (s, 3H), 5.50 (s, 1H), 6.90 (m, 3H), 7.16- 7.36 (m, 11H); IR (KBr) ν_{max}/cm^{-1}: 1638, 1240, 1041, 1048, 717, 841.

Benzhydryl 4-nitrophenyl ether (6c). ^{1}H-NMR (400 MHz, δ_H , $CDCl_3$): 5.51 (s, 1H), 6.90 (d, 2H, J=8Hz), 7.16-7.35 (m, 10H), 8.3 (d, 2H, J=8Hz); IR (KBr) ν_{max}/cm^{-1}: 1605, 1550, 1319, 1240, 1040, 1045, 710, 840.

Benzhydryl phenyl ether (7c). ^{1}H-NMR (400 MHz, δ_H , $CDCl_3$): 5.50 (s, 1H), 6.92 (m, 3H), 7.14-7.38 (m, 12H); IR (KBr) ν_{max}/cm^{-1}: 1643, 1245, 1041, 1050, 718, 840.

Benzhydryl *t*-butyl ether (12c). ^{1}H-NMR (400 MHz, δ_H , $CDCl_3$): 1,20 (s, 9H), 5.35 (s, 1H), 7.11-7.30 (m, 10H); IR (KBr) ν_{max}/cm^{-1}: 1246, 1038, 1525,1600, 715.

Benzhydryl allyl ether (13c). ^{1}H-NMR (400 MHz, δ_H , $CDCl_3$): 3.81 (d, 2H, J=3Hz), 5.20 (m, 2H), 5.43 (s, 1H), 6.01 (m, 1H), 7.15-722 (m, 10H); IR (KBr) ν_{max}/cm^{-1}: 1585, 1220, 1030, 1520,1580, 710.

Benzhydryl isopropyl ether (15c). ^{1}H-NMR (400 MHz, δ_H , $CDCl_3$): 1.21 (6H, d, J=6Hz), 3.68 (1H, sp, J=6Hz), 5.32 (s, 1H), 7.16-7.25 (10H, m); IR (KBr) ν_{max}/cm^{-1}: 1250, 1040, 1520,1600, 710.

Benzhydryl methyl ether (16c). ^{1}H-NMR (400 MHz, δ_H , $CDCl_3$): 3.48 (3H, s), 5.37 (1H, s) 7.31-7.40 (10H, m); IR (KBr) ν_{max}/cm^{-1}: 1240, 1030, 1510,1595, 720.

Benzhydryl benzyl ether (17c). ^{1}H-NMR (400 MHz, δ_H , $CDCl_3$): 4.50 (s, 2H), 5.39 (s, 1H) 7.11-7.35 (m, 15H); IR (KBr) ν_{max}/cm^{-1}: 1640, 1250, 1040, 1050, 705, 840.

RESULTS AND DISCUSSION

The heterogeneous catalytic synthesis of DPME from benzyl alcohol derivatives, allylic and aliphatic alcohols using Preyssler heteropolyacids supported onto silica gel at the indicated times and temperatures is reported and the products are identified by TLC (Scheme 1).

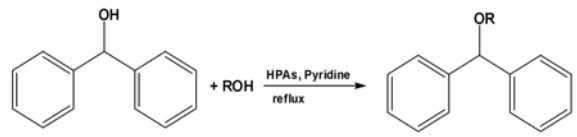

Scheme 1. Synthesis of DPME from alcohols and phenols using heteropolyacid catalysts

The reaction conditions were optimized by studying the effects of alcohol type, reaction time, catalyst type and other important factors, such as the solvent that controls the yield of diphenylmethyl ethers. The reaction was performed using various heteropolyacid catalysts. For preparing DPM-ethers, methanol, benzhydrol and various heteropolyacid (HPAs) catalysts were used under different conditions (Tables 1a, 1b, 1c).

The preparation of DPME starting from methanol and benzhydrol was tested under various conditions (temperature and solvent), using the bulk catalyst. The reaction gives higher yields in pyridine than in chloroform solution. The reaction was completed in 1 h at 115 °C, with pyridine as a solvent and 95% DPME was obtained (Table 1c, entry 16).

We performed the reaction under the same conditions for the protection of substituted phenols. The reactions proceeded efficiently with good yields. The nature of the substituents had no effect on the conversion rates (Table 1c, entries 1, 2, 6).

Silica supported Preyssler catalysts gave similar yields, also providing easy separation, simple recycling and recovery. The recycled heteropolyacid catalysts were used in reaction without loss of activity.

Effect of the alcohol type

The reaction with primary alcohols gave DPME in higher yields compared with secondary alcohols (Table 1c, entries 14 and 15). In benzylic alcohols with electron-donating substituents DPME was obtained with a higher yield than in alcohols with electron-withdrawing groups (Table 1a, entries 9-16). This can be attributed to the activating effect of the substituents.

Effect of the reaction temperature

The reaction was carried out at two temperatures: room temperature (lowest temperature) and reflux temperature (highest temperature, 115ºC). The maximum yield was reached at the reflux temperature (115ºC). This effect was expected since increasing the temperature apparently favours the acceleration of the forward reaction. In general, at room temperature (25ºC) no product was obtained.

Reusability of the catalyst

In order to know whether the catalysts would succumb to poisoning and loss of catalytic activity, the catalyst was recovered after the reaction and reused in the esterification reactions. These studies were performed with all forms of Preyssler catalysts. We have found that Preyssler catalysts can be reused several times without any appreciable loss of activity. IR spectra of the resulting solids indicated that the catalyst can be recovered without structural degradation. After several consecutive recoveries the catalytic activity only slightly

decreased, pointing to the stability and retention capability of the polyanion. Similar results were obtained for DPME of phenol (88% yield, Table 1c, entry 7).

Effect of the solvent

Preparation of DPME from benzhydrol and alcohols or phenols using heteropolyacid catalysts were carried out in various solvents, such as pyridine and chloroform. We have found that pyridine is the most effective solvent because of its solubility in polar and non-polar conditions, which corresponds to the activity of heteropolyacids in polar and non-polar solvents and systems. The results are shown in Table 2. The product yields were in the order: pyridine > chloroform. It is noteworthy to mention that even prolonged heating of the reactants in neat pyridine and chloroform in absence of catalyst did not give products.

Effect of the reaction time

Typical time courses of the reactions with various types of alcohols and phenols are shown in Tables 1a-c at reflux temperatures. The results show that in the initial stage, the reaction proceeds

rapidly. The effect of reaction time on DPME percent yield indicates that the latter strongly depends on reaction time. The best reaction time

Table 1a. Preparation of DPME from alcohols, phenols and benzhydrol using bulk Preyssler catalysts and silica supported Preyssler catalysts under reflux at different times with pyridine as a solvent

Entry	Alcohol	[a]Time (h)	[c]Yield(%) H_{14}-P_5	[c]Yield(%) $H_{14}P_5Mo$	[c]Yield(%) $H_{14}P_5/SiO_2$ (50%)	[c]Yield(%) H_{14}-P_5/SiO_2 (40%)
1	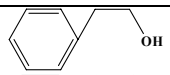	1	92	90	90(90,89)[b]	88(88,87)[b]
2	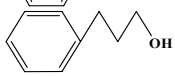	1.5	93	91.5	91(90,89)[b]	88.5
3	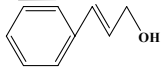	1	96.5	94	95(94,94)[b]	93(93,92)[b]
4	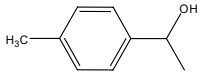	1	90(90,89)[b]	87.5	88.5	87(87,86)[b]
5	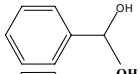	1.5	86	83	85	83(83,82)[b]
6	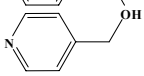	2	70(70,69)[b]	66	68.5	67
7	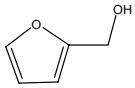	2	75	73.5	73(72,72)[b]	72
8	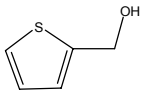	2	78(77,77)[b]	76	77(76, 75)[b]	75.5
9	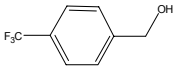	2.5	46.5	43.5	45	42.5
10	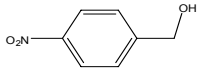	1.5	63	61.5	61	59.5
11	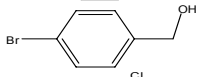	1.5	59.5	57	57.5	56
12	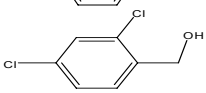	2.5	49.5	46	48(47,46)[b]	47
13	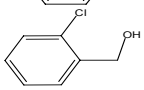	2	51	47	50(50,49)[b]	47
14	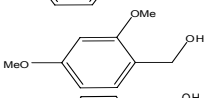	0.5	94(94,93)[b]	91	93(93,92)[b]	91(90,90)[b]
15	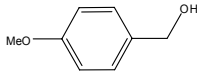	1	90.5(90,89)[b]	87(87,85.5)[b]	88	87(87,86)[b]
16	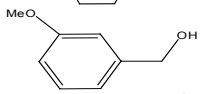	1.5	86	83	85	82.5(82,1)[b]
17	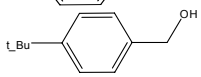	2.25	92(91,90.5)[b]	87	90(90,89)[b]	87
18	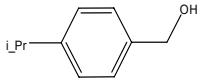	2.25	90(90,89)[b]	86.5	88(88,87)[b]	84.5

19	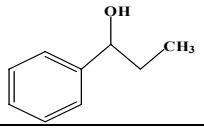	1.5	88	84	86.5	85(85,84)[b]

[b] In parentheses, yields obtained in the first and second reuse of the catalyst. [a,b,c]Yields analyzed by GC.

Table 1b. Preparation of DPME from from alcohols, phenols and benzydrol using Preyssler catalysts and its silica supported under reflux, different times and pyridine as solvent

Entry	Alcohol	[a]Time (h)	[c]Yield(%) H_{14}-P_5	[c]Yield(%) $H_{14}P_5Mo$	[c]Yield(%) H_{14}-P_5/SiO_2 (50%)	[c]Yield(%) H_{14}-P_5/SiO_2 (40%)
1	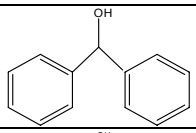	1	96(96,95)[b]	93(92.5,91.5)[b]	94(94,93.5)[b]	93(93,92)[b]
2	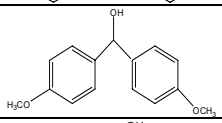	1	98	95.5	96.5	94
3	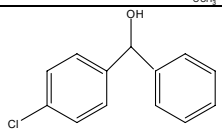	1.5	95	92	92.5	91
4	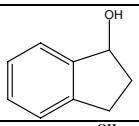	1.25	92	91	90	89
5	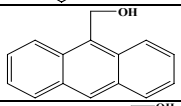	2.5	83	81.5	80.5	78
6	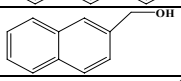	2.5	78	75.5	76.5	75
7	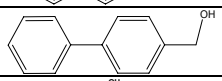	1.5	71	68	70	69
8	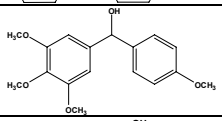	2	91.5	90	89	86.5
9	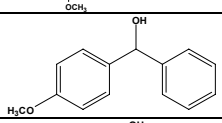	1.5	96(96,95)[b]	95(94,92.5)[b]	95(95,94)[b]	93.5(93,92.5)[b]
10	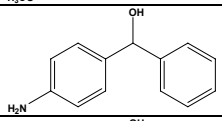	2	93.5	92	90.5	88
11	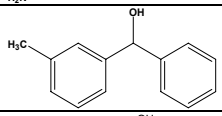	1.5	94.5	92.5	91.5	90
12	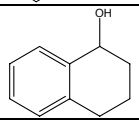	2	69.5	67.5	67	65
13	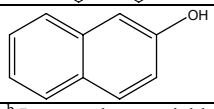	1.5	82	80	79.5	78.5

[b] In parentheses, yields obtained in the first and second reuse of the catalyst. [a,b,c]Yields analyzed by GC.

Table 1c. Preparation of DPME from from alcohols, phenols and benzydrol using Preyssler catalysts and its silica supported under reflux, different times and pyridine as solvent

Entry	Alcohol	[b]Time (h)	[c]Yield(%) H_{14}-P_5	[c]Yield(%) $H_{14}P_5Mo$	[c]Yield(%) H_{14}-P_5/SiO_2 (50%)	[c]Yield(%) H_{14}-P_5/SiO_2 (40%)
1	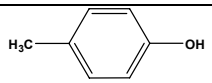	1	89.5(89.5,89) [b]	88(88,87) [b]	87.5(87,86) [b]	86.5(86,85.5) [b]
2	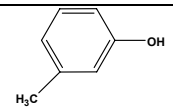	1	85	83.5	84	82
3	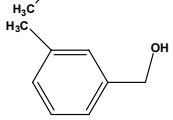	1.5	86	84	83.5	82
4	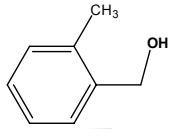	1.25	88	87	87	86
6	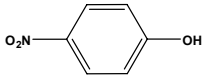	1	83	81.5	81	79
7	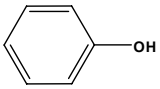	1	88(88,87) [b]	86	81	77
8	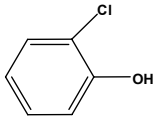	2.5	76	73.5	74.5	73.5
9	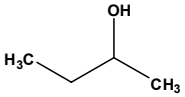	1	91	89	89	88
10	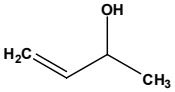	1	96	94.5	94	92.5
11	**n-C_8H1_7-CH_2-OH**	1	93	87	87.5	86
12	**$(CH_3)_3COH$**	1.5	87(87,86) [b]	85(85,84) [b]	84.5(84.5,84) [b]	82(82,81) [b]
13	**CH_2=CH-CH_2OH**	1	89	90	91	90
14	**CH_3-$(CH_2)_2CH_2OH$**	1	94	86	86	85
15	**CH_3CH-$OHCH_3$**	1	91	90	90	88
16	**CH_3OH**	1	95	91	91.5	91
17	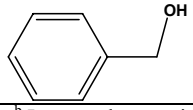	1	85	84	82.5	80

[b] In parentheses, yields obtained in the first and second reuse of the catalyst. [a,b,c]Yields analyzed by GC.

Table 2. Preparation of DPME from from alcohols, phenols and benzydrol using Preyssler, heteropolyacids catalysts under reflux, different times and chloroform as solvent

Entry	Alcohol	[a]Time (h)	[b]Yield(%) $H_{14}[NaP_5W_{30}O_{110}]$	[c]Yield(%) $H_{14}[NaP_5W_{29}MoO_{110}]$
1	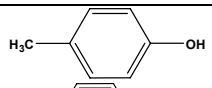	1	84.5	83
2	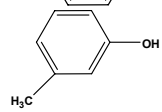	1	81	80
3	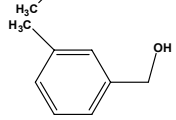	1.5	82	80.5
4	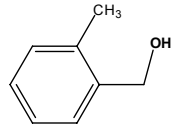	1.25	83.5	81.5
6	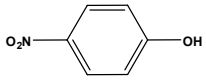	1	79	77
7	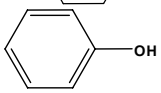	1	85.5	83.5
8	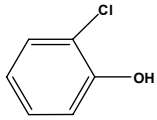	2.5	73.5	72
9	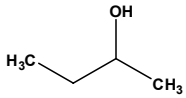	1	88	86.5
10	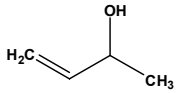	1	92.5	91
11	**n-C_8H1_7-CH_2-OH**	1	90	88.5
12	**$(CH_3)_3COH$**	1.5	84.5	82
13	**CH_2=CH-CH_2OH**	1	86	84.5
14	**CH_3-$(CH_2)_2CH_2OH$**	1	91.5	89.5
15	**CH_3CH-$OHCH_3$**	1	87	85
16	**CH_3OH**	1	91	89.5
17	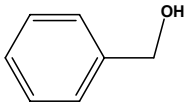	1	80.5	78.5
17	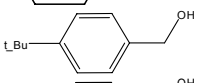	2.25	92(91,90.5) [b]	87
18	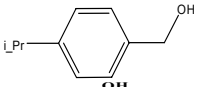	2.25	90(90,89)[b]	86.5
19	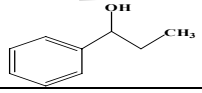	1.5	88	84

[a,b,c]Yields analyzed by GC.

was found to be 1 h at reflux temperature. At any reaction time, $H_{14}[NaP_5W_{30}O_{110}]$ was found to be the most active heteropolyacid catalyst.

Effect of the catalyst type

The reaction of DPME preparation was followed by GC. The yields are shown in Tables 1a-c. According to the results, the highest yield was

achieved in the presence of $H_{14}[NaP_5W_{30}O_{110}]$, ($H_{14}$–$P_5$) and $H_{14}[NaP_5W_{29}MoO_{110}]$, ($H_{14}$–$P_5Mo$) as catalysts. The Preyssler catalysts used in this system gave similar results. Along with the bulk catalyst we used $H_{14}[NaP_5W_{29}MoO_{110}]/SiO_2$ and $H_{14}[NaP_5W_{30}O_{110}]/SiO_2$ for comparative purposes; very similar yields were obtained in comparable reaction times (Table 1a-c). Furthermore, the use of the supported catalyst allows its easy separation and recovery for immediate reutilization. The highest yield of the products was achieved using $H_{14}[NaP_5W_{30}O_{110}]$ as a catalyst.

Comparison of the catalysts (Tables 1a-c) showed that $H_{14}[NaP_5W_{30}O_{110}]$ is the catalyst of choice. In all cases the supported polyacid was less active than the non-supported one.

CONCLUSIONS

The preparation of DPME of alcohols and phenols in the presence of an inexpensive, reusable, easy to handle, non-corrosive, highly hydrolytic, thermally stable and environmentally benign Preyssler heteropolyacid catalyst was studied. This catalyst offers advantages as regards simplicity of operation due to the heterogeneous nature of reaction, easy work-up, high yields of products, high selectivity and recyclability of the catalyst. The catalyst can be easily recovered, regenerated and reused without loss of structure and appreciable activity, thus providing an economic and environmentally friendly method for DPME preparation.

Acknowledgements: *The authors are thankful to the Agricultural Researches & Services Center, Mashhad, Feyzabad, Iran, the Mashhad Islamic Azad University, the Chemistry Department, University of Oslo, Norway and the National Research Council of Canada for the support of this work. Special thanks are due to Professor Dr. J. (Hans) W. Scheeren from the Organic Chemistry Department, Radboud University Nijmegen, The Netherlands.*

REFERENCES

1. C.L. Hill, *Chem. Rev*., **98**, 1 (1998).
2. M. T. Pope, Heteropoly and Isopoly Oxometalates, Springer-Verlag, New York, 1983.
3. I.V. Kozhevnikov, *Catal. Rev. Sci. Eng*., **37**, 311 (1995). Kozhevnikov, I.V. Catalysis by Polyoxometalates. In Catalysts for fine chemical synthesis; Wiley & Sons: Chichester, UK, 2002; Volume 2, p. 216.
4. J.F. Keggin, *Nature*, **131**, 908 (1933).
5. G. B. McGarvey, J. B. Moffat, *J. Catal*., **128**, 69 (1991).
6. T. Okuhara, N. Mizuno, M. Misono, *Adv. Catal*., **41**, 113 (1996).
7. G.B. McGarvey, J. B. Moffat, *J. Catal*., **128**, 69 (1991).
8. T. Okuhara, T. Nishimura, K. Ohashi, M. Misono, *Chem. Lett*., 1201 (1990).
9. M.K. Harrup, C. Hill, L. J. Cardona, *Inorg. Chem*., 33 (1993).
10. M.H. Alizadeh, S.P. Harmalker, Y. Jeanenin, J. Martin-Frere, M.T. Pope, *J. Am. Chem. Soc*., **107**, 2662 (1985).
11. F.F. Bamoharram, M. M. Heravi, M. Roshani, M. Jahangir, A. Gharib, *A. J. Appl. Catal. A: Gen*., **302**, 42 (2006).
12. F.F. Bamoharram, M. M. Heravi, M. Roshani, A. Gharib, M. Jahangir, *J. Mol. Catal. A: Chem*., **252**, 90 (2006).
13. F.F. Bamoharram, M. M. Heravi, M. Roshani, M. Jahangir, A. Gharib, *Journal of Molecular Catalysis A: Chemical*., **271**, 126 (2007).
14. F.F. Bamoharram, M. M. Heravi, M. Roshani, A. Gharib, M. Jahangir, *J. Chinese Chem. Soc*.., **17**, 505 (2006).
15. V. Namboodiri, R. Varma, *Tetrahedron Lett*., **43**, 4593 (2002).
16. L. Lapatsanis, *Tetrahedron Lett*., **19**, 3943 (1978).
17. S. Stavber, M. Zupan, M. *Tetrahedron Lett*., **34**, 4355 (1993).
18. D. Dobson, A. Todd, J. Gilmore, *J. Synth. Commun*., **21**, 601 (1991).
19. R. Parades, R. Perez, *Tetrahedron Lett*., **39**, 2037 (1998).
20. M. Kolovos, C. Froussios, *Tetrahedron Lett*., **25**, 3909 (1984).
21. S. Sugsawa, K. Fujiwara, *Org. Synth. Coll*., **4**, 72 (1963).
22. G. Sharma, T. Prasad, A. Mahalingam, *Tetrahedron Lett*., **42**, 759 (2001).

КАТАЛИТИЧНА СИНТЕЗА НА ДИФЕНИЛ-МЕТИЛОВИ ЕТЕРИ (DPME) ИЗПОЛЗВАЙКИ PREYSSLER‘ОВА КИСЕЛИНА $H_{14}[NaP_5W_{30}O_{110}]$ И PREYSSLER‘ОВ КАТАЛИЗАТОР ВЪРХУ ПОДЛОЖКА ОТ СИЛИЦИЕВ ДИОКСИД

А. Гариб [1,2], М. Джахангир[1], М. Рошани [1], Я. (Ханс) В. Схеерен[3]

[1]*Деапартамент по химия, Ислямски университет „Азад“, Машхад, Иран*
[2]*Център за селско-стопански изследвания и услуги, Машхад, Иран*
[3]*Клъстер за молекулна химия, Департамент по органична химия,Университет Радбоуд в Наймехен, Нидерландия*

Постъпила на 4 септември, 2010 г.; коригирана и приета на 18 март, 2011 г.

(Резюме)

Съобщава се за получаването на дифенил-метилови етери от бензихидрол и алкохоли или феноли с помощта на Preyssler‘ова киселина и катализатори от херетерополикиселини (HPA), нанесени върху подложка от силициев диоксид. Тази евтина и екологично-съобразна (зелена) синтеза предлага задоволителни добиви. Катализаторът лесно се възстановява и може да се използва многократно без загуба на каталитична активност.

Bulgarian Chemical Communications, Volume 44, Number 1 (pp. 20 – 25) 2012

Comparison between four equations of state in predicting the temperature and density dependencies of the parameters of the average effective pair potential for dense methane

M. Souri

Payame Noor University, Iran

Received: January 4, 2011; Revised March 1, 2011

In this work, four equations of state, namely MSRK, RK, Jan-Tsai and Nasrifar-Jalali were compared in predicting the parameters of the average effective pair potential for dense methane at various temperatures and densities. All equations of state show temperature and density dependencies for ε/k and σ: σ increases with temperature and ε decreases, while σ increases and ε decreases as density decreases.

Key Words: Average effective pair potential; Lennard-Jones potential; Equation of state

1. INTRODUCTION

Methane represents the most spherical molecule. The phase diagram of condensed methane is experimentally well investigated and exhibits a disordered phase upon solidification [1,2].

In statistical mechanics, the light and small methane molecule plays a key role. Its liquid phase represents the natural choice for investigating orientational effects upon spatial structural ordering and for examining the complex dynamic problem of translational - rotational coupling. Also, as the first representative of the homologous series of saturated hydrocarbons, the CH_4 molecule has vital importance for the description of the systematic changes in experimental physical and chemical properties with increasing number of CH_2 increments in alkanes and in relating these changes to particular molecular characteristics. Thus, it is not surprising that a huge number of potential models have been developed for modeling the liquid phase of methane [3].

The Lennard–Jones potential is:

$$u(r) = \frac{n\varepsilon}{n-m}\left(\frac{n}{m}\right)^{\frac{m}{n-m}}\left\{\left(\frac{\sigma}{r}\right)^{n} - \left(\frac{\sigma}{r}\right)^{m}\right\} \qquad (1)$$

where σ is the separation at which the potential is zero, ε is the depth of the potential well and n and m are integers.

Lennard–Jones potential is a qualitative realistic potential and is the most frequently used potential for gaseous and liquid systems even at dense fluid conditions. It is a simple pair potential function that possesses both repulsive and attractive London forces and has been extensively used owing to its simplicity [4,5].

Our aim in this work was to predict the temperature and density dependency of the Lennard-Jones potential, as an Average Effective Pair Potential (AEPP). Parsafar *et al*. [6] studied the density and temperature dependency of the Lennard-Jones parameters of dense fluids using linear isotherm regularity (LIR). Nasehzade and Azizi [7] introduced a new simple method to estimate the Lennard-Jones parameters for rare gases and *n*-alkanes at any desired temperature range from triple point to boiling point. Their approach was based on experimental data for the heat of vaporization, free energy of solution, as well as on the application of the scaled-particle theory (SPT) and other new expressions that give the free energy of cavity formation ΔG_c, in hard sphere fluids [8,9].

The state dependency of the Effective Pair Potential (EPP) parameters, the well depth, ε, and the intermolecular separation at constant σ, have been previously studied by some investigators *via* radial distribution function calculations and shape factor theory [10,11].

The interaction potential of an isolated pair is different from that of the pair in the presence of other molecules. This difference can be attributed to the effect of the medium on the molecular charge

* To whom all correspondence should be sent:
E-mail: msouri@pnu.ac.ir

© 2012 Bulgarian Academy of Sciences, Union of Chemists in Bulgaria

distribution. In the absence of such an effect, the interaction potential of two isolated molecules depends on their intermolecular separation (for simple spherical molecules). However, this effect is important in dense fluids. Based on this idea, the concept of the EPP, which includes the effects of the medium plus the isolated pair interaction potential, was introduced. Such a potential is considered to be the interaction of two nearest neighbor molecules in which all of their longer-range interactions are added to it. Since the effect of a fluid medium on the electronic distribution of molecules is included, the total potential energy of the fluid can be represented exactly as the sum of all average effective pair interaction energies. Therefore, the pairwise additivity of the potential energy in terms of the AEPP is an exact treatment (if one can include all long-range potentials in AEPP) and the total potential energy of a fluid can be written as:

$$U = N/2\bar{u}z \qquad (2)$$

where $\bar{u}$ is the AEPP, N is the number of molecules, and z is the average coordination number [6].

2. THEORY

In this work, four equations of state were compared in predicting temperature and density dependency of Lennard- Jones parameters.

The Redlich- Kwong equation of state is:

$$P = \frac{RT}{V-b} - \frac{a}{T^{0.5}V(V+b)} \qquad (3)$$

$$a = \frac{0.42748R^2T_C^{2.5}}{P_C} \qquad b = \frac{0.08664RT_C}{P_C}$$

where P, T, V and R are pressure, temperature, volume and gas constant, respectively (see [12]). a and b are parameters of the equation of state Tc.and Pc are the critical parameters of methane:

$$T_C = 190.564K \quad \text{and} \quad P_C = 4.59\times10^6\,Pa$$

U, internal energy, can be derived from each equation of state by the following steps:

i) $P_{th} = T(\frac{\partial P}{\partial T})_V$

ii) $P_{in} = P_{tot} - P_{th}$

iii) $P_{in} = -(\frac{\partial U}{\partial V})_T$

where P_{th} is the thermal pressure and P_{in} is the internal pressure.

For Redlich- Kwong equation of state, the expression for the internal energy has the form:

$$U = \frac{1.5a}{b\sqrt{T}}(-\frac{b}{V} + \frac{b^2}{V^2} - \frac{b^3}{V^3} + ...) \qquad (4)$$

or:

$$U = \frac{1.5a}{b\sqrt{T}}(-b\rho + b^2\rho^2 - b^3\rho^3 + ...)$$

On the other hand, using the (9,3) Lennard-Jones potential function as an EPP and applying eq. (2), the internal energy will be:

$$U = 1.299R(\varepsilon/k)Z(T,\rho)(\sigma^9\rho^3 - \sigma^3\rho) + 3RT \qquad (5)$$

where the first term is the configurational energy and the second one is the kinetic energy of the fluid.

One can assume that:

$$Z(T,\rho) = A(T) + B(T)\rho \qquad (6)$$

This is a simple function for the coordination number.

Inserting eq. (6) in eq. (5) and comparing the expression obtained for the internal energy with eq. (4) yields:

$$\sigma = (b^3\frac{A}{B})^{\frac{1}{6}} \qquad (7)$$

and

$$\varepsilon/k = \frac{1.5a}{1.299RA\sigma^3\sqrt{T_C}} \qquad (8)$$

Inserting eq. (7) and eq. (8) in eq. (5):

$$\left(\frac{(U-3RT)\sqrt{T_C}}{1.5a\rho} - b^3\rho^3 + 1\right)\Big/\rho = \frac{A}{B}b^3\rho - \frac{B}{A} \qquad (9)$$

The solution of eq. (9) provides a value of A/B for any values of U, ρ and T. Therefore σ can be obtained at any condition.

An expression for U can be derived from each equation of state that is listed in the Appendix. (Eq. 4 is an expression for the internal energy derived from Redlich- Kwong equation of state. Similar

derivation could be done for each equation of state in the Appendix). Comparing these expressions with eq. (5) using the method discussed above, permits to calculate σ values for each data point. The results of such calculations are summarized in Table 1.

The temperature dependency of σ for the RK EoS is shown in Figure 1. At any constant temperature σ decreases with density, but at higher temperatures the slope of variation is greater. In addition, at high densities the temperature dependency of σ is negligible and its values obtained at different temperatures are similar.

The other EoS exhibit analogous trends.

Figure 2 shows the density dependency of σ obtained from different equations of state at constant temperature, 400 K. As is shown, σ decreases with density at constant temperature. Although different equations of state do not predict the same value for σ at constant density, still within the range of data the profiles of Jan-Tsai, Nasrifar-Jalali and MSRK equations of state are parallel. In addition, σ values obtained from RK and MSRK equations of state show a considerable agreement with each other. Since the MSRK is a modified form of RK EoS, such similarity was expected.

One can observe a similar trend at any constant temperature.

One can write eq. (5) as follows:

$$U - 3RT = 1.299R\,\varepsilon/k\,A(1+\frac{B}{A}\rho)(\sigma^9\rho^3 - \sigma^3\rho) \quad (9)$$

where ε/k and A are unknown. Therefore:

$$y = \frac{U - 3RT}{1.299R(1+\frac{B}{A}\rho)(\sigma^9\rho^3 - \sigma^3\rho)} \quad (10)$$

where

$$y = A\,\varepsilon/k \quad \text{or} \quad \ln y = \ln A + \ln \varepsilon/k$$

Assuming that A is a function of T, such as $A = e^{\frac{\beta}{T}}$, one also has:

$$\ln y = \ln \varepsilon/k + \beta/T \quad (11)$$

ln y in terms of *1/T*is not a straight line. Therefore *ε/k* is not a constant value. We suggest the following equation for y:

$$\ln y = a\ln(\rho/T) + b(\ln(\rho/T))^2 + \beta/T \quad (12)$$

Table 1. Parameter σ, calculated for methane at given conditions. (The experimental data for the internal energy of methane are taken from Ref. [13])

σ/Å				U	ρ	T/K
Nasrifar-Jalali	Jan-Tsai	MSRK	R-K	(Jmol^{-1})	(moLlit^{-1})	
6.65	5.25	5.28	5.29	14830	12.00	580
6.25	4.96	4.96	4.96	14500	13.69	580
5.97	4.77	4.74	4.74	14240	15.09	580
6.42	5.10	5.10	5.09	13880	12.36	560
6.05	4.85	4.80	4.79	13560	14.05	560
5.79	4.86	4.60	4.59	13290	15.46	560
6.20	4.98	4.92	4.91	12960	12.74	540
5.85	4.76	4.65	4.63	12620	14.44	540
5.62	4.61	4.47	4.45	12360	15.85	540
5.97	4.87	4.75	4.72	12040	13.14	520
5.65	4.67	4.51	4.48	11700	14.85	520
5.43	4.54	4.36	4.32	11440	16.25	520
5.75	4.77	4.60	4.55	11140	13.58	500
5.45	4.60	4.39	4.34	10800	15.29	500
5.25	4.48	4.26	4.21	10530	16.63	500
5.10	4.39	4.16	3.12	10320	17.85	500
5.01	4.35	4.11	4.06	10140	18.35	500
4.90	4.26	4.03	3.99	9995	19.74	500
3.95	4.21	3.99	3.95	9872	205.2	500
5.13	4.70	4.36	4.24	7615	12.68	400
4.92	4.59	4.23	4.12	7305	14.09	400
4.64	4.43	4.08	3.99	6837	16.25	400
4.45	4.35	3.99	3.91	6497	17.37	400
4.37	4.24	3.92	3.85	6238	19.16	400
4.30	4.18	3.88	3.81	6032	20.24	400
4.24	4.13	3.84	3.78	5866	21.16	400
4.20	4.09	3.81	3.76	5730	21.97	400
4.17	4.05	3.79	3.74	5616	22.68	360
4.85	4.69	4.31	4.17	6349	12.42	360
4.61	4.56	4.17	4.05	5955	14.15	360
4.45	4.46	4.08	3.98	5617	15.52	360
4.26	4.32	3.97	3.89	5191	17.59	360
4.45	4.45	4.07	3.97	3806	13.17	300
4.34	4.60	3.20	4.08	4323	14.38	300
4.23	4.52	4.12	4.02	4039	15.38	300
4.03	4.35	3.99	3.90	3442	16.94	300
3.96	4.28	3.93	3.86	3165	18.14	300
3.86	4.18	3.86	3.80	2760	19.93	300
3.81	4.11	3.81	3.75	2472	21.27	300
3.77	4.05	3.77	3.72	2253	22.33	300
3.75	4.01	3.75	3.70	2081	23.22	300
3.91	4.29	3.95	3.89	2027	17.89	260
3.80	4.16	3.85	3.80	1485	20.19	260
3.67	4.10	3.80	3.76	1137	21.27	260
3.71	4.03	3.76	3.72	886.5	22.87	260
3.69	3.98	3.73	3.69	695	23.80	260
4.07	4.37	4.02	3.99	568.6	16.60	200
3.95	4.20	3.89	3.87	-147.4	19.59	200
3.89	4.12	3.83	3.81	-509	21.06	200

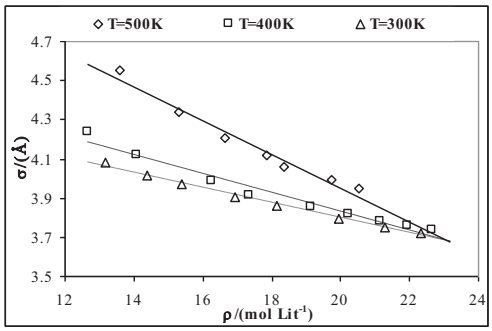

Fig. 1. Parameter σ in terms of density for RK equation of state at different temperatures.

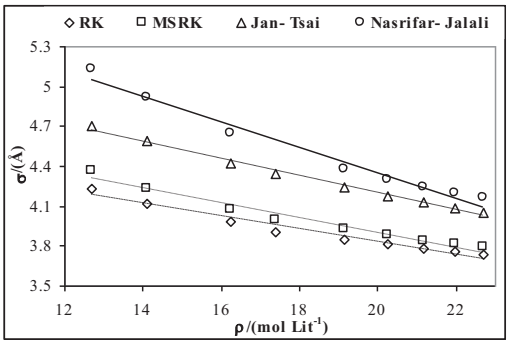

Fig. 2. Parameter σ vs density for different equations of state at constant temperature 400K.

This equation shows that ε/*k* is a function of temperature and density. Fitting of about 120 data points in eq. (12) with SIGMAPLOT software gave α, *b* and β with a negligible standard error. The parameters α, *b* and β and the relative standard errors for each equation of state are summarized in Table 2.

Eq. (12) indicated that:

$$\ln \varepsilon/k = a \ln(\rho/T) + b(\ln(\rho/T))^2 \qquad (13)$$

Therefore ε/*k* can be calculated for each temperature and density. The results of such calculations for each EoS are shown in Table 3.

Table 2. Fitting results for different equation of states

	RK		MSRK		Jan- Tsai	
	value	St. err.	value	St. err.	value	St. err.
α	-4.313	0.0893	-4.425	0.09446	-5.970	0.2401
b	-0.7875	0.02266	-0.8109	0.02396	-1.225	0.06089
β	246.8	20.87	225.8	22.06	74.05	56.07

Figure 3 shows the temperature dependency of ε/*k* for the RK EoS. This plot suggests that as the temperature increases, ε/*k* decreases. Such dependency can be observed for the other EoSs as well.

Figure 4 shows the density dependency of ε/*k* obtained from different EoSs at constant temperature *T* = 500 K. For all EoSs examined ε/*k* increases with density. As can be seen, the ε/*k* values, obtained with the RK and MSRK EoSs are close together. Similar trend is observed at other constant temperatures.

Table 3. Parameter ε/*k*, calculated for methane at given conditions

ε/*k* (K)			U ($Jmol^{-1}$)	ρ ($mol\ L^{-1}$)	T (K)
Jan-Tsai	MSRK	R-K			
136.82	15183	136.20	14830	12.00	580
231.74	18359	165.33	14500	13.69	580
329.06	21024	189.85	14240	15.09	580
178.52	17158	153.01	13880	12.36	560
282.27	204.85	183.47	13560	14.05	560
388.01	232.95	209.28	13290	15.46	560
224.84	192.95	171.58	12960	12.74	540
338.93	228.37	204.05	12620	14.44	540
450.55	256.55	229.81	12360	15.85	540
276.80	216.66	192.77	12040	13.14	520
399.06	252.83	225.86	11700	14.85	520
516.25	280.65	251.10	11440	16.25	520
333.04	241.65	215.58	11140	13.58	500
462.63	277.46	248.09	10800	15.29	500
582.36	304.26	272.18	10530	16.63	500
702.98	325.84	291.18	10320	17.85	500
765.27	338.53	302.87	10140	18.35	500
920.08	357.43	318.74	9995	19.74	500
1020.1	369.46	329.11	9872	20.52	500
392.71	267.20	239.30	10250	14.04	480
528.73	301.55	269.97	9911	15.74	480
683.57	329.98	294.46	9643	17.43	480
779.45	347.26	309.81	9428	18.27	480
303.00	244.38	219.55	9844	12.34	460
455.42	291.78	262.11	9381	14.54	460
598.93	324.35	290.52	9036	16.23	460
733.63	348.23	310.90	8769	17.60	460
859.35	366.64	326.38	8556	18.74	460

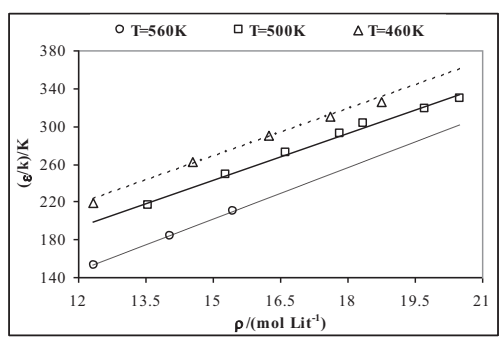

Fig. 3. Search for density dependency of the ε/*k* resulting from RK equation of state at different temperatures.

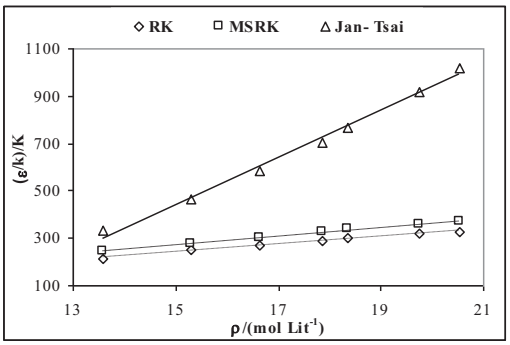

Fig. 4. Parameter ε/*k* in terms of density for various equations of state at constant temperature 500K.

3. CONCLUSION

Parsafar *et al*. [6] have shown that the parameters of the AEPP, σ and ε, are independent of density. Application of the CWA-VM theory (Chandler-Week-Andersen perturbation theory [14-17], analytically modified by the Verlet and Weis theory [18-19]) indicated that the obtained values of Lennard-Jones pair potential parameters are not constant and are dependent on temperature, so that when the temperature increases, σ increases and ε/*k* decreases [20].

As demonstrated above, σ and ε/*k* are dependent on temperature for all EoSs discussed.

Furthermore, the value of σ increases with temperature, while ε/*k* decreases. This is in agreement with previously reported results. When the parameter σ increases the repulsive branch of the potential shifts toward the longer separations. Therefore we may expect that as T increases, the potential well ε, decreases [6].

Potential parameters show density dependency: increasing density causes a decrease in σ values and an increase in ε/*k*. The reason behind this is the compression of the dense phase and the low free space between molecules. When density increases, molecules will pack closer together and σ decreases, which in its turn causes the shift in the repulsive branch of the potential toward shorter separations and the increase in ε/*k* values.

APPENDIX: The equations of state used

A1. *Redlich- Kwong equation of state [12]*

$$P = \frac{RT}{V-b} - \frac{a}{T^{0.5}V(V+b)}$$

$$a = \frac{0.42748 R^2 T_C^{2.5}}{P_C} \qquad b = \frac{0.08664 RT_C}{P_C}$$

A2*. Jan-Tsai equation of state [21]:*

$$P = \frac{RT}{V-b} - \frac{a}{V^2 + ubV + wb^2}$$

$$\alpha = [1 + m_1 \ln(T_r)]^2$$

$$\alpha' = \frac{2m_1}{T}[1 + m_1 \ln(T_r)]$$

$$m_1 = -0.3936 - 0.6353\omega + 0.1132\omega^2 + 0.07673/Z_C$$

$$a = a_C \alpha$$

$$a' = a_C \alpha'$$

$$a_C = \frac{\Omega_a R^2 T_C^2}{P_C}$$

$$b = \frac{\Omega_b R T_C}{P_C}$$

$$\Omega_b = \frac{1 - 3\xi_c}{u-1}$$

$$\Omega_a = 3\xi_c^2 + (u-w)\Omega_b^2 + u\Omega_b$$

$$\xi_c = 0.0889 + 0.750 Z_C$$

$$u = \frac{2.277}{Z_C} - 5.975$$

$$w = -u(\Omega_b + 1) - \xi_c^2 \frac{3 - \xi_c/\Omega_b}{\Omega_b}$$

A3*. MSRK (modified Soave Redlich- Kwong) equation of state [22]:*

$$P = \frac{RT}{V-b} - \frac{a}{V(V+b)}$$

$$a_c = 0.4286 \frac{R^2 T_C^2}{P_C}$$

$$b = 0.08664 \frac{RT_C}{P_C}$$

$$a = a_c \alpha(T_r)$$

$$\alpha(T_r) = [1 + C_1(1-\sqrt{T_r}) + C_2(1-\sqrt{T_r})^2 + C_3(1-\sqrt{T_r})^3]^2 \quad \text{for } T_r \le 1$$

$$\alpha(T_r) = [1 + C_1(1-\sqrt{T_r})]^2 \quad \text{for } T_r > 1$$

A4*. Nasrifar-Jalali equation of state [23]:*

$$Z = 1 + \frac{a_1\xi + a_2\xi^2}{(1-\xi)^2} - \frac{(Z_m - 2)\xi\Gamma}{1 + \xi\Gamma}$$

$$Z_m = \frac{1}{3}(4\sqrt{2}\pi)R^3 - 1$$

$$\xi = \frac{V_0}{V} \qquad V_0 = N_A \sigma^3 / \sqrt{2}$$

$$\Gamma = \exp(\varepsilon/kT) - 1$$

For methane: R=2,
$\sigma = 3.487 \times 10^{-10}$ *m*; $\varepsilon/k = 62.589$ K.

REFERENCES

1. N.J. Trappeniers, T. Wassenaar, J.C. Abels, *Physica* A, **98,** 289 (1979).
2. G.M. Van Waveren, J,P.J. Michels, N.J. Tappeniers, *Physica* B, **139/140,** 144 (1989).
3. H. Stassen, *Theochem,* **464,**107 (1999).
4. N. A. Walker, D.M. Lamb, S.T. Adamy, *Phys. Chem,.* **982,** 3679 (1989).
5. L.L. Lee, Molecular Thermodynamics of Nonideal Fluids, Butterworth Publishers, Stoneham, MA, 1988.
6. G. Parsafar, F. Kermanpour, B. Najafi, *Phys. Chem*. B, **103,** 7287 (1999).
7. A. Nasehzade, K. Azizi, ICCT-2000, Dalhousie University, Canada, 2000, 6-11 Aug.
8. R.A. Peiroti, *J. Phys. Chem*., **69,** 281 (1965).
9. D.V. Matyushov, B.M. Ladanyi, *J. Chem. Phys*., **107,** 5815 (1997).
10. T.M. Reed. K.E. Gubbins, Applied Statistical Mechanics, McGraw-Hill, New York, 1993.
11. G.D.Fisher, T.W. Leland Jr., *Ind. Eng. Chem. Fundam.,* **9,** 537 (1970).
12. M. Modell and R. Reid, Thermodynamics and its Applications, Prentice-Hal, Inc., New Jersy, 1983, p. 152.
13. B.A. Younglove, J.F. Ely, *J. Phys. Chem. Ref. Data*, **16,** 577 (1987).
14. D. Chandler, J.D. Weeks, *Phys. Rev. Lett*., **25,**149 (1970).
15. D. Chandler, J. Weeks, h.c. Andersen, *J. Chem. Phys.,* **54,** 5237 (1971).
16. H.C. Andersen, D. Chandler, J.D. Weeks, *Adv. Chem. Phys.,* **34,** 105 (1976).
17. D. Chandler, J.D. Weeks, H.C. Andersen, *Science,* **220,** 787 (1983).
18. L. Verlet, J.J. Weis, *Phys. Rev,*. **A5,** 939 (1972).
19. L. Verlet, J.J. Weis, *Mol. Phys*., **24,** 1013 (1972).
20. A. Nasehzadeh, M. Mohseni, K. Azizi, *Theochem*, **589/590,** 329 (2002).
21. D.S. Jan and F.N. Tsai, *Can. J. Chem. Eng*., **69,** 992 (1991).
22. P.M. Mathias, T.W. Copeman, *Fluid Phase Equilibria*, **42,** 63 (1988).
23. Kh. Nasrifar and F. Jalali, *Fluid Phase Equilibria*, **207,** 167 (2003).

СРАВНЕНИЕ МЕЖДУ ЧЕТИРИ УРАВНЕНИЯ НА СЪСТОЯНИЕТО ЗА ПРЕДСКАЗВАНЕ НА ЗАВИСИМОСТИТЕ НА ПАРАМЕТРИТЕ НА СРЕДНИТЕ ЕФЕКТИВНИ ПОТЕНЦИАЛИ НА МЕТАН ОТ ТЕМПЕРАТУРАТА И ПЛЪТНОСТТА

М. Сури
Университет “Паяме Нур”, Иран
Постъпила на 4 януари, 2011 г.; коригирана на 1 март, 2011 г.

(Резюме)

В тази работа са сравнени четири уравнения на състоянието (MSRK, RK, Jan-Tsai and Nasrifar-Jalali) при предсказване на осреднени ефективни потенциали (ε/k и σ) на метан при различни стойности на температура и плътност. Всички уравнения на състоянието, показват, че съществува зависимост между температура и потенциалите и между плътност ε/k и σ, както следва: с увеличаване на температурата σ се увеличава и ε намалява, докато при намаляване на плътността σ се увеличава, а ε намалява.

Bulgarian Chemical Communications, Volume 44, Number 1 (pp. 26 – 30) 2012

Detecting admixtures of vegetable oils in sunflower oil using physico-chemical methods

Kr. Nikolova*, M. Perifanova-Nemska, G. Uzunova

University of Food Technologies, Department of Physics 4002 Plovdiv, Bulgaria

Received January 4, 2011; Revised May 3, 2011

Systems of sunflower oil containing rapeseed oil or cotton oil were studied. Data on the color characteristics of the specified sample mixtures in CIE *La* b** and XYZ colorimetric systems were obtained. The metric brightness, purity of color and metric angle were determined. Regressive dependencies between the specified parameters and the concentration of rapeseed or cotton oil admixtures were found, which permit the quantitative determination of the admixture content. The qualitative detection of the latter is possible using transmission spectra in the visible region and infrared spectra.

Key words: vegetable oils, infrared spectroscopy, color characteristics, fatty acid composition

INTRODUCTION

In recent years the purity of sunflower oil has become of great importance. There are different methods for identifying admixtures in it. These methods include determining the iodine number, saponification number, density, fatty acid composition (FAC) and viscosimetric measurements [1].

Some authors have used data on the content of fatty acids, triglycerides, tocopherols, etc., for detecting vegetable oil admixtures in sunflower oil and olive oil [2, 3]. However, detecting admixtures by determining their physicochemical characteristics is a difficult process, as the fatty acids found in various oils are almost the same. Most of the analytical techniques for the detection of adulterants rely upon chromatographic methods such as gas and liquid chromatography (GC and HPLC) [4–6]. The latter methods are expensive and time-consuming. That calls for cheaper, faster and simpler methods for detecting admixtures of other vegetable oils in sunflower oil.

The objectives of this study are as follows:

to investigate the potential and efficiency of infrared spectroscopy for detecting vegetable oil admixtures in sunflower oil as a fast, non-destructive and cheap method;

to use the possibilities of colorimetric analysis in the quantitative identification and determination of the admixtures.

MATERIALS AND METHODS

In the experiments commercially available sunflower oil (Bulgaria), cottonseed oil (Turkey) and rapeseed oil (France), as well as mixtures of sunflower oil / cotton oil and sunflower oil / rapeseed oil with concentrations of the admixtures ranging between 10% and 50 % were investigated.

Fatty acid composition of the pure oils (sunflower, rapeseed and cottonseed) was determined by gas chromatography. The total fatty acid composition was determined by GC after transmethylation of the respective sample with 2N methanolic KOH at 50 ºC according to Christie [7]. Fatty acid methyl esters (FAME) were purified by silica gel TLC on 20×20 cm plates covered with 0.2 mm Silica gel 60 G layer (Merck, Darmstadt, Germany) with mobile phase n-hexane:acetone 100:8 (by volume). GC was performed on a HP 5890 (Hewlett Packard GmbH, Austria) gas chromatograph equipped with a 30 m × 0.25 mm (I.D.) capillary InnoWax column (cross-linked PEG, Hewlett Packard GmbH, Austria) and a FID. The column temperature was programmed from 165 ºC to 240 ºC at a rate of 4 ºC/min and held at each value for 10 min; injector and detector temperatures were 260 ºC. Nitrogen was the carrier gas at a flow rate of 0.8 cm^3/min; split was 100:1. Identification was performed by

* To whom all correspondence should be sent:
E-mail: kr.nikolova@abv.bg

© 2012 Bulgarian Academy of Sciences, Union of Chemists in Bulgaria

comparison of retention times with those of a standard mixture of fatty acids subjected to GC under identical experimental conditions [8].

The specified colorimetric system was selected because of its suitability for working with pigments, simple use and possibility of assessing the resulting colors obtained by mixing pigments. The samples were poured into 10 mm-wide cuvettes. The color parameters (index of lightness L^*, chroma C^* and hue h_{ab}) corresponding to the uniform color space CIELab [9], were determined on a Lovibond PFX 880 device using a standard light source at wavelengths from 420 nm to 710 nm selected by means of 16 narrow-band interference filters. These filters have translucency peaks at every 20 nm but the measuring system was programmed in such a way as to interpolate light at intervals of 5 nm. Lovibond PFX 880 was used for determining the β -carotene and chlorophyll content in the sunflower oil and its double mixtures with rapeseed oil and cotton oil. The device features a special program through which the β -carotene and chlorophyll contents in the product are determined from the readings obtained from the RYBN color scale, designed for determining the color characteristics of transparent products.

Parameters such as chroma (C^*) and hue (h_{ab}) are defined by formulas (1) and (2):

$$C^* = \left[(a^*)^2 + (b^*)^2\right]^{1/2}, \quad (1)$$

$$h_{ab} = \arctan\left(\frac{b^*}{a^*}\right) \quad (2)$$

The infrared spectra of sunflower oil and of its double mixtures with 50% content of rapeseed or cotton oil, respectively, were obtained. The spectra were collected using a Nicolet 6700 FTIR spectrometer with a spectral resolution of 2 cm^{-1} , accumulating 32 scans.

To record spectra, approx. 50 μL of the oil was dissolved in 5 % CCl_4. The cuvette used was 4 mm thick and 10 mm wide. The cuvette was carefully cleaned by twice scrubbing with hexane followed by acetone and was dried with a soft tissue before filling with the next sample. The transmission IR spectrum of all diluted standards and oil samples were recorded under the same parameters and background was subtracted from each one. These spectra were recorded as absorbance values at each data point. The spectral reconstruction was carried out in two steps:

-The spectrum of the diluent was subtracted from the spectrum of the diluted oil to eliminate the spectral contributions to measure the dilution factor (r).

-The resulting spectrum was then multiplied by $(1-r)^{-1}$ to correct for dilution as to reconstitute the oil spectrum.

For the sunflower oil and all sample systems, the transmission spectra within the interval from 400 nm to 750 nm were measured on the Lovibond PFX 880 device.

RESULTS AND DISCUSSION

The results for the fatty acid composition of the pure vegetable oils are given in Table 1.

Table 1. Fatty acid composition of sunflower, rapeseed and cottonseed oils

Fatty Acid, %	Sunflower oil	Cottonseed oil	Rapeseed oil
C14:0	-	0.7	-
C16:0	9.7	23.5	5.1
C16:1	0.3	0.6	0.3
C18:0	4.8	2.6	1.9
C18:1	28.2	20.6	66.3
C18:2	56.7	51.0	17.4
C18:3	-	0.3	7.1
C20:0	0.3	0.4	0.7
C20:1	-	-	1.2
C22:0	-	0.3	-

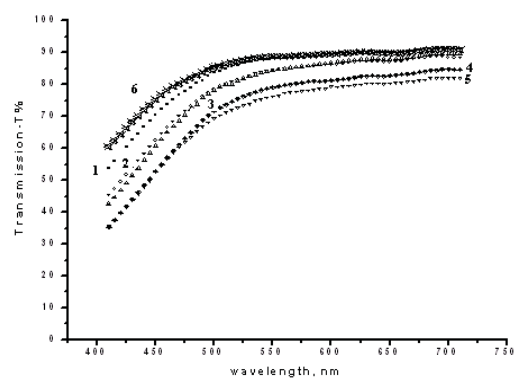

Fig. 1. Transmission spectra of sunflower oil and of its double mixtures with cotton oil. 1-10% cotton oil+90 % sunflower oil; 2–20% cotton oil+80 % sunflower oil; 3–30% cotton oil+70 % sunflower oil; 4-40% cotton oil+60 % sunflower oil; 5-50% cotton oil+50 % sunflower oil; 6- sunflower oil.

The transmission spectra of sunflower oil and of its double mixtures with cotton and rapeseed oil are presented in Figures 1 and 2. The addition of cotton oil to sunflower oil creates turbidity and lowers the product transmittance. The latter is a sign of the presence of an admixture in sunflower oil. It cannot,

however, serve to identify the admixture as cotton oil due to the lack of a characteristic absorption band. It is evident from the graph that the area under the spectrum decreases with the content of cotton oil in the mixture. The linear dependence *Area* = –84.78.C +25656 is found with a correlation coefficient R = 0.9.

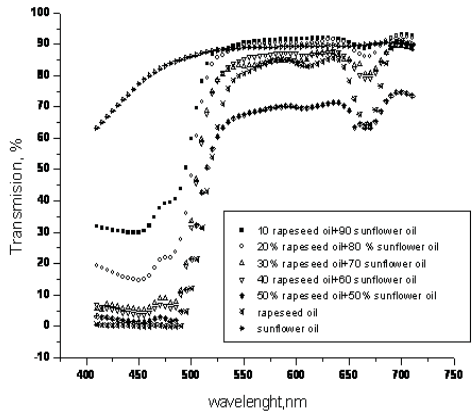

Fig. 2. Transmission spectra of sunflower oil and of its double mixtures with rapeseed oil

The presence of rapeseed oil admixture in sunflower oil, however, can easily be detected on the basis of the translucency spectrum in the visible range. Rapeseed oil has a marked absorption band in the interval from 630 nm to 680 nm, and there is no such band in the sunflower oil. The presence of rapeseed oil admixture up to 10 % results in the appearance of an absorption band typical of rapeseed oil. This fact can be used for the fast and easy detection of rapeseed oil in sunflower oil. In the case of low concentrations (C≤ 20%) of rapeseed oil, transmission abruptly drops in the spectral range from 400 nm to 500 nm. The presence of 10% rapeseed oil in sunflower oil leads to a two-fold decrease in transmission at λ = 420 nm. The characteristic absorption band in the 630 to 680 nm spectral range and the transmission between 15 % and 40 % in the 400 nm to 500 nm range present an opportunity for the identification of small concentrations (below 10%) of rapeseed oil.

The transmission coefficient T at λ = 690*nm* decreases with the concentration of cottonseed oil in model systems of sunflower and cottonseed oils. A regression dependence of the type *T = f (C)* with a correlation coefficient R = 0.88 was established as T = –0.14× C + 92.27. A dependence of the same type was valid for model systems of sunflower and rapeseed oils at λ = 670*nm* with *T=–0.28C+89=65* and a correlation coefficient *R*= 0.89, where C is the admixture concentration. The dependence of the transmission on the admixture concentration was determined at λ = 690*nm* nm which is the transmission minimum of rapeseed oil.

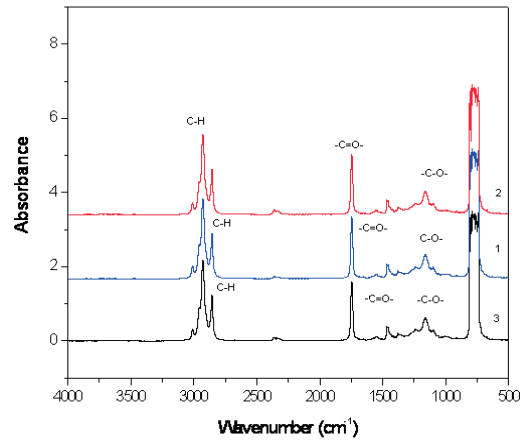

Fig.3. Infrared spectra of sunflower oil and of its mixtures with cotton and rapeseed oil 1-sunflower oil, 2–50% cottonseed oil+50% sunflower oil, 3–50% rapeseed oil+50% sunflower.

The biggest changes in the transmission for the admixtures of rapeseed oil in sunflower oil are in the 400 nm to 500 nm spectral range. For each of the two groups used as substitutes of sunflower oil, correlations between transmission T and concentration C were looked for at λ = 470*nm* nm, at which largest differences were registered. For admixtures of rapeseed oil in sunflower oil the exponential dependence T = 65.11 × $e^{-0.057}$ with R^2= 0.99 was found. For the same wavelength, the difference in transmission for cotton and sunflower oil is smaller and the dependence is linear, namely, T = –0.416C + 79.93 with *R*= 0.95.

The infrared spectra of sunflower oil and its double mixtures with rapeseed and cotton oil in a proportion of 1:1 in the interval from 500 cm^{-1} to 4000 cm^{-1} are presented in Figure 3.

Two peaks observed at 1747 cm^{-1} and 1160 cm^{-1} are due to the stretching vibrations of the aldehyde group (*C=O*) and ester group (*C–O*), respectively. In the region of the former peak, infrared energy is absorbed due to the carbon-oxygen bonds in the oil and it is often used for determining the level of oxidation.

There also are two peaks attributed to the bending vibrations in methylene (CH_2) groups and C-H stretching vibrations, which appear at 1465 cm^{-1} and 2929 cm^{-1}, respectively.

For the specified wavelengths 2929 cm^{-1} and 1747 cm^{-1}, the peak height increases upon addition of cotton oil, and decreases when the

same concentration of rapeseed oil is added. A similar decrease in the peak height is observed when corn and soybean oil are added as admixtures to olive oil [10].

The investigation carried out shows that infrared spectroscopy makes it possible to detect cotton oil and rapeseed oil admixtures in sunflower oil. In future studies, the obtained results will be used for identifying correlation dependencies between the peak height or peak area in the infrared spectrum and the concentration of the admixture in sunflower oil.

The β -carotene and chlorophyll content of sunflower oil and of its double mixtures with cotton oil and rapeseed oil was investigated. The obtained data are presented in Table 2.

Table 2. Data on the chlorophyll *a* and β-carotene content in sunflower oil and in its double mixtures with cotton oil and rapeseed oil.

Concentration of the admixture C %	Sunflower oil+ rapeseed oil			Sunflower oil + cotton oil		
	x	β - carotene ppm	Chlor ophyll *a* ppm	x	β - carotene ppm	Chlor ophyll *a* ppm
10	0.3803	15.36	0.162	0.3266	3.52	0
20	0.4145	25.54	0.286	0.3329	4.87	0
30	0.4323	34.10	0.397	0.3348	5.30	0
40	0.4487	43.73	0.504	0.3383	6.05	0
50	0.4579	53.25	0.597	0.3410	6.58	0
sunflower oil	0.3202	2.23	0	0.3202	2.23	0

Table 3 Color parameters of sunflower oil and its double mixtures with cotton oil or rapeseed oil.

Concentration of the admixture. C %	Sunflower oil + rapeseed oil						Sunflower oil + cotton oil					
	L	a	b	ΔE_{ab}	C	h_{ab}	L	a	b	ΔE_{ab}	C	h_{ab}
10	93.72	-11.07	48.41	41.30	49.66	-77.11	94.57	-3.93	12.08	3.05	12.70	-71.98
20	92.71	-13.62	72.36	65.35	73.63	-79.34	93.16	-4.68	15.98	7.21	16.65	-73.68
30	90.70	-13.63	86.33	79.26	87.40	-81.03	92.75	-4.96	17.16	8.48	17.86	-73.88
40	90.03	-13.40	100	92.81	100.89	-82.37	88.65	-5.05	18.76	11.61	19.43	-74.93
50	82.30	-11.09	102.06	95.40	102.66	-83.80	90.56	-5.25	20.55	12.37	21.21	-75.67
0	95.51	-3.06	7.93	-	8.50	-68.90	94.87	-3.19	9.14	-	9.68	-70.76

There is no chlorophyll in pure sunflower oil, and the β -carotene content is low, ranging from 2.23 ppm to 2.61 ppm. The presence of cotton oil admixture in sunflower oil results in an increase of the β -carotene content to 6.58 ppm, and the presence of rapeseed oil admixture - to 53.25 ppm. The presence of chlorophyll *a* in sunflower oil from 0.162 ppm to 0.597 ppm is a sign of the presence of rapeseed oil from 10% to 50%. When cotton oil is added, the chlorophyll *a* content in sunflower oil remains unchanged and cannot therefore be used as a parameter for detecting cotton oil admixtures in sunflower oil. Oil with 3 – 7 ppm of β -carotene contains cotton oil admixtures, and oil with above 10 ppm of β -carotene contains rapeseed oil admixtures. The dependence between the transmission coefficient at $\lambda = 670nm$ and the content of chlorophyll in the rapeseed oil-containing samples was obtained: $T = -4.46\ Chlorophyl + 94.23$ with a correlation coefficient R = 0.95.

For the different brands of sunflower oil, as well as for each of the investigated sample systems, data on the color coordinates a^* and b^* in the CIE La^*b^* colorimetric system were obtained; the color coordinate x in XYZ colorimetric system, as well as the metric lightness L^*, the metric chroma C^* and the metric angle of the hue of the color h_{ab} were calculated. The color differences ΔE_{ab} between sunflower oil and its double mixtures with rapeseed or cotton oil were calculated. The data are presented in Table 3. The translucency spectra were recorded using a 1 cm wide cuvette, without dilution.

The data presented in Table 3 clearly show that the addition of cotton oil or rapeseed oil admixtures leads to an increase in the values of the color coordinate $в^*$. This fact indicates that both admixtures lead to an enhancement of the yellow hue of the product. The higher values of the color coordinate x are connected with the higher β-carotene content.

The presence of admixtures in sunflower oil causes turbidity, and hence a decrease in the value of the metric lightness L^* of the product. The presence of cotton oil admixtures leads to a decrease in the specified value by 2 or 3 units, while the presence of rapeseed oil leads to a decrease in the L^*value up to 10 units. There is a correlation dependency between the metric lightness L^* and the concentration of the admixture when rapeseed oil is added to sunflower oil: $L^* = -0.1689\ ^*C + 95.75$ with a

correlation factor R= 0.96, but this dependency, when cotton oil admixture is added, has a relatively low correlation factor, and is, therefore, not mentioned in the discussion.

Table 4. Correlation dependency between the color parameters and the concentration of admixtures in the sample.

Sunflower oil + rapeseed oil		Sunflower oil+ cotton oil	
Linear dependences	R	Linear dependences	R
ΔE_{ab}=1.3564*C+34.131	0.93	ΔE_{ab} =0.2305*C+1.6282	0.95
h_{ab}= – 0.1639*C–75.815	0.99	h_{ab} = 0.0864*C–71.43	0.95
x = 0.0026*C+0.3439	0.93	x =0.0004*C+0.3232	0.80

The knowledge of the type of the admixture in sunflower oil and the color characteristics of the sample makes it possible to determine the concentration of the admixture. For this purpose, linear regression dependencies of the type $\Delta E_{ab} = f(C)$, $h_{ab} = f(C)$ and $x = f(C)$ were identified. The specified dependencies, together with their correlation factors, are presented in Table 4.

CONCLUSIONS

It is possible to detect admixtures of rapeseed oil in concentrations from 10 to 50 % to sunflower oil on the basis of the translucency spectrum in the visible range and the presence of an absorption band at 670 nm. An absorption band in the interval from 630 nm to 680 nm and a transmission coefficient between 15% and 40% in the 400 to 500 nm range of a sunflower oil sample is a solid indication of the presence of low concentrations (up to 20%) of rapeseed oil adulterant.

The adulteration of sunflower oil by cottonseed oil (up to 50%) leads to a decrease in the transmission coefficient T in the interval from 400 to 500 nm. There is no absorption band found in the visible spectrum.

In the infrared spectrum at a fixed λ, the peak height increases with the addition of cottonseed oil and decreases with the addition of up to 50% of rapeseed oil. Through the infrared spectrum it is possible to detect adulterants of rapeseed or cottonseed oils in quantities lower then 50%. Future studies are recommended to investigate the relationship between the characteristics of the IR spectra and the concentration of adulterant oils in the range from zero to 25%.

REFERENCES

1. G. Tous, in: *Analysis and characterization of oils, fats and fat products*, H. A. Boekenoogen (eds), Interscience, London, 1968, p.315.
2. R. Aparicio, M. T. Morales, Alonso, *J. Agricultural and Food Chemistry*, **45**, 1076 (1997).
3. M. Dennis, *Analyst*, **123**, 151R (1998).
4. R. Aparicio, R. Aparicio-Ruoz, *J Chromatogr A.*, **881**, 93 (2000).
5. M. Tsimidou, R. Macrae, *Food Chem.,* **25**, 251 (1987).
6. N. K. Andrikopoulos, I. G. Giannakis and V. Tzamtzis, *J. Cromatogr. Sci*., **39,** 137 (2001).
7. W. W. Christie, in*: Lipid Analysis*, The Oily Press, Bridgewater, England, 2003, p. 2345.
8. Animal and vegetable fat and oils. Determination of methyl esters of fatty acids - Gas chromatographic method. ISO 5508, 2000
9. Commission Internationale de l' Elairage. Recommendations on uniform color spaces, color difference equations, psychometric color terms. CIE publication no 15 (F. 1. 3. 1.) 1971, supplement 2, Bureau Central de la Commission Internationale de l' Elairage, Vienna, 1978
10. M. D. Guillen, N. Gabo, *J. Sci. Food and Agriculture,* **75**, 1, (1997).

ОТКРИВАНЕ НА ПРИМЕСИ ОТ РАСТИТЕЛНИ МАСЛА В СЛЪНЧОГЛЕДОВО МАСЛО ЧРЕЗ ОПТИЧНИ МЕТОДИ

Кр. Николова, М. Перифанова-Немска, Г. Узунова

Университет по хранителни технологии, Пловдив

Постъпила 4 януари, 2011 г.; преработена на 3 май, 2011 г.

(Резюме)

В настоящата работа са изследвани моделни системи от слънчогледово масло в смес с рапично или памучно. Получени са данни за цветовите характеристики на посочените моделни смеси в CIE *La*b** и XYZ колориметрични системи. Определени са метричната светлота, чистотата на цвета и метричният ъгъл. Показано е, че съществуват регресионни зависимости между посочените параметри и концентрацията на примеса от рапично или памучно масло. Чрез тях е възможно количественото определяне на примеса, а качественото му откриване е възможно чрез получаване на спектъра на пропускане във видимата част на спектъра и провеждане на инфрачервена спектроскопия.

Bulgarian Chemical Communications, Volume 44, Number 1 (pp. 31 – 40) 2012

Physical stability of detonation nanodiamonds in liquid lubricants

G. St. Cholakov*, V. B. Toteva, St. D. Janev, St. G. Staykov, K. G. Stanulov

Department of Organic Synthesis and Fuels, University of Chemical Technology and Metallurgy, 8 boul. "Kl. Ohridsky", Sofia 1756, Bulgaria

Received January 10, 2011; Revised April 24, 2011

The aggregation of detonation nanodiamonds hinders their wider implementation and requires application-oriented studies and selection of stabilizers, which do not interfere with the rest of the components in the product in which they are used.

The aim of this work was to study the effect of typical lubricant additives on the sedimentation stability of nanodiamond powders in non-polar media (liquid paraffin). The low temperature stability of lubricating oils with nanodiamonds was also evaluated experimentally.

The used powders (nanodiamonds, ND and nanodiamonds with 40 % soot, NDS 40) were with sizes typical for commercial industrial nanodiamonds. Experimental evidence is presented that they contain a significant amount of aggregates with larger than nano-sizes.

Conventional laboratory mechano-chemical disaggregation, in the presence of experimentally selected best additives, ensure that more than 50 % of the NDS stays in the upper-most layer of the paraffin concentrate after 90 days of storage, while mild homogenization recovers around 70 % of the powder.

The mechano-chemical disaggregation was not so effective for ND. Similar stability was achieved when it was combined with a technology in which the concentrate was prepared from water suspension, by evaporation of the water in the presence of the stabilizer and some paraffin.

The NDS and ND powders slightly influence the low temperature stability of automotive oils, but their effect should be checked.

Keywords: detonation nanodiamonds; mechano-chemical disintegration; oil suspensions; sedimentation stability; lubricating oils, low temperature stability.

1. INTRODUCTION

Detonation of carbon-containing explosives under conditions of negative oxygen balance produces nanodiamond crystals with dimensions below 100 nm (NCDs) and/or below 10 nm (ultrananocrystalline diamonds, UNCD) [1], together with soot and other impurities, that have to be removed. Different purification methods have been suggested, but the most widely used involve treatment with oxidative agents in water suspension [2–4]. Soot might be only partially removed for some applications [5].

Depending on their size and specific conditions of formation, detonation diamonds might exhibit unique physical (highly developed surface) and chemical (active surface functional groups) properties [6]. These properties allow for a wide range of potential applications [5-8]. However, there are serious problems, which have to be solved in order to put nanodiamond production on an industrial scale [9] and increase it significantly from the estimated 7 tons sold world-wide in 2008 [10].

The presence of active functional groups, obtained on the surface of both soot and nanodiamonds during their synthesis and/or purification, leads to formation in storage, of aggregates in which the original 4 – 5 nm sized nanoparticles, become chemically bonded [11]. There is evidence that aggregated particles with above micron dimensions are found in significant amounts in the water suspensions and dry powders offered on the market [8, 12].

Preserving the size and storage stability of the suspensions with disaggregated powders as a serious problem, especially in non-polar media, has been recognized fairly recently. It is complicated by the many interrelated factors, which influence its adequate solutions [13, 14]. The increase of the aggregates in storage compromises the inherent advantages of nanodiamond powders and seriously impairs their properties for different applications. Disaggregation methods and chemical

*To whom all correspondence should be sent.
E-mail: cholakov@uctm.edu

© 2012 Bulgarian Academy of Sciences, Union of Chemists in Bulgaria

modifications for preserving the size and storage stability of the disaggregated powders in suspension have been suggested [5-14]. Typically, most surface groups are transformed into a particular type (e.g., –OH or –COOH), which facilitates further chemical reactions – for instance, esterification[15]. More sophisticated modifications can produce hydrophopic, fluorinated, borated, etc. nanodiamonds [1, 3, 14–16].

However, the choice of a particular combination of methods should be application-oriented in terms of specific requirements for particle size and physical stability, possible interactions with other components in the final product, price-effect ratio, etc. Hereunder, we shall illustrate these specific requirements for the application of nanodiamonds in lubricants.

The interest in the lubricating properties of novel carbon materials stems from the present use of nanodiamonds for creating very efficient thin solid lubricating films on metal substrates, and to their potential "ball bearing effect" when introduced as suspensions in lubricants [5, 17–20]. The typical application in the former case is lubrication in vacuum (e.g., in space) and in the latter case more conventional and much less expensive products - lubricating oils, greases, etc. are targeted.

Numerous lubricating additives with nanodiamonds are being advertized on the market. Their positive effect on lubrication reported in different publications, can be characterized as significant [17–20] or very high [5, 21, 22], though at least in one paper [23] negative results for a nanodiamond additive in automotive oils are presented.

Nanodiamonds can be used in two types of conventional lubricating products: liquid (i.e., oils) and plastic (i.e., greases, pastes, etc.). Modern liquid lubricants are synergistic combinations of hydrocarbon and/or synthetic base oils, and additives which ensure adequate performance according to a preset specification. The chemical types of the used components depend on the particular application of the oils [24]. Moreover, different producers might employ chemically different additive compounds to achieve the lubricating, oxidation, rheological, etc. properties of their products [25].

Solid additives that can be solubilized in micelles of organic surfactants and form stable colloid solutions are incorporated into the respective lubricating oils in their production [26]. Micro- and nano-sized solid particles of metals, MoS_2, graphite, fluorine polymers, etc. [27] for liquid lubricants are offered as "Do It Yourself (DIY)" oil suspensions, which the consumer might add to commercial oils. Nanodiamonds fall in the same category and presently are commercialized as concentrated suspensions in oil [28, 29].

There is a need for systematic studies of engineering problems, concerning the whole field of application of nanodiamonds in non-polar media and pertaining not only to lubricants. These include specification of acceptable particle size and sedimentation stability, compatibility of stabilizers/modifications with other compounds in the same product (e. g, base oil and lubricant additives), influence of the powders not only on the targeted functional properties (e.g., lubrication), but also on other important properties of the final product (e. g., low temperature properties, oxidation stability), etc.

Previously, we developed a method for UV-VIS determination of the concentration of nanodiamond powders in non-polar media [28], and applied it for estimation of the sedimentation stability of suspensions of nanodiamonds with soot (NDS) and pure nanodiamonds (ND), stabilized with different surfactants [29].

The aim of this work is to study the effect of typical lubricant additives on the sedimentation stability of ND and NDS in non-polar media (liquid paraffin). The low temperature stability of lubricating oils with nano-diamonds is also evaluated.

2. EXPERIMENTAL

2.1. Nanodiamond powders and concentrated suspensions in liquid paraffin

We used two powder samples, produced in the Space Research Institute (SRI) of the Bulgarian Academy of Sciences– a blend of nanodiamond and soot, containing 40 % nanodiamond (denoted as NDS 40) and – pure nanodiamonds (denoted as ND). In SRI, after the detonation, soot from both powders had been removed by treatment with a boiled mixture of sulfuric acid and potassium bichromate, followed by moderate thermal oxidation with HNO_3 and washing with de-ionized water to pH 7. The water suspensions of the powders had been finally subjected to ultrasonic treatment.

The average particle size distribution of the used powders, obtained from SRI as water suspensions (Fig. 1), was determined by photometric sedimentation analysis with a Shimadzu Centrifugal Particle Size Analyzer, Type SA–CP–2.

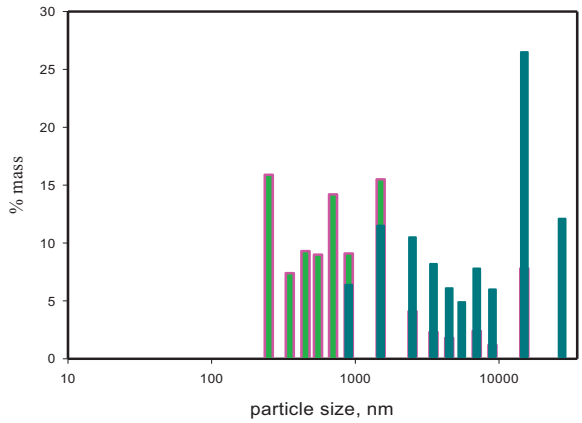

Fig. 1. Size distribution in the used nanodiamond samples: ■ - ND; ■ - NDS 40.

The NDS 40 sample has considerably larger aggregates than the ND sample, some of which are more than 10 microns in size. Both samples are comparable to the typical commercial industrial nanodiamonds, analyzed by Osawa [12], with dynamic light scattering. More information about the used powders can be found in publications by our colleagues from SRI [30–32].

Evidently, the aggregates in both samples used could be crushed and chemically modified by sophisticated techniques. However, for our studies on implementation of nanodiamonds in conventional automotive oils, it was important to start our work with the sizes, typical for commercial powders, available at a reasonable price.

The suspensions in liquid paraffin (kinematic viscosity at 40 ºC = 32.82 $mm^2 s^{-1}$; density at 20 ºC = 842.5 kg m^{-3}; its GC analysis is given in [28]), were prepared either from the dry powders, or from their water suspensions. When the model suspensions were prepared from dry powders, firstly a paste containing approx. 20 % powder was obtained by homogenizing weighed amounts of powder and liquid paraffin with a laboratory homogenizer with shearing blades for 10 sec at rotation speed of 10 000 rpm. For mechano-chemical disintegration, the respective stabilizer was included in the paste, which was then disintegrated in six subsequent 10 sec. runs for a total of one minute. The applied technology for the particular pastes is noted in the respective Tables. The concentration of the powder in all pastes was determined in parallel by the UV-VIS method, and gravimetrically, after centrifugation of the suspensions in hexane. In the latter case, the hexane was removed from the separated oil phase in a rotary vacuum evaporator, and from the powder – in a vacuum drying oven.

The powder suspensions in paraffin were prepared by weighing calculated amounts of the respective paste, stabilizer(s) and liquid paraffin in laboratory flasks, followed by mixing with a conventional laboratory stirrer for 30 min at 60 ºC, conventional laboratory ultrasonic treatment, and again mechanical stirring under the described conditions. The preparation of oil suspensions from water suspensions of the powders is described later in the text.

2.2. Stabilizers and lubricating oils

Nanodiamond powders might be stabilized with different surface-active substances [33]. However, it is an advantage if the stabilizers are compounds involved in the potential application of the powders. Therefore, in continuation of our previous studies [29], in the present work we have tested the combinations of the additives and packages, typical for gear and automotive oils, shown in Table 1. The influence of the powder suspensions on the pour point temperatures was studied in three typical petroleum oils. The first one was SAE 90 base oil (SAE is the US Society of Automotive Engineers), used as received by the manufacturer – the “Prista Oil” Company, Bulgaria. The second oil was prepared in our laboratory by dissolving a required amount of the auto gear oil package 1 in the base oil at concentration, recommended by the package producer for SAE 90 API GL 5 automotive gear oil(API is the American Petroleum Institute). The third oil was a commercial sample of SAE 15W/40 API SJ/CF engine oil, bought from a gasoline station. It is mineral oil based and widely used in gasoline and diesel engines on the road in many countries.

2.3. Methods of analysis

The method for the estimation of the concentration of NDS 40 and ND in oil concentrates with UV–VIS has been described in detail in [29]. The sedimentation stability [28] was studied by determination with UV–VIS of the concentration of the powder in the upper 0.5 cm layer of the paraffin concentrates, stored in closed laboratory test tubes. The tubes were kept at room temperature in the laboratory. Samples for the sedimentation stability studies were taken after 0, 20, 75 and 90 days of storage, thus characterizing, respectively, initial, short, medium and long-term stability in their potential application. Additionally, recovery of the stability of the concentrate after

long-term storage was tested after 1 min stabilization of the 75 or 90 days samples with a conventional laboratory tube-shaking machine. Thus, it is also application-oriented, though in DYI applications vigorous shaking of the pack, often containing a ball, is used.The FT–IR spectra of all liquid samples were recorded with a "FT–IR Equinox" spectrophotometer ("Bruker Corporation") in thin film, and those of the powders – in the standard thin tablets, prepared with KBr.

Table 1. Description of the lubricant additives and packages tested as stabilizers.

Stabilizers	Description by the supplier[a]
Gear oil package 1	Additive package for automotive gear oils, containing S, P, N
Gear oil package 2	Additive package for automotive gear oils, containing S, P, N
Motor oil DD package 1	Overbased Ca detergent + N-containing dispersant
Motor oil DD package 2	Detergent and dispersant (DD) additive package
Finished motor oil package 1	Motor oil additive package, containing S, P, N, B, Zn, Mg
Finished motor oil package 2	Motor oil additive package, containing S, P, N, Zn, Ca, Mg
Motor oil additive 1	Thermostable polyalkenyl succinimide dispersant
Motor oil additive 2	Overbased Ca alkylaryl sulphonate
Motor oil additive 3	Neutral Ca alkylaryl sulphonate

[a)] The single capital letters are the symbols of the respective chemical elements.

The amount of calcium in the additives and the oils was determined by inductively coupled plasma atomic emission spectrometry (ICP AES), following the ASTM D 4951 method on a "Varian Vista MPX", with a detector with CCD matrix. Sulphur was determined by the ASTM D 4951 method and checked with Wavelength-Dispersive X–Ray Fluorescence Spectroscopy (ASTM D 4927 method). The reason for determination of sulphur by two methods was that its concentration turned out to be somewhat higher than that given by additive manufacturers. Both methods confirmed the sulfur concentrations presented in the respective Table.

The pour point temperatures were determined according to the ASTM D 97 method.

3. RESULTS AND DISCUSSION

3.1. Stability in liquid paraffin of NDS 40 suspensions, stabilized with lubricant additive packages and additives

Our previous work with individual additives and additive packages [28] implied that succinimide dispersants and alkylarilsulphonate detergents are promising stabilizers for concentrated suspensions that can be used in lubricants. More importantly, it demonstrated that engine oil additive packages, which contain such additives, have also a stabilizing effect. The tested gear oil packages and additives could not stabilize the suspensions. Inorganic alkalinity, solubilized in the overbased sulphonates showed a negative effect as compared to the neutral sulphonates tested. For polymeric dispersants the presence of an imide group improved stability. Table 2 summarizes the most important results for suspensions, containing 3 % NDS 40. The stability at 15 min after preparation is given as an indication of the easiness of initial dispersion. The Table includes also a binary combination of the better stabilizers, which within experimental error [28], does not show synergistic action of additives 1 and 3.

In general, the amount of stabilized powder after short-term and medium-term storage in all samples is low, but the recovery after 75 days for some of them is satisfactory.

The above observations determined our further experiments, namely we studied systematically the short-term stability of gear oil package 1 with combinations of three engine oil additives. In engine oils these additives are expected to adsorb on soot and prevent its flocculation. It was important to establish if there might be antagonism between the gear oil package and the engine oil additive stabilizers, which might compromise their effect. The amount of NDS 40 was decreased, in order to estimate the effect of lower powder concentrations. Fig. 2 shows the obtained results

With the lower powder concentration the short-term stability is improved. For all samples the stabilizing effect decreases with decreasing the amount of the stabilizer. However, the polyalkenyl succinimide additive 1 shows some positive effect (i.e. higher stability than the proportional to its concentration), while the other two additives have a negative effect. Thus, this additive is more appropriate for stabilizing NDS 40 in gear oils. This is important because additives without metal are preferred in these oils.

3.2. Stability of NDS 40 paraffin suspensions, prepared with binary additives and mechano-chemical disintegration.

Our next experiments were targeted on improving medium and long-term stability. We tested systematically combinations of the two best

Table 2. Stability of paraffin suspensions of 3 % NDS 40[a].

No	Stabilizers[b]	Stability, % of initial			
		15 min	20 days	75 days	Recovery, 75 days
1	Auto gear oil package 1	47.54	0.0	-	-
2	Auto gear oil Package 2	44.53	3.1	-	-
3	Engine oil DD[b] package 1	99.02	54.0	11.9	37.2
4	Engine oil DD Package 2	95.49	42.8	20.5	61.8
5	Finished engine oil package 1	76.26	54.6	7.2	81.7
6	Finished engine oil package 2	90.59	56.7	12.9	74.0
7	Engine oil additive 1	89.92	17.6	9.1	65.1
8	Engine oil additive 2	85.62	37.0	11.1	34.1
9	Engine oil additive 3	97.22	61.5	19.2	84.0
10	0.50 Add. 1 + 0.50 Add. 3	93.94	36.9	24.3	54.4

a) From dry powder, without mechano-chemical disintegration.

b) "DD" stands for "Dispersant and Detergent" – i.e. packages of dispersant and detergent additives for engine oils that can be bought separately.

Table 3. Stability of 3 % NDS 40 suspensions from paste, with additives 1 and 3[a]

Sample	Stabilizers (mixtures in mass ratios)	Sedimentation stability, % of initial			
		20 days	75 days	90 days	Recovery, 90 days
25	Motor oil additive 1	71.46	58.51	57.07	72.98
26	0.75 Add. 1 + 0.25 Add. 3	77.57	62.33	60.94	75.43
27	0.50 Add. 1 + 0.50 Add. 3	59.50	45.61	40.72	60.87
28	0.25 Add. 1 + 0.75 Add. 3	66.01	-	51.72	67.73
29	Motor oil additive 3	62.59	63.34	59.80	67.32

a) From dry powder, with mechano-chemical disintegration.

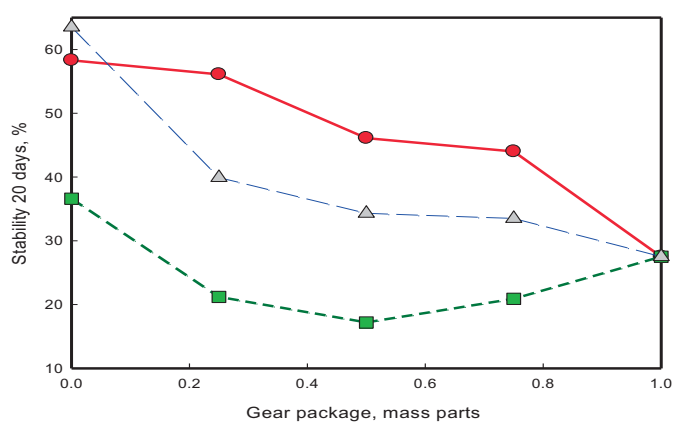

Fig. 2. Stability of paraffin suspensions of 2 % NDS 40 with mixtures of gear oil package 1 and engine oil additives: **(●)**-additive 1;**(■)**-additive 2; **(▲)**- additive 3.

stabilizers, including them in the pastes and increasing the disintegration time with the view to achieve mechano-chemical crushing of some aggregates. Table 3 presents the obtained results.

It shows that more than half of the powder stays suspended even after 90 days of storage. The recovered stability is somewhat lower than the best results achieved previously. The observed synergism for sample 26 and antagonism for sample 27 needs further studies, although the respective result in Table 1 provides some relevant evidence for the latter sample. However, we decided not to perform such studies at this stage because of the modeling approach of this work, done in paraffin. In a DIY product the used oil for the suspensions would be of higher viscosity and the recovery more effective, thus minimizing the practical importance of the observed effects.

Our next task was to study the effect of the applied mechano-chemical disintegration of NDS 40. For this purpose, the oils and the powders from the pastes with individual additives had been separated by centrifugation and the respective FT-IR spectra had been recorded. Fig. 3 shows the FT-IR spectra of additive 1, the oil (liquid paraffin) and the powder, obtained by centrifugation of the paste from which the suspension with additive 1 had been prepared.

The spectrum of additive 1 (Fig. 3, up) among the peaks of hydrocarbon groups, shows two peaks characteristic for succinimides: vibrations of –NH-groups (a wide peak at 3448.7 cm^{-1}) and vibrations of >C=O groups (a sharp peak at 1704.9 cm^{-1}). In the oil spectrum (Fig. 3, up) the first peak disappears, and the second one (at 1705.7 cm^{-1}) has a much lower intensity.

In the spectra of the crushed NDS 40 powder (Fig. 3, down) the –NH- peak is identified at 3442.5 cm^{-1}, and the peak of the >C=O groups is at 1697.5 cm^{-1}. These peaks are not present in the spectra of the liquid paraffin or the NDS 40 powder used to prepare the suspension (Fig. 3, down). Thus, the FT-IR spectra on Fig. 3 confirm the assumption that additive 1 has been adsorbed on the powder during the preparation of the paste.

Table 4. Active elements in Additive 3, its paste with NDS 40[a], and the oil from the paste after centrifugation.

Samples	Concentration, %	
	Sulphur	Calcium
Additive 3	5.16	2.78
Oil portion of paste	1.04	0.55
Oil, obtained from the paste by centrifugation	0.23	0.17
Calc. reduction in separated oil as compared to oil in paste, %	77.9	69.1

[a)] From dry powder, with mechano-chemical disintegration.

The adsorption of the alkylaryl sulphonate additive 3 is supported by FT-IR spectra (peak of S=O vibrations for the additive at 1212.4 cm^{-1}). However, the spectra are not presented here, because the adsorption of additive 3 is confirmed more profoundly by the data presented in Table 4. According to these data a significant portion of additive 3 is not present in the oil, obtained after centrifugation, and presumably has been adsorbed on the surface of the powder. The effect of the mechano-chemical dis-integration of NDS 40 in the presence additive 1 on the powder size distribution is presented in Fig. 5.

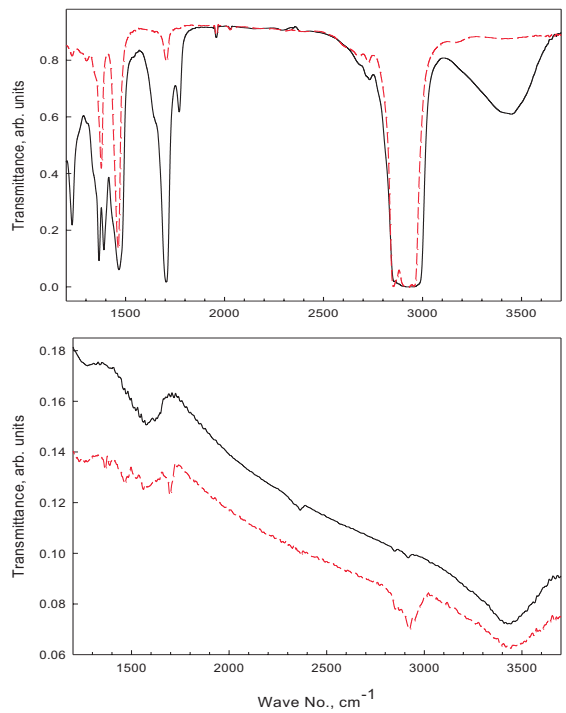

Fig. 3. FT-IR spectra indicating adsorption of the polyalkenyl succinimide additive 1 on the NDS 40 powder. Up: Straight line - Additive 1 (thin film); Dashed line - oil, separated from the paste, containing additive 1 (thin film). Down: Straight line - NDS 40 powder (tablet); Dashed line - NDS 40 powder, separated from the paste (tablet).

3.3. Sedimentation stability of liquid paraffin suspensions with pure nanodiamonds.

Table 5 presents the results for the sedimentation stability of the paraffin suspensions of pure nanodiamond powder (ND), prepared with additives 1 and 3.

The pastes for the first two samples were obtained from dry powders, without mechano-chemical stabilization. As expected, the results were not satisfactory. The next two samples were prepared with mechano-chemical disintegration, as those with NDS. A certain improvement was achieved, but the effect was lower than for the NDS samples. The last two samples were prepared from water suspensions of the ND powder, into which portions of paraffin and additive were added, and the water was evaporated. The rest of the paraffin and additive needed to prepare pastes with approx. 20 % powder were then added, and the pastes were mechano-chemically disintegrated. The developed

Table 5. Sedimentation stability of paraffin suspensions with nanodiamond powder (ND).

Sample	Technology	Sedimentation stability, %			
		20 days	75 days	90 days	Recovery
30	Dry powder, paste with Add. 1	23.80	-	16.00	30.00
31	Dry powder, paste with Add. 3	39.12	-	28.20	56.90
32[a]	Dry powder, paste with Add. 1	54.75	37.83	28.70	70.43
33[a]	Dry powder, paste with Add. 3	44.60	37.27	31.81	86.70
34[a]	Water suspension and paste, add. 1	68.20	44.60	46.50	79.10
35[a]	Water suspension and paste, add. 3	82.60	70.50	65.20	84.70

[a] With mechano-chemical disintegration.

Table 6. Active elements in Additive 3, its paste with ND[a], and the oil from the paste after centrifugation

Samples	Concentration, %	
	Sulphur	Calcium
Additive 3	5.16	2.78
Oil portion of paste	2.58	1.39
Oil, obtained from the paste by centrifugation	1.51	0.58
Calc. reduction in separated oil, as compared to oil in paste, %	58.53	41.73

[a] From water suspension, with mechano-chemical disintegration.

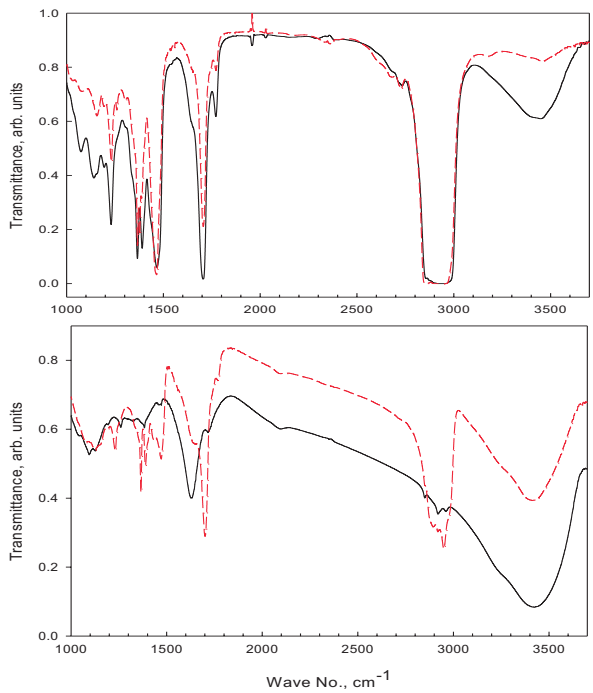

Fig. 4. FT-IR spectra indicating adsorption of polyalkenyl succinimide additive 1 on pure nanodiamond. Up: FT-IR spectra (thin films) of additive 1 - straight line and the oil, separated from the nanodiamond paste containing it - dashed line. Down: FT-IR spectra (tablets) of the used nanodiamond - straight line and the nanodiamond, separated from the paste containing additive 1 - dashed line.

preliminary treatment of the water suspensions brought up the stability of the ND suspensions to the levels achieved with the NDS powder.

Fig. 4 shows the FT-IR spectra of the polyalkenyl succinimide additive 1, the oil (liquid paraffin) and the powder, obtained by centrifugation of the paste from which the suspension with additive 1 had been prepared.

The two characteristic peaks of additive 1: vibrations of –NH- groups (a wide peak at 3448.7 cm^{-1}) and vibrations of >C=O groups (a sharp peak at 1704.9 cm^{-1}) are clearly seen on Fig. 4 (up). Their intensity in the oil centrifuged from the paste is lower, though not so profound as in Fig. 3. Fig. 4 (down) also shows the appearance of the characteristic additive peaks, though the wide peak at 3100 – 3600 cm^{-1} might include –OH, $-NH_2$ and >NH groups present on the original nanodiamond powder surface, as well. In general the spectra with nanodiamonds are more complex than with the NDS 40 blend. They suggest more complex interactions between the additive and the functional groups on the nanodiamond surface.

Table 6 presents the content of the active elements in the alkylaryl sulphonate additive 3, its nanodiamond paste, and the oil from the paste after centrifugation. Again a considerable amount of the additive is not present in the oil, centrifuged from the paste, and has remained on the nanodiamond powder surface.

Fig. 5 presents the effect of the mechano-chemical disintegration in the presence of additive 1 on the size distribution of both the NDS and ND powders. The analysis was performed on samples taken from the respective freshly prepared paraffin suspensions. The comparison with Fig. 1 clearly shows that the larger aggregates have been crushed, with effect similar to ball milling [33].

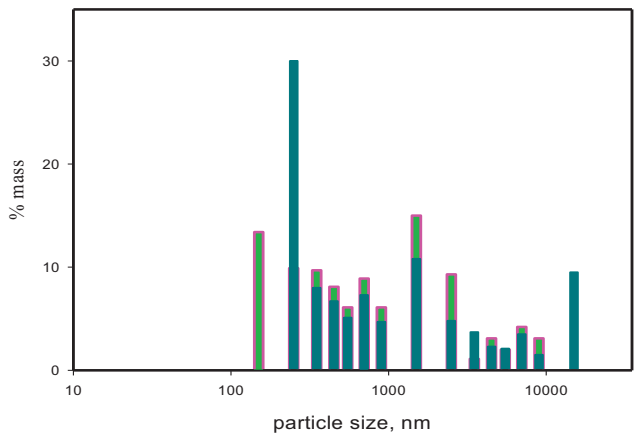

Fig. 5. Size distribution of the mechano-chemically disintegrated nanodiamond samples: - ND in the presence of additive 1; - NDS 40 in the presence of additive 1.

Table 7. Pour temperatures of lubricating oils with NDS 40 and ND.

Sample	Pour point, ^{o}C
Base gear oil (specification) +	(less than -18)
no additive	-19
5% liquid paraffin	-19
5 % concentrate of NDS 40 with Additive 1	-19
5 % concentrate of NDS 40 with Additive 3	-19
5 % concentrate of ND with Additive 1	-19
5 % concentrate of ND with Additive 3	-18
Automotive gear oil SAE 90 API GL 5 (specification) +	(less than -18)
no additive	-20
5% liquid parafin	-19
5 % concentrate of NDS 40 with Additive 1	-19
5 % concentrate of NDS 40 with Additive 3	-16
5 % concentrate of ND with Additive 1	-17
5 % concentrate of ND with Additive 3	-17
Motor oil 15W/40 API SJ/CD (specification) +	(less than -27)
no additive	less than -32
5% liquid parafin	less than -30
5 % concentrate of NDS 40 with Additive 1	less than -30
5 % concentrate of NDS 40 with Additive 3	less than -30
5 % concentrate of ND with Additive 1	less than -30
5 % concentrate of ND with Additive 3	less than -30

3.4. Low temperature stability of lubricating oils with NDS and ND

As shown in the introduction, the effect of nanodiamonds on lubricating properties has been widely studied. However, the requirement that they should not impair the rest of the important properties of the original lubricant – oxidation stability, low temperature and anticorrosion properties, demulsibility, etc. seems to be neglected. Chou and Lee [19] recently showed that addition of nanodiamond particles, depending on their size and the additives in the lubricant, might increase the viscosity of lubricating oils. Hereunder, we present results on the influence of nanodiamond concentrates on the low temperature stability of three oils, accessed by their pour point temperatures (Table 7). The pour point temperature is indicative of depletion at low temperatures of high molecular mass *n*-alkanes from the oil. Experimental data of the influence of the powders on this phenomenon is needed, because the particles might become centers for the crystallization of the alkanes.

The results in Table 7 show that, within the error of the analysis, the concentrates slightly influence the pour point temperatures of the oils. This is very important, especially for multi-grade fuel economy engine oils, which have to pass more sophisticated tests related to low temperature properties [24, 25]. In any case, our results show that the pour point temperature should always be tested when developing nanodiamond suspensions for different

oils, because particular combinations of powder stabilizers and lubricant additive packages might impair the low temperature properties of the doped oil.

CONCLUSIONS

The sedimentation stability of the studied nanodiamonds (ND) and their blends with soot (NDS) in paraffin was estimated after 20, 75 and 90 days of storage. Recoverability of the initial stability by mild homogenization was also tested. Typical additives for automotive gear and engine oils, their packages and binary combinations were evaluated as stabilizers. The obtained results show:

- Dispersant and detergent additives for engine oils and their packages are effective stabilizers. Succinimides and neutral sulphonates showed best results.
- The ND sample was more difficult to stabilize than its 40 % blend with soot (NDS 40), which can be explained with the fact that these additives are designed to disperse soot and coke particles.
- Mechano-chemical disaggregation with a laboratory homogenizer with razor blades was also evaluated. Both tested additives adsorbed on the surfaces of NDS 40 and ND, and some of the larger aggregates were crushed.
- With the selected stabilizers and mechano-chemical disaggregation more than 50 % of the NDS stayed in the upper layer of the paraffin concentrate after 90 days of storage, with recovery of around 70 % of the initial stability with mild homogenization. Higher stability is expected when more viscous hydrocarbon oils are used for the concentrates.
- The mechano-chemical disaggregation was not so effective for ND. Similar to the NDS results were achieved, when it was combined with evaporation of the water in the presence of the stabilizer and the paraffin.
- The NDS and ND powders slightly influence the low temperature stability of tested lubricating oils, but their effect should always be checked.

Acknowledgement: *The authors acknowledge with gratitude that the present work was supported by a grant from the Bulgarian National Science Fund under the provisions of Project No. NT 3-03/2004.*

REFERENCES.

1. B. I. Kharissov, O.V. Kharissova and L. Chávez-Guerrero. Synthesis Techniques, Properties, and Applications of Nanodiamonds, *Synth React Inorg M*, **40**, 2, 84 (2010).
2. V. Yu. Dolmatov, M. V. Veretennikova, V. A. Marchukov, and V. G. Sushchev. Currently Available Methods of Industrial Nanodiamond Synthesis. *Phys. Solid State,* **46**, 4, 611 (2004).
3. S. Osswald, G. Yushin, V. Mochalin, S. O. Kucheyev, and Yu. Gogotsi. Control of sp2/sp3 Carbon Ratio and Surface Chemistry of Nanodiamond Powders by Selective Oxidation in Air. *J. Am. Chem. Soc.* **128**, 11635 (2006).
4. P. A. Vityaz. The State of the Art and Prospects of Detonation-Synthesis Nanodiamond Applications in Belarus. *Phys. Solid State*, **46**, 4, 606 (2004).
5. V. E. Red'kin. Lubricants with Ultradisperse Diamond-Graphite Powder. *Chem. Technol. Fuels Oils*, **40**, 3, 164 (2004).
6. *Ultrananocrystalline Diamond Synthesis, Properties, and Applications*. Eds. O. A. Shenderova, D. M. Gruen, William Andrew Publishing, New York, U.S.A, 2006.
7. O. Auciello, A. V. Sumant. Status review of the science and technology of ultrananocrystalline diamond (UNCD™) films and application to multifunctional devices. *Diamond Relat. Mater.*, **19**, 699 (2010).
8. A. M. Schrand, S. A. Hens, A. C. Suzanne and O. A. Shenderova. Nanodiamond Particles: Properties and Perspectives for Bioapplications, *Crit. Rev. Solid State Mater. Sci*, **34**, 1, 18 (2009).
9. V. V. Danilenko. Nanodiamonds: Problems and Prospects. *J. Superhard Mat.*, **32**, 5, 301 (2010).
10. A. Vul. Detonation nanodiamonds. New Challenges and Applications. 2nd International forum on nanotechnologies, *Rusnanotech 09*, 6-8 october 2009, Moscow.
11. A. S. Barnard. Self-assembly in nanodiamond agglutinates. *J. Mater. Chem.*, **18**, 4038 (2008).
12. E. Osawa. Monodisperse single nanodiamond particulates. *Pure Appl. Chem.*, **80**, 7, 1365 (2008).
13. M. V. Korobov, M. M. Batuk, N. V. Avramenko, N. I. Ivanova, N. N. Rozhkova and E. Osawa. Aggregate structure of "single-nano buckydiamond" in gel and dried powder by differential scanning calorimetry and nitrogen adsorption. *Diamond Relat. Mater.*, **19**, 665 (2010).
14. V. N. Mochalin and Yu. Gogotsi. Wet Chemistry Route to Hydrophobic Blue Fluorescent Nanodiamond. *J. Am. Chem. Soc.*, **131**, 4594 (2009).
15. A. Krueger, Th. Boedeker. Deagglomeration and functionalisation of detonation nanodiamond with long alkyl chains. *Diamond Relat. Mater.*, **17**, 1367 (2008).
16. W.-W. Zheng, Yi-H. Hsieh, Yu-Ch. Chiu, S.-Jhu Cai, Ch.-L. Cheng and Ch. Chen. Organic functionalization of ultradispersed nanodiamond: synthesis and applications. *J. Mater. Chem.*, **19**, 8432 (2009).
17. M. Amaral, C.S. Abreu, A.J.S. Fernandes, F.J. Oliveira, J.R. Gomes, R.F. Silva. Nanodiamond-based tribosystems. *Surf Coat Tech*, **204**, 1962 (2010).

18. C.A. Charitidis. Nanomechanical and nanotribological properties of carbon-based thin films: A review. *Int J Refract Met H*, **28**, 51 (2010).
19. C.-C. Chou, S.-H. Lee, Tribological behavior of nanodiamond-dispersed lubricants on carbon steels and aluminum alloy, *Wear,* **269,** 11–12, 757 (2010).
20. D. X. Peng, Y. Kang, R. M. Hwang, S.S. Shyr, Y.P. Chang. Tribological properties of diamond and SiO_2 nanoparticles added in parafin. *Trib. Int.*, **42**, 911 (2009).
21. V. Yu. Dolmatov. Detonation Nanodiamonds in Oils and Lubricants. *J. Superhard Mat.*, **32**, 1, 14 (2010).
22. M. G. Ivanov, S. V. Pavlyshko, D. M. Ivanov, I. Petrov, O. Shenderova. Synergistic Compositions of Colloidal Nanodiamond as Lubricant Additive, *J. Vac. Sci. Technol*. **B** 28, 4, 869 (2010).
23. Y.Y. Wu, W.C. Tsui, T.C. Liu. Experimental analysis of tribological properties of lubricating oils with nanoparticle additives. *Wear*, **262**, 819 (2007).
24. *Lubricant additives: chemistry and applications*. Ed. L. Rudnick, 2nd ed., CRC Press, Taylor & Francis, Boca Raton – London - New York, 2009.
25. *Chemistry and Technology of Lubricants*. Eds. R. M. Mortier, M. F. Fox, S. T. Orszulik, 3rd ed., Springer, Dordrecht - Heidelberg - London - New York, 2010.
26. J. Galsworthy, St. Hammond and D. Hone. Oil-soluble colloidal additives. *Curr Opin Colloid In*, **5**, 274 (2000).
27. *Nanolubricants*. Eds. J. M. Martin, N. Ohmae, John Wiley & Sons, Ltd, 2008.
28. G. St. Cholakov, N. Georgiev, Chr. Ivanova, K. G. Stanulov. Stability of Ultradisperse Diamond Powders in Oil Suspensions. *Journ. Univ. Chem. Techn. Met.*, **40**, 4, 299 (2005).
29. G. St. Cholakov, N. Georgiev, Chr. Ivanova, K. G. Stanulov. An Express Method for Estimation of the Concentration of Ultradisperse Diamond Powder in Oil. *Journ. Univ. Chem. Techn. Met.* 40 (2005), 4, 291 - 298.
30. D. Mitev, R. Dimitrova, M. Spassova, Ch. Minchev, S. Stavrev. Surface peculiarities of detonation nanodiamonds in dependence of fabrication and purification methods. *Diamond Relat. Mater.*, **16**, 776 (2007).
31. T. Tsoncheva, V. Mavrodinova, L. Ivanova, M. Dimitrov, S. Stavrev, Ch. Minchev, *J. Mol. Catal. A: Chem.* **259**, 223 (2006).
32. V. Mavrodinova, M. Popova, I. Kolev, S. Stavrev, Ch. Minchev. Effect of the preparation conditions of Ni-supported shock-wave synthesized nanodiamond catalysts. FT-IR and catalytic considerations. *Appl. Surf. Sci.* **253**, 7115 (2007).
33. Y. Zhu, X. Xu, B. Wang, Zh. Feng. Surface modification and dispersion of nanodiamond in clean oil. *China Part*, **2**, 3, 132 (2004).

ФИЗИЧЕСКА СТАБИЛНОСТ НА ДЕТОНАЦИОННИ НАНОДИАМАНТИ В ТЕЧНИ СМАЗОЧНИ МАТЕРИАЛИ

Г. Ст. Чолаков*, В. Б. Тотева, Ст. Д. Янев, Ст. Г. Стайков, К. Г. Станулов

Катедра „Органичен синтез и горива", Химикотехнологичен и металургичен университет, бул. "Климент Охридски", София 1756, България

Постъпила на 10 януари, 2011 г.; коригирана на 21 април, 2011 г.

(Резюме)

Агрегирането на детонационните нанодиаманти спъва по-широкото им използване и изисква изследвания, ориентирани към конкретното приложение, и стабилизатори, които да не взаимодействат негативно с останалите компоненти на продукта.

Основната цел на работата беше да изследва ефекта на типични присадки за смазочни материали върху седиментационната стабилност на нанодиамантени прахове в неполярна среда (течен парафин). Оценена беше експериментално и нискотемпературната стабилност на смазочни масла с нанодиаманти.

Използваните прахове (нанодиаманти, ND и нанодиаманти с 40 % сажди, NDS 40) бяха с размери, типични за продаваните индустриални нанодиаманти. Представени са експериментални резултати, че те съдържат значително количество агрегати с по-големи от нано размери.

При използване на лабораторно механо-химическо дезинтегриране, в присъствие на експериментално подбраните най-добри присадки, над 50 % от NDS 40 остават в най-горния слой на парафиновия концентрат след 90-дневно съхранение, а около 70 % от праха се суспендират отново след умерено хомогенизиране.

Механо-химичното дезинтегриране не беше толкова ефективно при ND. Подобна стабилност беше постигната, когато то беше комбинирано с технология за приготвяне на концентрата чрез изпаряване на водата от водна суспензия в присъствие на стабилизатора и известно количество парафин.

Праховете NDS 40 и ND слабо влияят върху нискотемпературната стабилност на изпитаните смазочни масла, но техния ефект трябва винаги да се проверява.

Bulgarian Chemical Communications, Volume 44, Number 1 (pp. 41 – 51) 2012

Inhibitive action of malachite green-Zn^{2+} system

V.Johnsirani[1], S. Rajendran*[1,2], J. Sathiyabama[1], T.S. Muthumegala[1], A.Krishnaveni[3], N. Hajara Beevi[4]

1. PG and Research Department of Chemistry, GTN Arts College, Dindigul – 624005, Tamil Nadu, India.

2. RVS School of Engineering and Technology, Dindigul-624 005, Tamil Nadu, India.
3. Department of Chemistry, Yadava College, Madurai, India.
4. Department of Chemistry, B.S. Abdur Rahman University, Vandalur, Chennai-600048, India.

Received January 7, 2011; Revised March 29, 2011

The inhibition efficiency (IE) of malachite green- (MG) Zn^{2+} system in controlling corrosion of carbon steel in well water containing 665 pm of Cl^-(model corrosion medium) has been evaluated by weight loss method. Weight loss study reveals that the formulation consisting of 30 ppm of MG and 25 ppm of Zn^{2+} has 95% inhibition efficiency in controlling corrosion of carbon steel immersed in well water (model corrosion medium). Synergistic parameters suggest that a synergistic effect exists between MG and Zn^{2+}. Polarization study reveals that this system functions as cathodic type inhibitor controlling cathodic reaction predominantly. AC impedance spectra reveals that a protective film is formed on the metal surface. The FTIR spectra reveals that the protective film consists of Fe^{2+}-MG complex. This is further confirmed by UV-visible spectra and fluorescence spectra. The colour of the dye can be removed by electrolysis using platinised titanium as anode and graphite as cathode.

Keywords : Carbon steel, corrosion inhibition, malachite green, F-Test, synergism parameter

INTRODUCTION

Several compounds such as nitrates [1,2] phosphates [3,4] silicates [5] sodium salicylate [6] sodium cinnamate [7] molybdates [8,9] phosphonic acids [10,12] polyacrylamide [13] and caffeine [14,15] have been used as corrosion inhibitors. Talati and Gandhi have studied the effect of some dyes as corrosion inhibitors for B26S aluminium in hydrochloric acid [16,18]. The inhibition efficiency (IE) of triphenylmethane dyes such as Victoria blue, fast green, light green, malachite green, fuchsine base, fuchsine acid, crystal violet and methyl violet 6B in controlling corrosion of aluminium in phosphonic acid has been studied by Talati and Daraji using mass and polarization studies [19]. Several dyes such as Nile blue, indigo carmine organic dyes [20], crystal violet [21], congo red [22], methylene blue [23], basic yellow 13 [24], fluorescein [25], methyl orange [26], and eriochrome black-T [27] have been used as corrosion inhibitors. The present work is undertaken to investigate (i) the inhibition efficiency of malachite green in controlling corrosion of carbon steel immersed in well water (model corrosion medium) (Table 1) in the absence and presence of zinc ions; (ii) the influence of pH and immersion period on the inhibition efficiency and (iii) the protective film by UV-visible reflectance, FTIR and fluorescence spectra.

Table 1: Physico –chemical parameters of well water (model corrosion medium)

Parameter	Well Water
pH	8.38
Conductivity	3110 µmhos/cm
Total dissolved solids	2013 ppm
Chloride	665 ppm
Sulphate	14 ppm
Total hardness	1100 ppm

MATERIALS AND METHODS

Preparation of the specimens

Carbon steel specimens (0.026% S, 0.06% P, 0.4% Mn, 0.1% C and rest iron) of the dimensions 1.0 × 4.0 × 0.2 cm were polished to a mirror finish, degreased with trichloroethylene, and used for the weight-loss method and surface examination studies.

Mass-loss method

Determination of surface area of the specimens

The length, breadth and the thickness of carbon

* To whom all correspondence should be sent:
E-mail: E-mail: srmjoany@sify.com

© 2012 Bulgarian Academy of Sciences, Union of Chemists in Bulgaria

steel specimens and the radius of the holes were determined with the help of vernier calipers of high precision and the surface areas of the specimens were calculated.

Weighing the specimens before and after corrosion

All the weighing of the carbon steel specimens before and after corrosion were carried out using Shimadzu Balance-AY62.

Determination of corrosion rate

The weighed specimen in triplicate were suspended by means of glass hooks in 100 ml beakers containing 100 ml various test solutions and after 24 hours of immersion, the specimens were taken out, washed in running water, dried and weighed. From the change in weights of the specimen, corrosion rates were calculated using the following relationship.

$$\text{Corrosion rate} = \frac{\text{Loss in weight (mg)}}{\text{Surface area of the specimen (dm}^2) \times \text{period of immersion (days)}}$$

Corrosion inhibition efficiency (IE) was then calculated using the equation.

$$IE = 100\,[1-(W_2/W_1)]\ \%,$$

where W_1 is the corrosion rate in absence of inhibitor; W_2 is the corrosion rate in presence of inhibitor.

Surface examination study

The carbon steel specimens were immersed in various test solutions for a period of one day. After one day, the specimens were taken out and dried. The nature of the film formed on the surface of metal specimen was analyzed by surface analysis technique, namely, FTIR, UV-visible reflectance and fluorescence spectroscopy.

The UV-Visible Spectra

The UV-visible reflectance spectra were recorded using Hitachi U-3400 spectrophotometer. The same instrument was used for recording UV-visible absorption spectra of aqueous solutions also.

Luminescence spectra

The luminescence spectra of solution and the film formed on the metal surface were recorded using Hitachi 650–10 S fluorescence spectrophotometer equipped with 150 W Xenon lamp and a Hamamatsu R 928 F photomultiplier tube.

Potentiodynamic polarization study

Potentiodynamic polarization studies were carried out using CHI electro chemical impedance analyzer, model 660 A. A three electrode cell assembly was used. The working electrode was a rectangular specimen of carbon steel with one face of the electrode exposed and the rest shielded with red lacquer. A saturated calomel electrode (SCE) was used as a reference electrode and a rectangular platinum toil was used as the counter electrode.

The working electrode and platinum electrode were immersed in well water (model corrosion medium) in the absence and presence of inhibitor saturated calomel electrode was connected with the test solution through a salt bridge. Potential (E) vs log current (I) plots were then recorded. Corrosion potential (E_{corr}) and Tafel slopes b_a and b_c were determined from E vs log I plots.

AC impedance measurements

A CHI electrochemical impedance analyzer (Model 660A) was used for AC impedance measurements. A time interval of 5 to 10 minutes was given for the system to reach the stable open circuit potential. The real part (Z') and imaginary part (Z") of the cell impedance were measured in ohms for various frequencies. The R_t (charge transfer resistance) and C_{dl} (double layer capacitance) values were calculated. Equivalent circuit diagram is shown in Scheme 1.

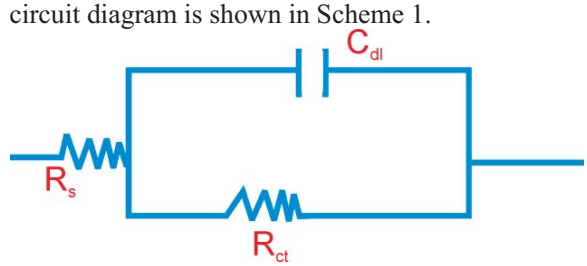

Scheme 1: Equivalent circuit diagram

Synergism parameters

Synergism parameters are indications of synergistic effect existing between two inhibitors.

Synergism parameters were calculated using the relation

$$S_I = \left| 1 - \theta_{1+2} / 1 - \theta'_{1+2} \right|$$

where $\theta_{1+2} = (\theta_1 + \theta_2) - (\theta_1 \times \theta_2)$;
- θ_1= surface coverage of substance 1;
- θ_2= surface coverage of substance 2;

-where θ'_{1+2} = combined surface coverage of substance 1 & 2.

Analysis of variance (F-Test)

F-test was carried out to investigate whether the synergistic effect between CAE and Zn^{2+} was statistically significant.

Analysis of the results of the mass loss method

The calculated inhibition efficiencies (IE) of malachite green in controlling the corrosion of carbon steel immersed in well water (model corrosion medium) both in the absence and presence of zinc ion have been tabulated in Table 2 and 3. The calculated values indicate the ability of malachite green to be a good corrosion inhibitor. The inhibition efficiency is found to be enhanced in the presence of zinc ion. The formulation consisting of 30 ppm of MG and 25 ppm of Zn^{2+} offers 95% inhibition efficiency.

Table 2: Corrosion rates (CR) of carbon steel in well water (model corrosion medium) in the absence and presence of inhibitors and the inhibition efficiencies obtained by mass loss method. Inhibitor system: Malachite green (MG) + Zn^{2+} .Period of immersion: 1 day

MG ppm	Zn^{2+} ppm	CR mdd	IE %
0	0	42.72	--
10	0	16.36	61
30	0	15.45	63
50	0	8.18	80
70	0	7.27	82
90	0	2.72	93

Table 3 : Corrosion rates (CR) of carbon steel in well water (model corrosion medium) in the absence and presence of inhibitors and the inhibition efficiencies obtained by mass loss method. Inhibitor system : Malachite green (MG) + Zn^{2+}. Period of immersion: 1 day

MG ppm	Zn^{2+} ppm	CR mdd	IE %
0	25	18.18	17
10	25	4.54	75
30	25	2.14	95
50	25	2.72	85
70	25	2.72	85
90	25	0.90	80

Influence of immersion period on the corrosion inhibition of carbon steel in well water (model corrosion medium) by MG + Zn^{2+} system

The corrosion rates of carbon steel in the presence of the inhibitor system in well water (model corrosion medium) for different durations of immersion are tabulated in Table 3.

The IE of 30 ppm MG–25 pm Zn^{2+} system is found to decrease as the immersion period

Table 4: Corrosion rates (CR) of carbon steel in well water (model corrosion medium) in the absence and presence of inhibitors and the inhibition efficiencies obtained by mass loss method. Inhibitor system: Malachite green (MG) + Zn^{2+}. Period of immersion: 1 day

MG ppm	Zn^{2+} ppm	CR mdd	IE %
0	50	9.09	23
10	50	5.45	40
30	50	4.54	50
50	50	3.63	60
70	50	2.72	70
90	50	0.90	90

increases. This indicates that the protective film formed on the metal surface is unable to withstand the continuous attack of corrosive ions such as Cl^- ion (665 ppm) present in well water (model corrosion medium). There is a competition between the formation of $FeCl_2$ (and also $FeCl_3$) and Fe^{2+}–MG complex on the anodic sites of the metal surface. Analysis of results suggests that the formation of $FeCl_2$ is more favoured than the formation of Fe^{2+}-MG complex. Similar observation has been made by Selvaraj et al., [28], while studying corrosion behaviour of carbon steel in presence of polyvinyl pyrrolidone.

Table 5 : Influence of immersion period on the inhibition efficiency of the MG (30 pm) - Zn^{2+} (25 pm) Corrosion rates of carbon steel in well water (model corrosion medium) in the presence and absence of the inhibitor system and the inhibition efficiencies obtained by the mass loss method
Inhibitor system : MG (30 ppm) + Zn^{2+} (25 ppm).

MG ppm	Zn^{2+} ppm	Immersion period days	Corrosion Rate mdd	Inhibition efficiency %
0	0	1	42.72	--
30	25	1	0.90	95
0	0	3	47.31	--
30	25	3	4.73	90
0	0	5	49.25	--
30	25	5	5.42	89
0	0	7	54.01	--
30	25	7	9.18	83

Influence of pH on inhibition efficiency of malachite green Zn^{2+} system

Corrosion rates of carbon steel in well water (model corrosion medium) in the presence of the inhibitor system at different pH values and the IE are tabulated in Table 6.

At pH 8, the IE of MG Zn^{2+} system is 90%. When the pH is lowered to 6 (by the addition of

dil.H_2SO_4), the IE decreases to 88 due to the attack of H^+ ion present in the acid, on protective film formed on the metal surface. When the pH decreased from 8 to 7 (by addition of diluted H_2SO_4). The IE decreases from 90 to 83. This is due to the fact that the protective film formed on the metal surface is broken by the attack of H^+ ion [29]. The IE at pH 6 is found to be greater than that at pH 7. This is explained as follows: The inhibitor contains amino groups. When acid is added (pH = 6), protonation of amines takes place. Nitrogen atom attains positive charge. This positive charge and the (Fe^{2+}) positive charge on the metal are coordinated through the chloride ions (665 ppm) which are also present on the metal surface. Thus, when acid is added (pH=6), inhibition efficiency increases.

Table 6: Influence of pH on the inhibition efficiency of MG (30 ppm) - Zn^{2+} (25 pm). Corrosion rates of carbon steel in well water (model corrosion medium) at different pH and the inhibition efficiencies obtained by the mass loss method. Inhibitor system : MG (30 pm) – Zn^{2+} 25 ppm. Immersion period: 1 day.

MG ppm	Zn^{2+} ppm	pH	Corrosion Rate mdd	IE %
0	0	7	30.27	--
30	25	7	5.15	83
0	0	8	42.72	--
30	25	8	1.82	90
0	0	6	32.78	--
30	25	6	3.93	88

Influence of CTAB, SDS on the IE of MG + Zn^{2+} system

Influence of CTAB

The corrosion rates of carbon steel in well water (model corrosion medium) containing Zn^{2+} – MG inhibitor formulation for various concentrations of N-Cetyl–N,N,N-trimethyl ammonium bromide (CTAB) are tabulated in Table 7.

Table 7: Influence of CTAB on the IE of MG + Zn^{2+} system. Corrosion rates of carbon steel in well water (model corrosion medium) in the presence and absence of the inhibitor system and the inhibition efficiencies obtained by mass loss method
Inhibitor system : MG + Zn^{2+} + CTAB

MG ppm	Zn^{2+} ppm	CTAB ppm	CR mdd	IE %
30	25	0	2.14	95
30	25	5	6.36	73
30	25	10	0.15	34
30	25	15	9.09	61
30	25	20	9.09	61
30	25	25	4.54	80

It is seen that as the concentration of CTAB (a cationic surfactant) increases, the IE increases and then decreases and again increases. The decrease in IE at a given concentration of CTAB is due to the fact, that at this concentration of CTAB, monomers are formed. Hence more number of CTAB molecules are adsorbed on metal surface. Hence IE increases, at higher concentrations of CTAB [30]. Similar observations have been made by. CTAB is a biocide [31]. It can control the corrosion caused by bacteria. The present study reveals that the formulation consisting of MG, Zn^{2+} and CTAB has excellent corrosion inhibitor efficiency. This formulation may find application in cooling water systems, provided the experiments are carried out at high temperature and under dynamic condition.

Influence of SDS on the IE of MG + Zn^{2+} system

The corrosion rates of carbon steel in well water (model corrosion medium) containing Zn^{2+} + MG

Table 8: Influence of SDS on the IE of MG + Zn^{2+} system. Corrosion rates of carbon steel in well water (model corrosion medium) in presence and absence of the inhibitor system and the inhibition efficiencies obtained by the mass loss method. Inhibitor system : MG + Zn^{2+} + SDS

MG ppm	Zn^{2+} ppm	SDS	CR mdd	IE %
30	25	0	2.14	95
30	25	5	12.73	53
30	25	10	9.09	66
30	25	15	8.18	70
30	25	20	5.45	80
30	25	25	4.54	83

inhibitor formulation for various concentrations of sodium dodecyl sulphate (SDS) are tabulated in Table 8.

When various concentrations of an anionic surfactant, SDS, were added to the inhibitor system, the inhibition efficiency decreased and reached a minimum and then increased. A micelle would have been formed at the minimum efficiency concentration. Afterwards the micelles would have been converted into monomer, which improved the inhibition efficiency. When more amount of SDS is added, SDS exists as monomer. These monomers are easily adsorbed on the metal surface. A protective film is formed. This prevents corrosion of metal SDS is a biocide [32]. This formulation may find application in cooling water systems, provided the experiments are carried out at high temperature and dynamic condition.

Synergism parameters

Synergism parameters have been calculated to evaluate the synergistic effect existing between two inhibitors [33–37]. There is synergistic effect when

the value of the synergism parameter is greater than 1.

The synergism parameters are given in Table 9. It is observed that the value of synergism parameter is greater than 1. This suggests that a synergistic effect exists between MG and Zn^{2+}. It is also interesting to note that the values of S_I are slightly smaller in the case of 50 ppm of Zn^{2+}, when compared with 25 ppm of Zn^{2+} (Fig.1). This is in agreement with inhibition efficiencies obtained by weight loss method. Thus the values of synergism parameter give a quantitative picture of synergism existing between two inhibitors.

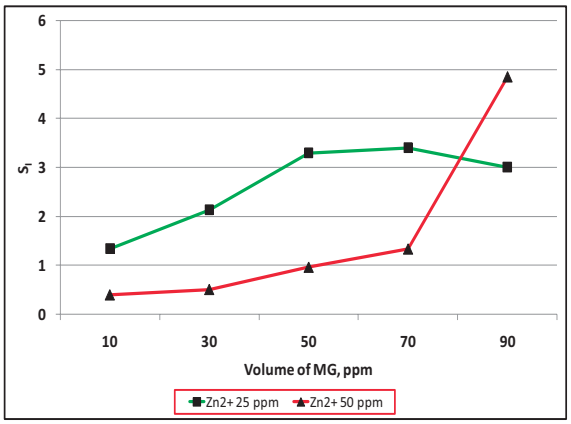

Fig. 1. Synergism parameters as a function of concentration of MG.

Table 9: Synergism parameters derived from inhibition efficiencies (surface coverage, θ)of MG-Zn^{2+} system

MG ppm	Zn^{2+}		S_I
	0 ppm	25 ppm	
0	--	17	--
10	61	75	1.345
30	63	95	2.142
50	80	85	3.293
70	82	85	3.404
90	93	80	3.01

Table 10 : Synergism parameters derived from inhibitor efficiencies (surface coverage, θ)of MG-Zn^{2+}

MG ppm	Zn^{2+}		S_I
	0 ppm	50 ppm	
0	-	23	-
10	61	40	0.399
30	63	50	0.510
50	80	60	0.965
70	82	70	1.338
90	93	90	4.861

Analysis of variance (ANOVA)

F-test was carried out to find out whether the influence of Zn^{2+} on the inhibition efficiencies of MG is statistically significant [38-40]. The results are given in Tables 11 and 12.

In Table 11, the influence of 25 ppm of Zn^{2+} on the inhibition efficiencies of 7, 10, 30, 50, 70 and 90 pm MG is investigated. The obtained F-value 0.1071 is statistically insignificant, since it is less than the critical F-value 5.32, for 1,8 degrees of freedom at 0.1071 level of significance. Therefore, it is calculated that the influence of 25 ppm of Zn^{2+} on the inhibition efficiencies of various concentration of MG is not statistically significant.

In Table 12, the influence of 50 ppm of Zn^{2+} on the inhibition efficiencies of 10 ppm, 30 ppm, 50 pm, 70 ppm, 90 ppm of MG is investigated. The obtained F-value 0.4052 is statistically insignificant

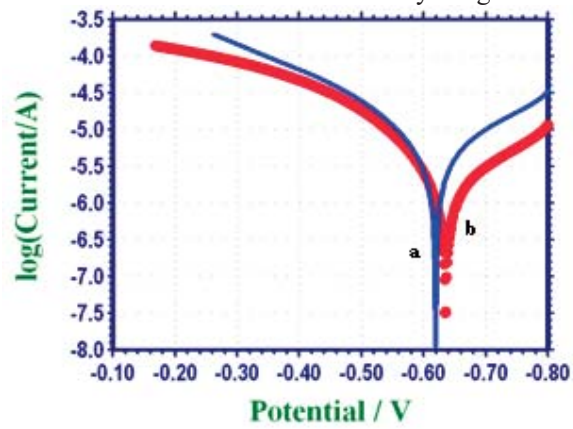

Fig. 2. Polarization curves of carbon steel immersed in various test solutions. (a) -Well water (model corrosion medium).(b) -Well water (model corrosion medium) + MG 30 ppm + Zn^{2+} 25 ppm.

since it is less than the critical F-value 5.32, for 1,8 degrees of freedom at 0.4052 level of significance. Therefore, it is concluded that the influence of 50 ppm of Zn^{2+} on the inhibition efficiencies of various concentrations of MG is not statistically significant.

Table 11: Distribution of F-value between the inhibition efficiencies of various concentrations of MG (0 ppm of Zn^{2+}) the inhibition efficiencies of MG is the presence of 25 ppm of Zn^{2+}

Source of variance	Sum of squares	Degree of freedom	Mean square	F	Level of significance of F
Between	168.1	1	168.1	0.1071	p<0.05
Within	12547.232	8	1568.404		

Table 12: Distribution of F-value between the inhibition efficiencies of various concentrations of MG (0 ppm of Zn^{2+}) and the inhibition efficiencies of MG is the presence of 50 ppm of Zn^{2}

Source of variance	Sum of squares	Degree of freedom	Mean square	F	Level of significance of F
Between	476.1	1	476.1	0.4052	p < 0.05
Within	9398.84	8	1174.85		

Analysis of polarization curves

Polarization study has been used to detect the formation of protective film on the metal surface [41–45]. When a protective film is formed on the metal surface, the linear polarization resistance (LPR) increases and the corrosion current (I_{corr}) decreases. The potentiodynamic polarization curves of carbon steel immersed in various test solutions are shown in Fig.2. The corrosion parameters namely, corrosion potential (E_{corr}), Tafel slopes (b_c=cathodic; b_a=anodic), linear polarization

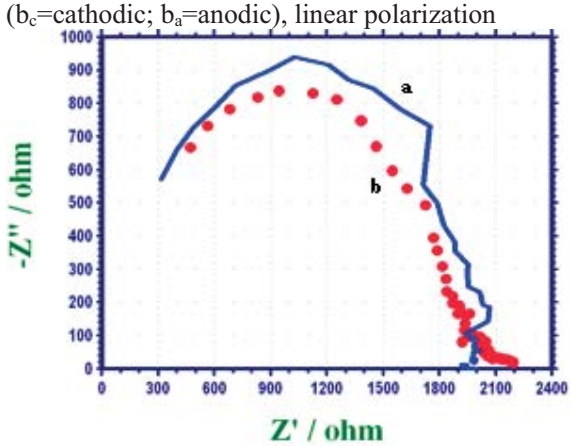

Fig. 3 : AC impedance spectra of carbon steel immersed in various test solutions (Nyquist plots). (a) - Well water (model corrosion medium); (b)- Well water (model corrosion medium) + MG 30 ppm +Zn^{2+} 25 ppm

resistance (LPR) and corrosion current (I_{corr}) are given in Table 13. When carbon steel is immersed in an aqueous solution containing well water (model corrosion medium) (665 ppm), the corrosion potential is –619 mV vs SCE. The formulation consisting of 30 ppm of malachite green solution (MG) and 25 ppm of Zn^{2+} shifts the corrosion potential to –635 mV vs SCE. This suggests that the cathodic reaction is controlled predominantly. The LPR value increases from 7.454×10^3 to 16.71×10^3 ohm cm^2. This suggests that a protective film is formed on the metal surface. Further the corrosion current decreases from 4.858×10^{-6} A/cm^2 to 2.029×10^{-6} A/cm^2. The IE calculated from corrosion current is 58%. This value is lower than the IE obtained by weight loss method (95%). The discrepancy may be explained by the fact that in electrochemical processes, the instantaneous corrosion current is measured.

Analysis of AC impedance spectra

AC impedance spectra have been studied to detect the formation of film on the metal surface. If a protective film is formed, the charge transfer resistance increases and double layer capacitance value decrease [46–50]. The AC impedance spectra of carbon steel immersed in various solutions are shown in Figs.3 and 4. The AC impedance parameter, namely charge transfer resistance (R_t) and double layer capacitance (C_{dl}) (derived from Nyquist plot) are given in Table 14.

Table 13. Potentiodynamic polarization curves of carbon steel immersed in various test solution

System	E_{corr} mV vs SCE	b_c mV/ decade	b_a mV/decade	LPR ohm cm^2	I_{corr} A/cm^2
Well water (model corrosion medium)	–619	193	147	7.454×10^3	4.858×10^{-6}
Well water (model corrosion medium) + MG 30 ppm + Zn^{2+} 25 ppm	–635	192	132	16.71×10^3	2.029×10^{-6}

However, in the case of the weight loss method, IE is calculated after a long time. The protective film formed is strengthened as the duration of immersion increases.

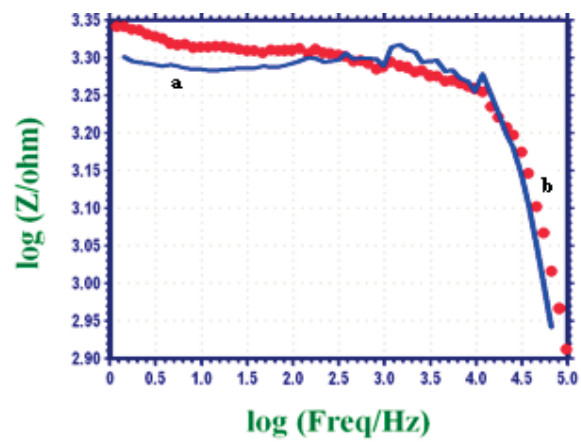

Fig. 4a. AC impedance spectra of carbon steel immersed in various test solutions (impedance – Bode plots). (a) - Well water (model corrosion medium); (b) - Well water (model corrosion medium) + MG 30 ppm + Zn^{2+} 25 ppm.

When carbon steel is immersed in aqueous solution containing well water (model corrosion medium). The R_t value is 1710 ohm cm^2 and C_{dl} value is 2.98×10^{-9} F/cm^2.

When MG and Zn^{2+} are added, the R_t value increases from 1710 ohm cm^2 to 1748 ohm cm^2 and C_{dl} value decrease from 2.98×10^9 F/cm^2 to 2.92×10^{-9} F/cm^2. This suggests that a protective film is formed on the surface of the metal. This accounts for the very high IE of MG Zn^{2+} system. Further there is increase in impedance, log (z/Ohm), value

from 3.909 to 3.343 (derived from Bode plot shown in Fig.4).

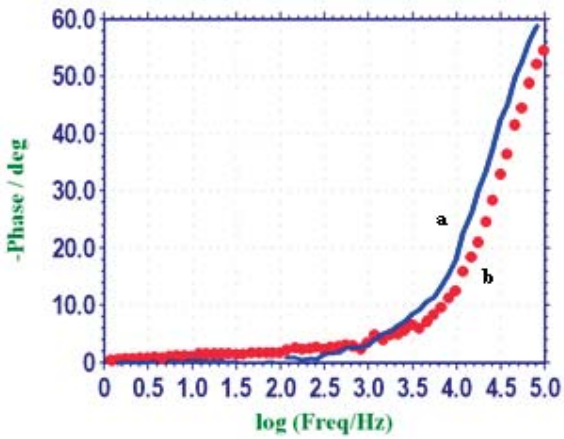

Fig. 4b. AC impedance spectra of carbon steel immersed in various test solutions (-phase – Bode plots).(a)-Well water (model corrosion medium (b) -Well water (model corrosion medium) + MG 30 ppm + Zn^{2+} 25 ppm.

In electrochemical studies, instantaneous corrosion rate is measured. But in weight loss method corrosion rate is measured after a longer period in the present study after one day. After a longer period the protective film becomes more compact and stable. This accounts for the discrepancy in IE, obtained from AC impedance spectra and from weight loss method.

Table 14: AC impedance parameters of carbon steel immersed in various test solution.

System	R_t ohm cm^2	C_{dl} F/cm^2	Impedance Value log(z/ohm)
Well water (model corrosion medium)	1710	2.98×10^{-9}	3.309
MG (30 ppm) + Zn^{2+} 25 ppm	1748	2.92×10^{-9}	3.343

Analysis of UV visible spectra

The UV-visible absorption spectrum of an aqueous solution of MG and Fe^{2+} (freshly prepared $FeSO_4$ solution) is shown in Fig. 5. Peaks appear at 202, 313, 423 and 615 nm. This is due to the Fe^{2+}-MG complex formed in solution [51,52].

The UV-visible reflectance spectrum of the film formed on the metal surface after immersion in the solution containing well water (model corrosion medium), 30 ppm of MG and 25 ppm of Zn^{2+} is shown in Fig. 6. Peaks appear at 202, 313, 423 and 615 nm.

These peaks match with those of the Fe^{2+}-MG complex in solution. Hence it is confirmed that the protective film consists of the Fe^{2+}-MG complex [53, 54].

Analysis of luminescence spectra

Fluorescence spectra were used to confirm the formation of a protective film on the metal surface during corrosion inhibition studies [55,56].

The luminescence spectrum (λ_{ex}=300 nm) of an aqueous solution of malachite green (MG) and freshly prepared Fe^{2+} ($FeSO_4.7H_2O$) is shown in Fig. 7(a). Peaks appear at 336 nm, 364 nm, 410 nm, 441 nm and 521 nm. This spectrum is due to the formation of a MG-Fe^{2+} complex in the solution.

The luminescence spectrum (λ_{ex}=300 nm) of the film formed on the metal surface after immersion in an aqueous solution containing well water (model corrosion medium), 30 ppm of MG, and 25 ppm of Zn^{2+} is shown in Fig. 7(b). Peaks appear at 335 nm, 364 nm, 410 nm, 440 nm and 520 nm. These peaks match with the peaks of the Fe^{2+}-MG complex formed in solution, which confirms that the protective film formed on the metal surface consists of the Fe^{2+}-MG complex.

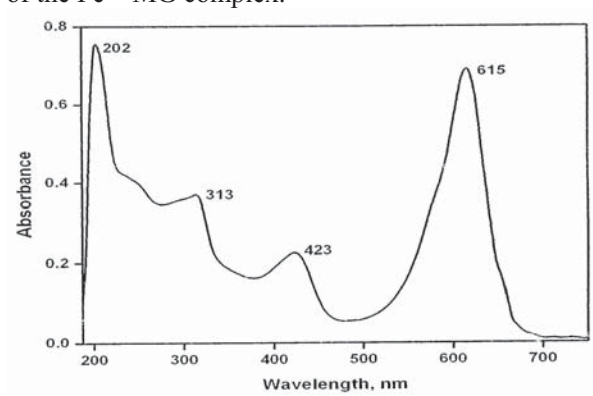

Fig.5. UV-visible absorption spectrum of an aqueous solution of MG + Fe^{2+} .

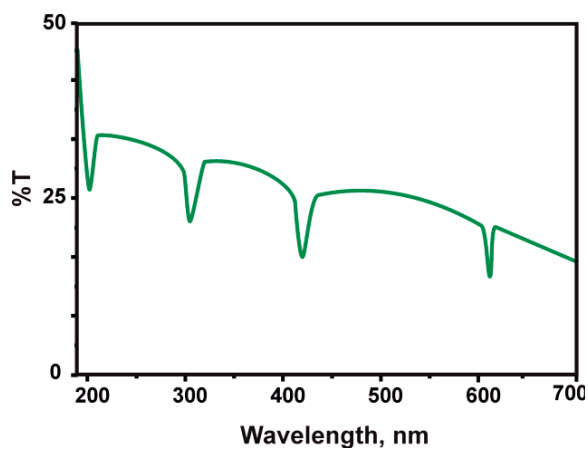

Fig. 6. The UV-visible reflectance spectrum of the film formed on metal after immersion in the solution containing Well water (model corrosion medium) + MG 30 ppm + Zn^{2+} 25 ppm/

Analysis of FTIR spectra

The structure of MG is shown in Scheme 2. The FTIR spectrum (KBr) of pure MG is shown in Fig. 8(a). The peak at 1616 cm^{-1} corresponds to aromatic -C=C- stretching frequency. The peak at 1319 cm^{-1} corresponds to $-N:$ stretching frequency. Thus the structure of MG, namely,

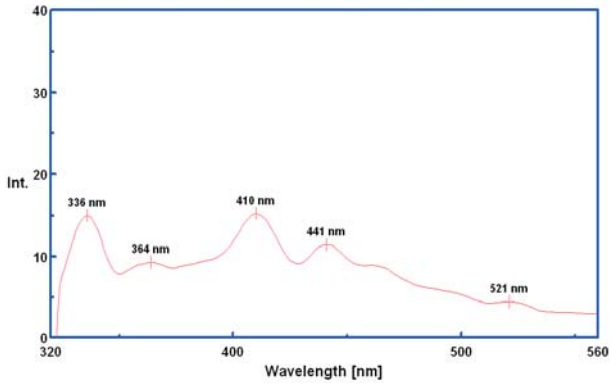

Fig.7a. The luminescence spectrum of an aqueous solution containing MG and Fe^{2+} .

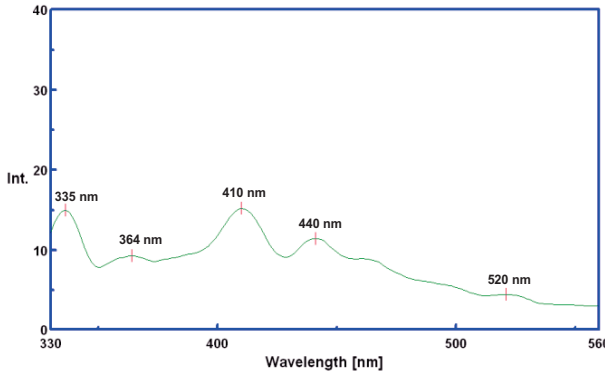

Fig.7b. The luminescence spectrum of the film formed on the metal surface after immersion in aqueous containing well water (model corrosion medium), 30 ppm of MG and 25 ppm of Zn^{2+}.

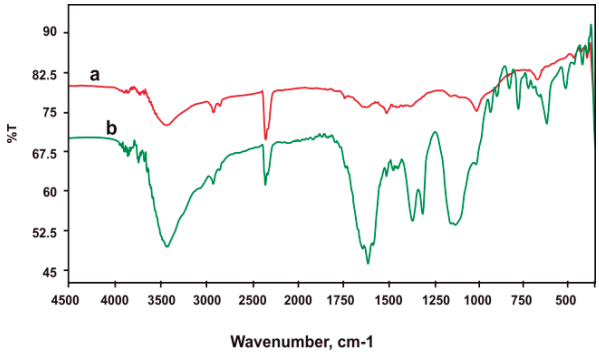

Fig.8: FTIR spectra. (a) pure MG; (b) - film formed on the carbon steel surface after immersion in a solution containing well water (model corrosion medium) + MG (30 ppm) + Zn^{2+} (25 ppm).

4-[(4-dimethylaminophenyl)-phenylmethyl-N,N-dimethyl aniline] is confirmed by FTIR [57].

The FTIR spectrum of the protective film formed on the surface of the metal after immersion in the well water (model corrosion medium) containing 25 ppm of Zn^{2+} and 30 ppm of MG is shown in Fig.8b. It is found that the disappearance of teritary nitrogen confirms the co-ordination through the $-N:$ atom. It is interesting to note that

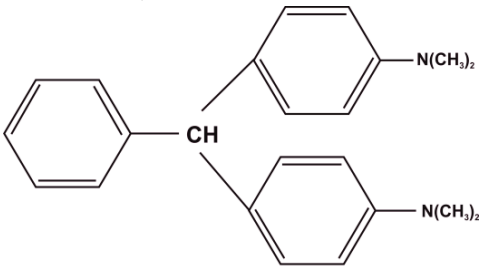

Scheme 2. Structure of Malachite Green

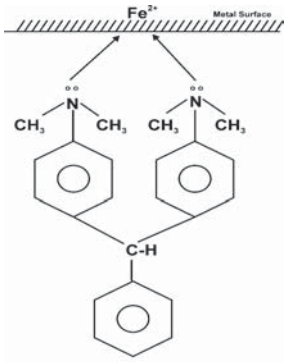

Scheme 3. Adsorption of MG on metal surface.

the aromatic π electron peak at 1616 cm^{-1} does not disappear in the FTIR spectrum of the protective film.It appears at 1616 cm^{-1} without shift, which indicates that the aromatic π-electrons do not participate in the coordination with Fe^{2+} on the metal surface. Thus, it is confirmed that the Fe^{2+}-MG complex on the metal surface is formed through coordination of electrons of nitrogen atoms and Fe^{2+} on the metal surface. The aromatic π-electrons do not participate in Fe^{2+}-MG complex formation. The probable structure of this complex is shown in Scheme 3.

Parallel coordination is not possible due to steric hindrance. Hence, perpendicular coordination takes place. The peak at 1350 cm^{-1} is due to zinc hydroxide. Thus, it follows from the FTIR spectral study that the protective film consists of the Fe^{2+}-MG complex.

Decolourisation process

Platinized titanium anode and graphite cathode were immersed in 100 ml of the solution to be decolorized. Current was passed for 10 minutes without addition of NaCl. Potential was 2 V; current density was 0.25 A/cm^2. There was no discoloration. When 1 g of NaCl was added (1% solution supporting electrolyte), partial discoloration took place after passing current for 10 minutes, due to the low concentration of sodium hypochlorite produced. However, it is very interesting to note that when 2 g of NaCl were added (2% solution), the solution was completely discolored within a few seconds. Hence this formulation, namely 2% solution of NaCl, platinized titanium anode, graphite cathode, current density of 0.125 A/cm^2 and potential of 2 V may be used for a few seconds to discolor the solution of MG (20 ppm). The supporting electrolyte plays an important role in the oxidation process [58,59]. When NaCl solution is electrolysed, the active species produced is Cl^+ which oxidizes the colored product into a colorless one (Scheme 4).

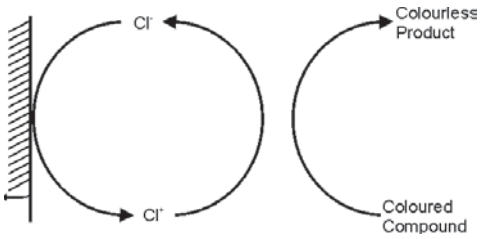

Scheme 4. Mechanism of decolourisation.

The optical density value for coloured solution before decolourisation was 0.38 and after decolourisation was 0.01. Hence the efficiency of decolourisation is 96%.

The optical density of the colored solution before discoloration was 0.38 and after discoloration - 0.01. Hence, the efficiency of discoloration is 96%.

The main objection for using dyes as corrosion inhibitors in cooling water systems is the color of dye.

The present study offered a method of discoloration of the colored inhibitor solutions.

Table 15: The decolourising efficiency

System	Current Density A/cm^2	Potential volts	NaCl g	OD	Efficiency %
MG before electrolysis	--	--	--	0.38	--
MG after electrolysis	0.125	2	2	0.01	96

CONCLUSION

The inhibition efficiency (IE) of the malachite green (MG)-Zn^{2+} system in controlling corrosion of carbon steel in well water containing 665 ppm of Cl^- (model corrosion medium) was evaluated by the mass-loss method. The present study leads to the following conclusions:

- The mass-loss study reveals that the formulation consisting of 30 ppm of MG and 25 ppm of Zn^{2+} has 95% inhibition efficiency in controlling corrosion of carbon steel immersed in well water (model corrosion medium).
- The values of the synergistic parameters point to a synergistic effect between MG and Zn^{2+}.
- The polarization study reveals that the formulation functions as a cathodic type inhibitor predominantly controlling the cathodic reaction.
- It follows from the AC impedance spectra that a protective film is formed on the metal surface.
- The FTIR spectra show that the protective film consists of the Fe^{2+}-MG complex, which is further confirmed by the UV-visible spectra and fluorescence spectra.
- The colour of the dye can be removed by electrolysis using platinized titanium as anode and graphite as cathode.

Acknowledgement: *The authors are thankful to UGC and to their managements for their encouragement.*

REFERENCES

1. M. Cohen, *Corrosion*, **32**, 461 (1976).
2. S. Sanyal, *Bull.Electrochem*., **6**, 392 (1990).
3. J.L. Mansa, W. Szybalski, *Corrosion,* **8**, 381 (1952).
4. K.S. Rajagopalan, K. Venu, *Indian J.Techn*., **6**, 239 (1968).
5. J.W. Wood, J.S. Beecher, P.S. Lawrence, *Corrosion*, **13**, 41 (1957).
6. E.V. Bogatyreva, S.A. Balezin, *Zh.Priklad. Khim*., **35**, 1071 (1962).
7. E.V. Bogatyreva, V.V. Nagaev, *Zh.Priklad. Khim*., **35**, 550 (1962).
8. S. Rajendran, B.V. Apparao, N. Palaniswamy, *J. Electro. Chem. Soc. India,* **47**, 43 (1998).
9. S. Rajendran, B.V. Apparao, A.Mani, N. Palaniswamy, *Anti-Corrosion Methods & Materials*, **45**, 25 (1998).
10. Y.I. Kuzentzov, T.I. Bardasheva, *Zashch Met*., **24**, 234 (1988).
11. K. Airey, R.D. Armstrong, T. Handside, *Corrosion Sci.*, **28**, 449 (1998).

12. S. Rajendran, B.V. Apparao, N. Palaniswamy, *Anti-Corrosion Methods & Materials*, **47**, 294 (2000).
13. S. Rajendran, B.V. Apparao, N. Palaniswamy, *Anti-Corrosion Methods & Materials*, **44**, 308 (1997).
14. S. Rajendran, S. Vaibhavi, N. Anthony, D.C. Trivedi, *Corrosion,* **59**, 529 (2003).
15. S. Rajendran, A.J. Amalraj, M.J. Joice, N. Anthony, D.C. Trivedi, M. Sunderavadivelu, *Corrosion Reviews*, **22**, 233 (2004).
16. J.D. Talati, D.K. Gandhi, *Werkst. Korros*., **33**, 155 (1982).
17. J.D. Talati, D.K. Gandhi, *Indian J. Technol*., **20**, 312 (1982).
18. J.D. Talati, D.K. Gandhi, *Corrosion*, **40,** 88 (1984).
19. J.D. Talati, J.M. Daraji, *J. Electrochem. Soc*. *India,* **35**, 175 (1986).
20. M. Abdeli, N.P. Ahmadi, R.A. Khosroshahi, Journal of Solid State Electrochemistry, **14**, 1317 (2010).
21. E.E. Oguzie, V.O. Njoku, C.K. Enenebeaku, C.O. Akalezi, C. Obi, *Corrosion Sci.*, **50**, 3480 (2008).
22. E.E. Oguzie, *Materials Chem. &Phys*., **87,** 212-217 (2004).
23. E.E. Oguzie, B.N. Okolue, E.E. Ebenso, G.N. Onuoha, A.J. Onuchukwu, *Materials Chem.&Phys*, **87,** 394-401 (2004).
24. H. Ashassi-Sorkhabi, B. Masoumi, P. Ejbari, E. Asghari, *J. Appl. Electrochem*., **39**, 1497 (2009).
25. J. Sathiyabama, S. Rajendran, J.A. Selvi, J. Jeyasundari, *Bul. Chem. Commun*., **41**, 374 (2009)
26. J. Sathiyabama, S. Rajendran, J.A. Selvi and A.J. Amalraj, *Ind.ian J. Chem. Technol*., **15**, 462 (2008).
27. J. Sathiyabama, S. Rajendran, J. Arockia Selvi, *Bull. Electrochem*., **22**, 363 (2006).
28. S.K. Selvaraj, A.J. Kennedy, A.J. Amalraj, S. Rajendran, N. Palaniswamy, *Corrosion Reviews*, **22**, 219 (2004).
29. A. Jeyashree, F. Rajammal Selvarani, J. Wilson Sahayaraj, A. John Amalraj, S. Rajendran, *Portug. Electrochim. Acta*, **27**, 23 (2009).
30. S. Rajendran, R. Maria Joany, N. Palaniswamy, *Corrosion Reviews*, **20,** 231 (2002).
31. S. Rajendran, B.V. Apparao, N. Palaniswamy, *Bull. Electrochem*., **13**, 441 (1997).
32. A. Leema Rose, F.R. Selva Rani, A.P.P. Regis, S. Rajendran, A. Krishnaveni, *Zastita Materijala*, **51**, 143 (2010).
33. S.A. Kanimozhi, S. Rajendran, *Int. J. Electrochem. Sci.*, **4**, 353 (2009).
34. N. Anthony, H. Benita Sherine, *Arabian J. Sci. Eng*., **35**, 41 (2010).
35. S. Rajendran, M. Agasta, R. Bama Devi, B. Shyamala Devi, K. Rajam, J. Jeyasundari, *Zastita Materijala*, **50**, 77 (2009).
36. S. Rajendran , S. Shamugapriya, T. Rajalakshmi, A. John Amalraj, *Corrosion*, **61** (2005) 685.
37. K. Anuradha, R.Vimala, B. Narayanaswamy, A. Arockia Selvi, S. Raji, *Chem. Eng. Commun*., **195**, 352 (2008).
38. S. Agnesia Kanimozhi, S. Rajendran, *The Open Corrosion*, **2**, 166 (2009).
39. S. Rajendran, A. Raji, J. Arockia Selvi, A. Rosaly, S. Thangasamy, EDUTRACKS**, 6**, 30 (2007).
40. S. Agnesia Kanimozhi, S. Rajendran, *The Open Corrosion Journal*, **2**, 166 (2009).
41. N. Antony, H. Bentia Sherine, S. Rajendran, Int. J. Engi. Sci. Technol., **2**, 2774 (2010).
42. S. Rajendran, M. Kalpana Devi, A. Peter Pascal Regis, A. John Amalraj, J. Jeya Sundari, M. Manivannan, *Zastita Materijala*, **50**, 131 (2009).
43. A. Raji, S. Rajendran, P. Sivaprabha, J. Arockia Selvi, B. Narayanasamy, J. Jeyasundari, *Zastita Materijala*, **50**, 153 (2009).
44. L. Rose, N. Antony, F.R. Selvarani, A.P.P. Regis, S. Rajendran, *Zastita Materijala*, **50**, 167 (2009).
45. S. Rajendran, M. Kanagamani, M. Sivakalaivani, J. Jeyasundari, B. Narayanasamy and K. Rajam, Zastita Materijala, 49, 19 (2008).
46. R. Kalaivani, B. Narayanasamy, J.A. Selvi, A.J. Amalraj, J. Jeyasundari, S. Rajendran, *Portug. Electrochim. Acta*, **27**, 177 (2009).
47. S. Rajendran, J. Jeyasundari, P. Usha, J.A. Selvi, B. Narayanasamy, A.P.P.Regis, P. Rengan, *Portug. Electrochim. Acta*, **27**, 153 (2009).
48. A. Jayashree, F. Rajammal Selvarani, J.W. Sahayaraj, A. John Amalraj and S. Rajendran, *Portugaliae Electrochim Acta*, **27**, 23 (2009).
49. J. Arockia Selvi, S. Rajendran, V. Ganga Sri, A. John Amal Raj, B. Narayanaswamy, *Portug. Electrochim. Acta*, **27**, 1 (2009).
50. P. Shanthy, P. Rengan, A. Thamarai Chelvan, K. Rathika, S. Rajendran, *Indian J. Chem. Technol.* **16**, 328 (2009).
51. S. Rajendran, R. Maria Joany, B.V. Apparoa, N. Palanisamy, *Indian J. Chem. Technol.,* **9**, 197 (2002).
52. S. Rajendran, B.R. Earnest John Peter, A.P.P. Regis, A.J. Amalraj, M. Sundaravadivelu, *Transactions of the SAEST*, 38, 11 (2003).
53. S. Rajendran, B.V. Aparao, N. Palaniswamy, *Anti-Corr. Meth. Mater.*, **45**, 338 (1998).
54. S. Rajendran, B.V. Apparao, N. Palaniswamy, *Anti-Corr. Meth. Mater*, **45**, 256 (1998).
55. S. Rajendran, S. Vaibhavi, N. Anthony, D.C. Trivedi, *Corrosion*, **59**, 529 (2003).
56. S. Rajendran, S.P. Sridevi, N. Anthony, Amalraj, M. Sundaravadivelu, *Anti-Corr. Meth. Mater*, **52**, 102 (2005).
57. R.M. Silverstein, G.C. Bassler, T.C. Morril, Spectrometric identification of organic compounds New York, NY, 95 (1986).
58. S. Rajendran, D.C.C. Trivedi, *J. Synthesis,* Feb.1995, p.153.
59. R.I. Dotson, R.W.I. Ynch, *J.Electrochem. Soc*., **128**, 798 (1981).

ИНХИБИРАЩО ДЕЙСТВИЕ НА СИСТЕМАТА Zn^{2+} -МАЛАХИТОВО ЗЕЛЕНО

В. Джонсирани[1], С. Раджендран[1,2], Дж. Сатябама[1], Т.С. Мутхумегала[1], А. Кришнавени[3], Н. Хаджара Бииви[4]

[1)] *Изследователски департамент по химия, GTN колеж по изкуствата, Диндигул – 624005, Тамил Наду,Индия*

[2)] *RVS Училище по инженерство и технология, Диндигул – 624005, Тамил Наду,Индия*

[3)] *Департамент по химия, Колеж Ядава, Мадурай, Индия*

[4)] *Департамент по химия, B.S. Университет Абдур Рахман, Вандалур,Ченаи-600048,Индия*

Постъпила на 7 януари, 2011 г.; коригирана на 29 март, 2011 г.

(Резюме)

Ефективността на инхибиране (IE) на системата Zn^{2+} - малахитово зелено (MG) при корозията на въглеродна стомана е оценена по метода за загуба на теглото. Използвана е моделна среда, съдържаща 665 ppm хлоридни йони. Изследванията показват, че препаратът, съдържащ 30 ppm от MG и 25 ppm от Zn^{2+} има инхибираща ефективност от 95% при използваната моделна среда. Има данни за синергизъм на MG и Zn^{2+}. Поляризационните изследвания показват, че системата работи като инхибитор от катоден тип, т.е. контролираща предимно катодната реакция. AC-импедансните спектри показват, че върху металната повърхност се образува защитен филм. FTIR-спектрите показват, че този филм се състои от комплекс между Fe^{2+} и багрилото. Този резултат е потвърден UV-Vis и флуоресцентна спектроскопия. Оцветяването може да се отстрани чрез електролиза при анод от платинизиран и графит като катод.

Bulgarian Chemical Communications, Volume 44, Number 1 (pp. 52 – 56) 2012

Flame AAS determination of trace amounts of Cu, Ni, Co, Cd and Pd in waters after preconcentration with 2-nitroso-1-naphthol

G. Gentscheva*, A. Petrov, E. Ivanova, I. Havezov

Bulgarian Academy of Sciences, Institute of General and Inorganic Chemistry, Acad. G. Bontchev Str., Bl. 11, BG-1113 Sofia, Bulgaria

Received January, 18, 2011; accepted February 20, 2011

Flame AAS was applied to the determination of micro trace amounts of Co, Ni, Cu, Cd and Pd in waters after precipitation of their complexes with 2-nitroso-1-napthol. The precipitate was separated from the sample solution by filtration through Millipore filter of 0.22 μm pore size under suction. It was dissolved with a minimum amount of ethanol and was subjected to flame AAS analysis. The detection limits of Co, Ni, Cu, Cd and Pd were 0.61, 0.64, 0.89, 0.10 and 0.60 μg l^{-1}, respectively. The method was validated using the reference material SPS-WW2 – Spectrapure Standards, Norway, and was applied for analysis of capture water and waste water.

***Keywords**:* Flame AAS, preconcentration, 2-nitroso-1-naphthol, waters, Co, Ni, Cu, Cd, Pd

INTRODUCTION

Waters are among the most often analyzed samples. A large number of elements occur as contaminants from natural processes, industrial activities and automobile traffic. The determination of the toxic trace elements Cd, Co, Cu, Ni and Pd in natural and waste waters is of significant interest in the monitoring of environmental pollution. The use of atomic absorption spectrometry for direct trace and ultra-trace analysis of these waters meets specific difficulties – e.g., insufficient sensitivity (flame AAS) or severe matrix interferences (graphite furnace AAS) [1]. Therefore, sample pretreatment is usually necessary to separate/ preconcentrate trace analytes prior to their AAS detection [2].

Solvent extraction is one of the most widely applied procedures for trace element preconcentration and separation with subsequent flame AAS analysis. The main reason for this is the higher sensitivity of the analysis of organic solutions in comparison with that of aqueous solutions. The trace metal ions are usually extracted as chelate complexes into the organic phase [3]. In solid phase extraction the chelate complexes of the metal ions are collected onto solid sorbents [4–6]. As chelate complexes are insoluble in aqueous solutions, they may be separated from the aqueous phase as precipitates without the addition of a solid sorbent. Depending on the adopted method of detection, the precipitates, separated by filtration, may be dissolved in a suitable solvent [7–9] or directly analyzed e.g., by X-ray fluorescence spectrometry [10, 11]. An essential advantage of the precipitation procedure is the possibility to handle large sample volumes achieving high preconcentration factors [12].

2-Nitroso-1-naphthol is a chelating reagent that has been used for on-line preconcentration of cobalt on a chelating microcolumn [13], for the spectrophotometric determination of ruthenium [14], as well as for the solid phase extraction of Th, Ti, Fe, Pb and Cr from waters [15]. There are no data in the literature for the preconcentration of Cu, Ni, Cd and Pd with 2-nitroso-1-naphthol.

The purpose of the present work was to study the possibilities for precipitation preconcentration of trace amounts of Cu, Ni, Co, Cd and Pd using 2-nitroso-1-naphthol with a view to their subsequent flame AAS determination. The method developed was validated using a reference material and was applied to the determination of traces of these elements in capture water and waste water.

EXPERIMENTAL

Instrumentation

A Thermo SOLAAR M5 flame atomic absorption spectrometer with deuterium background corrector was used in this study. All measurements were performed in air-acetylene flame under standard conditions except for the 10

* To whom all correspondence should be sent:
E-mail: gentg@svr.igic.bas.bg

© 2012 Bulgarian Academy of Sciences, Union of Chemists in Bulgaria

% reduction in the acetylene flow in the analysis of the ethanolic solutions.

Reagents

Analytical grade reagents and redistilled water were used throughout. The stock solutions of Ni, Co, Cu, Cd and Pd of concentration 1000 mg l^{-1} were prepared from Merck titrisols. Intermediate standard solutions were prepared by stepwise dilution of the stock solutions with ethanol. 2-Nitroso-1-naphthol (95%, Fluka), ethanol (96%, Merck), ammonia (25%, Merck), acetic acid (99–100%, Merck) and ammonium acetate (Merck) were used.

Buffer solutions for the pH range 5.0 – 7.0 were prepared from 0.5 mol l^{-1} ammonium acetate and were brought to the needed pH value with dilute ammonia or acetic acid. Durapore® membrane filters (Millipore), cat. No GVWP02500, 0.22 µm pore size were employed. A 1 % solution of 2-nitroso-1-naphthol was prepared in ethanol.

The reference material for measurement of elements in waste water SPS-WW2, Batch no.108, Spectrapure Standards AS (Oslo, Norway) was used.

Preconcentration procedure

150 ml of the water sample were mixed with 10 ml of buffer pH 6.5 and 11 ml of 1 % solution of 2-nitroso-1-naphthol. The mixture was stirred for 40 min on a shaking machine. The precipitate formed was filtered under suction through a membrane filter. The precipitate was transferred into a 5 ml volumetric flask, dissolved in ethanol and filled up to the mark with ethanol.

Blank samples were prepared by treating 150 ml of redistilled water in the described way. The calibration solutions were prepared by adding aliquots of the standard solutions of the analytes to precipitates obtained from blank samples prior to their dissolution in ethanol.

For the analysis of the reference material (RM) 20 ml aliquots (2 ml for the determination of Ni and Cu) were diluted to 150 ml with water and supplied with 10 ml buffer pH 6.5 and 11 ml reagent solution. The subsequent steps of the procedure were as described above.

RESULTS AND DISCUSSION

Calibration

The slopes of calibration curves prepared in ethanol and in a 1 % ethanolic solution of 2-nitroso-1-naphthol were compared. It was found that 2-nitroso-1-naphthol considerably suppressed the absorbance of the analyte elements (differences in the slopes between 20 and 40%). On the other hand, only part of the reagent added to the aqueous phase passed into the final concentrate. In order to eliminate calibration errors due to varying reagent concentrations, the calibration curves were prepared as described in the experimental part.

Effect of pH of complexation

The effect of pH was studied in the range 5.0–7.0 using model aqueous solutions of 50 ml volume and analyte concentration 0.2 µg ml^{-1} for nickel, cobalt and copper, 0.1 µg ml^{-1} for cadmium and 0.5 µg ml^{-1} for palladium. The obtained results are presented in Fig. 1. As can be seen, all analyte elements are quantitatively recovered (>95%) in the pH range 6–6.5.

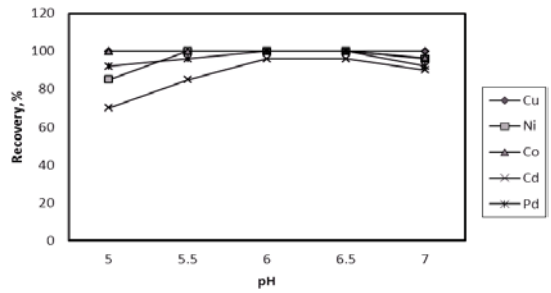

Fig. 1. Effect of pH on the recovery of Ni, Co, Cu, Cd and Pd with 2-nitroso-1-naphthol.

Effect of sample volume and amount of 2-nitroso-1-naphthol

The effect of sample volume on the recovery of the analyte elements was studied in the range from 20 to 250 ml. The results are shown in Fig. 2. As can be seen, the maximum sample volume allowing quantitative recovery of the analytes (>95%) is 160 ml. At higher sample volumes the recovery gradually decreases. For the quantitative preconcentration of nickel and cobalt sample volumes up to 200 ml were admissible.

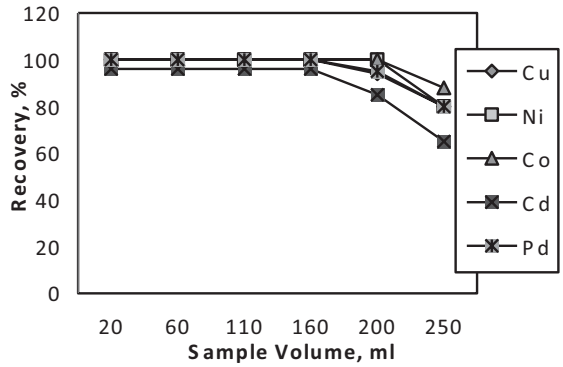

Fig. 2. Effect of sample volume on the recovery of Ni, Co, Cu, Cd and Pd with 2-nitroso-1-naphthol.

The amount of 2-nitroso-1-naphthol needed for the quantitative precipitation of the analyte elements at a 150 ml sample volume was optimized using increasing volumes of the 1% ethanolic 2-nitroso-1-naphthol solution. It was found that 10-12 ml was the optimal volume range of the reagent solution.

Effect of time of complexation

The effect of the time of complexation was studied over the range 15-60 min, see Fig. 3. As can be seen, the optimum time of complexation is 40 min. Longer time did not affect the recovery of the analytes.

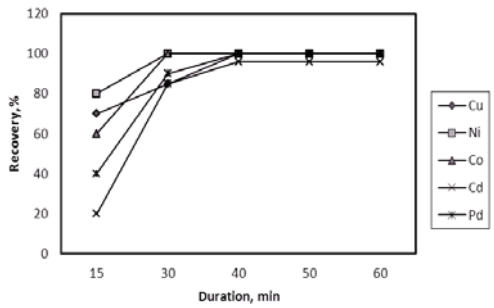

Fig. 3. Effect of time of complexation on the recovery of Ni, Co, Cu, Cd and Pd with 2-nitroso-1-naphthol

Interference studies

The precipitation of the analyte elements was studied in the presence of Na, K, Ca, Mg, Pb, Fe, Mn and Zn as possible matrix components (Table 1). No essential effects at the examined interferent levels on the recovery of the analytes were registered. The only exception was Cd with recoveries lower than 95%. Therefore, the standard addition method was adopted for Cd determination in further experiments.

Table 1. Effect of interferents on the determination of Cu, Ni, Co, Cd and Pd at the μg l^{-1} level

Interferent	Concentration, mg l^{-1}	Recovery, %				
		Cu	Ni	Co	Cd	Pd
Na	100	99±2	99±2	100±2	83±2	99±2
K	10	99±2	99±2	99±2	90±2	99±2
Ca	6	100±2	99±2	99±2	91±2	99±2
Mg	6	99±2	99±2	99±2	91±2	99±2
Pb	2	98±2	98±2	98±2	84±2	98±2
Fe	5	98±2	98±2	98±2	80±2	98±2
Mn	2	99±2	100±2	100±2	83±2	99±2
Zn	3	101±2	100±2	100±2	91±2	99±2

Analytical parameters

The detection limits (DL) were calculated as 3σ of the blank signals: Co - 0.64 μg l^{-1}, Ni – 0.61 μg l^{-1}, Cu - 0.89 μg l^{-1}, Cd – 0.10 μg l^{-1} and Pd - 0.60 μg l^{-1}. The precision of the results was characterized by an RSD of 1.5-2.0%.

The accuracy of the method was checked by analysis of the reference material SPS-WW2 (waste water). As the RM does not contain Pd, the "added-found" method was used. The recovery of the added concentrations of Pd (0.167 and 0.067 mg l^{-1}) was 98 and 103%, respectively. In order to check whether the concentrations of the analytes determined by the present method are undistinguishable from the certified values Welch's t-statistic evaluation was carried out according to [16]. The results obtained are shown in Table 2. As it can be seen, the values of t_{calc} are lower than the corresponding tabulated values at a probability of 0.05 and the corresponding effective degrees of freedom (ν_{eff}) for all analytes which points to the good accuracy of the results and confirm the validity of the proposed method.

Table 2. Measured (n = 5) and certified concentrations and t-statistic

	Ni	Co	Cu	Cd
Measured concentration, ng ml^{-1}	4945±65	300,8±4,4	1985±25	99,3±1,7
Certified concentration, ng ml^{-1}	5000±25	300±2	2000±10	100±0.5
t calc	1,70	0,35	1,19	0,84
ν_{eff} *	6,22	7,17	6,42	5,27
t (0,05; ν_{eff})	2,45	2,36	2,45	2,57

* effective degrees of freedom

Application

The method was applied to the determination of traces of Cu, Ni, Co, Cd и Pd in capture water from

Table 3. Determination of Cu, Co, Ni, Cd and Pd in capture water from the region of an old copper mine (Bov, Bulgaria) and waste water from the copper plant "Assarel", Bulgaria

Sample	Capture water		Waste water	
Element	Concentration, mg l^{-1}	*u(c)*, mg l^{-1}	Concentration, mg l^{-1}	*u(c)*, mg l^{-1}
Ni	0.0068	0.00102	0.0350	0.00092
Co	0.0144	0.00097	0.0230	0.00093
Cu	0.0810	0.00378	0.4500	0.02529
Cd	0.0020	0.00007	0.0084	0.00023
Pd	< DL	–	< DL	–

a region close to an old copper mine (Bov, Bulgaria) and waste water from the copper-dressing plant "Assarel" in Bulgaria. The obtained results are shown in Table 3.

The results are given with their uncertainties. As can be seen, copper is the trace element with the highest content not only in the waste water sample, but also in the capture water sample. The latter may be attributed to the high residual level of this element in the environment of the former copper mine. The Pd content was below the DL of the method. It follows from the obtained results that the flame AAS determination of micro trace amounts of Co, Ni, Cu, and Cd in waters after precipitation of their complexes with 2-nitroso-1-napthol is applicable to the analysis of real water samples.

Acknowledgements: *The authors acknowledge the financial support by the National Science Fund of Bulgaria (National Centre for New Materials UNION, Contract No DCVP-02/2/2009).*

REFERENCES

1. T R. Dulski, Trace elemental analysis of metals – methods and techniques. Marcel Dekker, New York, 1999
2. B. S. Garg, R K Sharma, N. Bhojak, S. Mittal, *Microchem. J.* **, 61**, 94 (1999)
3. F. Pena-Pereira, I. Lavilla, C. Bendicho, *Anal Chim. Acta*, **669**, 1 (2010)
4. D. Pozebon, V.L. Dressler, A.J. Curtius, *Anal. Chim. Acta***, 438**, 215 (2001)
5. A.A. Ensafi, A.R. Ghaderi*, J. Kor. Chem. Soc*., **52**, 16 (2008)
6. C. Duran, A. Gundogdu, V.N. Bulut, M. Soylak, L. Elci, H.B. Sentürk, M.Tüfekci, *J. Hazard. Mat.*, **146**, 347 (2007)
7. S. Arpadjan, P. Petrova, J. Knutsson, *Eurasian J. Anal. Chem.***, 3**, 10 (2008)
8. I. Narin, M. Soylak, *Anal. Chim. Acta*, **493**, 205 (2003)
9. Ş. Saçmaci, Ş. Kartal, *Microchim Acta*, **170**, 75 (2010)
10. F.L. Melquiades, P.S. Parreira, M.J. Yabe, M.Z. Corazza, R. Funfas, C.R Appoloni,., *Talanta*, **73**, 121 (2007)
11. G. Gentscheva, J. Jordanov, E. Ivanova, V. Petrova and L. Vladeva, *Bulg. Chem. Comm*., **37**, 69 (2005)
12. R. E. Santelli, M. Gallego, M. Valcarcel, Analytical Chemistry, **61**, 1427 (1989)
13. A.M. Haji Shabani, S. Dadfarnia, K. Dehghan, *Talanta*, **59**, 719 (2003)
14. D. L. Manning, O. Menis, *Anal. Chem*., **34**, 94 (1962)
15. F. A. Aydin, M. Soylak, *J. Hazard. Mat.*, **173**, 669 (2010)
16. Statistical Methods in Analytical Chemistry, Peter C. Meier and Richard E. Zund, second edition, John Wiley & Sons, 2000

ПЛАМЪКОВО AAC ОПРЕДЕЛЯНЕ НА СЛЕДИ ОТ Cu, Ni, Co, Cd И Pd ВЪВ ВОДИ СЛЕД КОНЦЕНТРИРАНЕ С 2-НИТРОЗО-1-НАФТОЛ

Г. Генчева*, А. Петров, Е. Иванова, И. Хавезов

Българска академия на науките, Институт по обща и неорганична химия,
Ул. Акад. "Г. Бончев", бл. 11, BG-1113 София, България

Получена на 18 януари 2011 г., приета на 20 февруари 2011

Пламъкова AAC е използвана за определяне на следи от Co, Ni, Cu, Cd и Pd във води след утаяване на техни комплекси с 2-нитрозо-1-нафтол. Получената утайка е отделена от разтвора на пробата чрез филтруване през мембранен филтър с размер на порите 0.22 μm. Разтворена е в 5 ml етанол и е анализирана с помощта на пламъкова AAC. Границите на откриване за Co, Ni, Cu, Cd и Pd са съответно 0.61, 0.64, 0.89, 0.10 и 0.60 μg l^{-1}. Методът е валидиран с използване на референтен материал SPS-WW2 – Spectrapure Standards, Норвегия и е приложен за анализ на каптажна и отпадна вода.

Bulgarian Chemical Communications, Volume 44, Number 1 (pp. 57 – 63) 2012

Oxidative changes in some vegetable oils during heating at frying temperature

E. M. Marinova*, K. A. Seizova, I. R. Totseva, Svetlana S. Panayotova, Ilko N. Marekov, Svetlana M. Momchilova

Institute of Organic Chemistry with Centre of Phytochemistry - Bulgarian Academy of Sciences, 1113 Sofia, Bulgaria

Received February 15, 2011; Revised March 29, 2011

The oxidative changes in refined sunflower, grape seed, soybean, corn and olive oils caused by frying temperature were studied. The oxidative degradation of the oils was evaluated by monitoring their respective peroxide value (PV), oxidation stability (IP), content of conjugated dienes as absorbance at 232 nm (A_{232nm}), content of conjugated trienes as absorbance at 270 nm (A_{270nm}), changes in fatty acid composition (C18:2/C16:0), and content of total polar components (TPC). Results showed that olive oil has better stability against thermal oxidation when compared to polyunsaturated oils. On the other hand, corn and soybean oils (among unsaturated oils) are most resistant to oxidation at frying temperature. The best correlation was observed between the rate of decrease in C18:2/C16:0 ratio and the content of total polar components.

Key words: frying temperature; sunflower oil; grape seed oil; soybean oil; corn oil; olive oil

INTRODUCTION

In recent years the contribution of frying oils to total energy intake has markedly increased in the industrialized countries. This is mainly due to the rising consumption of deep-fried products, which are very popular because of their desirable flavour, colour, and crispy texture. Recently, much concern has been expressed on the biological effects of oxidized lipids, and there is increasing evidence that they may be detrimental to health [1, 2]. The chemistry of oxidation at high temperatures is very complex since both thermal and oxidative reactions are involved [3]. During the deep fat frying a number of chemical reactions takes place – hydrolysis, oxidation, thermal decomposition and polymerization. The chemical mechanism of thermal oxidation is principally the same as the autoxidation mechanism, but the thermal oxidation rate is faster than the autoxidation rate [4]. Oxidative stability is very important factor in oil quality especially for these used for frying because of the high temperature applied. Frying oil must have high oxidative stability during use. From a nutritional point of view, it should be taken into account that oils with high amounts of saturated fatty acids and fats containing *trans* fatty acids are less desirable for good health [5]. More over, highly saturated fatty acid composition of some industrial frying oils may represent a problem in case it is necessary to keep the product in the liquid state [6].

Vegetable oils like soybean, sunflower, corn etc. are often judged as very unstable for continuous frying due to their content of polyunsaturated fatty acids. On the other hand, the presence of natural substances such as tocopherols, oryzanol, sterol fraction, squalene etc., enhances their stability at higher temperatures [7].

Since many factors affect the rate of deterioration of fats used for deep-fat frying, no single procedure will be reliable under all conditions [8]. With prolonged heating time the accumulation of deterioration products leads to organoleptic failures and a decrease of the nutritive value. Deep-fat frying decreases the unsaturated fatty acids and increases polar material. Many methods have been used for determination of fat deterioration during frying. They include methods for assessment of peroxide value, iodine value dienes, fatty acids, polar components etc. For the quality control of frying fats or oils the determination of total polar parts is an approved standard method.

The aim of the present study was to investigate the high temperature performance of some vegetable oils as a function of heating duration at simulated frying temperature of 180°C. The oxidative degradation of the oils was evaluated by monitoring peroxide value (PV), oxidation stability (IP), content of conjugated dienes as

* To whom all correspondence should be sent:
E-mail: emma@orgchm.bas.bg

© 2012 Bulgarian Academy of Sciences, Union of Chemists in Bulgaria

absorbance at 232 nm (A_{232nm}), content of conjugated trienes as absorbance at 270 nm (A_{270nm}), changes in fatty acid composition (C16:0/C18:2), and content of total polar components (TPC).

MATERIALS AND METHODS

Samples. Commercially available samples of refined sunflower oil ("Papas olio", Yambol, Bulgaria) refined grape seed oil (Olitalia, Forli, Italy), refined soybean oil ((Olitalia, Forli, Italy), refined corn oil (Olin Yag Sanagyi, Edirne, Turkey) and refined olive (pomace) oil (Cotoliva, Dos Hermanas, Spain) were purchased from the local markets, Sofia, Bulgaria.

Simulated deep frying. Oil samples (5g) were placed into glass vessels with an internal diameter of 12 mm and heated continuously at 180 ± 5°C in an oven. At certain time intervals, samples from the oils were taken away and stored at -18°C until the parameters characterizing oxidation process were determined.

Ga*s chromatography of fatty acid methyl esters.* Fatty acid methyl esters (FAME) were prepared by acid-catalysed transesterification of the oil samples using 1% sulfuric acid in methanol [9]. If needed, the FAME were purified on silica gel G TLC plates developed with hexane-acetone (100:8, v/v) mobile phase. GC of the FAME was performed on a Shimadzu GC-17A gas chromatograph (Shimadzu Corp., Kyoto, Japan) equipped with a 30 m x 0.25 mm x 0.25 µm INNOWAX capillary column (Agilent Technologies, USA). The temperature gradient started from 165°C increased to 230°C with 4°C/min and held at this temperature for 15 min; injection volume was 1 µl. Injector and detector temperatures were 260°C and 280°C respectively. Nitrogen was the carrier gas at flow rate 0.8 ml/min. The analyses were performed in triplicate.

Determination of peroxide value (PV). The peroxide value was determined by modified iodometric method [10].

Measuring the content of conjugated dienes (CD) and trienes (CT). Content of conjugated dienes as absorbance at 232 nm (A_{232nm}) and content of conjugated trienes as absorbance at 270 nm (A_{270nm}), were determined by dissolving weighed-out samples in isooctane (0.1%) and reading the sample absorbance at 232 nm (A_{232nm}) and 270 nm (A_{270nm}), using a Cecil Series 8000 UV/VIS double-beam scanning spectrophotometer (Cecil Instruments Ltd., Cambridge, UK). The A_{232nm} (1%) and A_{270nm} (1%) were calculated from the absorbance reading.

Determination of the oxidative stability. Oxidation at 100°C (±0.2°C) was carried out by blowing air through the samples (2 g) in the dark at a rate of 50 ml/min. The process was followed by withdrawing samples at measured time intervals and estimating the degree of oxidation by determination of PV. Kinetic curves of PV accumulation were plotted. All of them represent a mean result of three independent experiments.

Determination of the amount of unchanged triacylglycerols (TAG) and total polar components (TPC). The amount of unchanged triacylglycerols (TAG) and polar components (PC) was determined after their separation by preparative thin-layer chromatography [11]. The developing system used was hexane – acetone (100:10). Upon registration of the triacylglycerol zone, the layers containing triacylglicerols and those corresponding to the polar components were scrapped off, transferred to glass columns and eluted with chloroform and methanol (2:1). The solvents were evaporated and test-tubes were weighed until constant weight was reached.

Statistical analysis. The coefficient of variation for the PV determination was 7-8% irrespective of the measured value. The reported values for the IP were a mean result from three independent experiments. The coefficient of variation ranged from 6-13% and was inversely related to the induction period. Linear relationships between parameters investigated were obtained using the Linear fit tool of Origin 6.1 software (OriginLab Corporation, One Roundhouse Plaza, Northampton MA, USA).

RESULTS AND DISCUSSION

The characteristics of the oils used in these experiments are given in Table 1. During heating each oil sample was analyzed periodically for PV, oxidation stability (IP determined at 100°C), absorption at 232 nm, absorption at 270 nm, fatty acid composition (18:2/16:0 ratio) and the content of total polar components (TPC).

Peroxide value (PV)

Whereas storage of oil leads to increases in peroxide value (PV), the use of oils for frying does not lead to substantial increases in PV because peroxides decompose spontaneously above 150°C [12, 13]. The changes in PV during heating of the oils investigated are presented in Fig. 1. It is shown that PVs are not representative for changes occurring with oil samples during heating at 180°C.

Table 1. Initial characteristics of the refined vegetable oils used in the experiments

Vegetable oil	PV (meq kg-1)	IP (h)	A232 (1%)	A268 (1%)	TPC (%)	Fatty acid composition					
						C16:0	C18:0	C20:0	C18:1	C18:2	C18:3
Sunflower	8.8	6.7	3.65	3.27	5	7.4	4.1	0.2	25.6	62.7	0.0
Grape	5.7	10.2	3.95	3.21	9	6.9	3.4	0.2	22.1	66.8	0.5
Soybean	4.0	11.5	5.07	4.29	5	9.8	3.4	0.6	25.1	55.6	5.6
Corn	6.9	12.0	3.35	1.51	7	10.4	1.8	1.0	28.1	58.5	1.0
Olive (pomace)	8.9	30.0	3.62	1.25	6	11.5	3.2	0.4	75.3	9.0	0.6

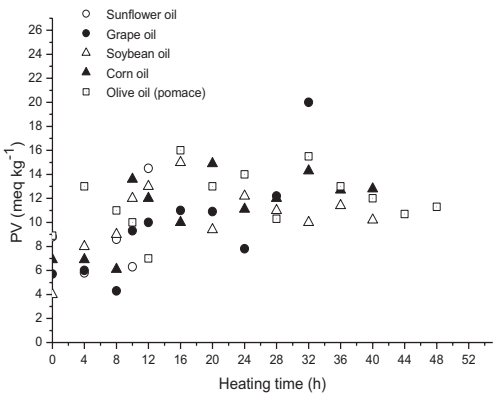

Fig. 1. Changes in the peroxide values (PV) of the oils during heating at 180°C.

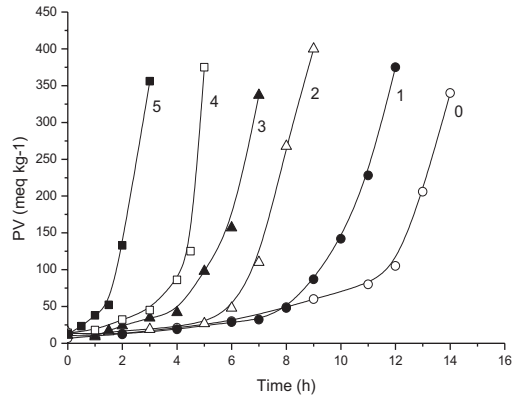

Fig. 2. Kinetic curves of peroxides accumulation during heating of corn oil after: 0 – 0 h; 1 - 10 h; 2 – 20 h; 3 – 24 h; 4 – 32 h; 5 – 36 h.

Oxidation stability

The oxidation stability (or induction period, IP) is defined as the time during which the oil's natural resistance to oxidation, due to the presence of naturally occurring antioxidants, inhibits oxidation [13]. Vegetable oils contain a range of components such as tocopherols, phenolics, sterols, etc. which are beneficial to oil stability during heating. Fig.2 illustrates, by way of example, the kinetic curves of peroxides accumulation during heating of corn oil. After processing all the kinetic curves obtained, the lengths of the IP were determined. It was established that the IPs decrease gradually with increasing thermal treatment in all oils investigated (Fig. 3). From the values of the regression line slopes, the rates of the decrease of oxidation stability (RDOS) are determined (Table 2). As shown from the results the values of RDOS decreased in the following order: olive oil ≈ sunflower oil > grape seed oil > soybean oil ≈ corn oil. Obviously, the oils rich in γ-tocopherol, in this paper soybean and corn oils [14] showed higher oxidation stabilities during treating at high temperature.

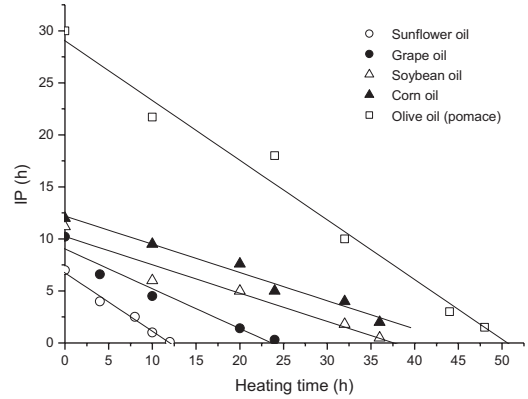

Fig. 3. Dependence of the induction periods (IP) on the heating times (h) of the oils.

Content of conjugated dienes (A_{232nm})

Thermal oxidation of unsaturated fatty acids is accompanied by considerable isomerization of double bonds leading to products containing *trans* double bonds and conjugated double bond systems [13].

From the Fig. 4A it is seen that UV absorbance at 232 nm tends to increase initially and then

plateau off during later stage of heating fat deterioration. This has been related to the establishment of equilibrium between the rate of formation of CD and the rate of formation of polymers formed by a Diels Alder reaction [4]. From the values of the regression line slopes the rates of CD accumulation (RCDA) during the first step of heating were determined (Fig.4B, Table 2). The results showed that the RCDA decreased in the following order: sunflower > grape seed > soybean > corn >olive oil. These data indicated that with respect to CD accumulation olive oil is most stable and among polyunsaturated oils - corn and soybean oils.

Table 2. Regression coefficients and coefficients of determination (r^2) from the linear regression of PV and CD

Vegetable oil	Rate of the decrease of IP	Rate of CD accumulation	Rate of the decrease C18:2 / C16:0 ratio
Sunflower	Y = 6.7 - 0.561x r^2 = 0.986	Y = 2.6 + 1.64x r^2 = 0.982	Y = 8.6 – 0.101x r^2 = 0.682
Grape	Y = 9.0 - 0.382x r^2 = 0.954	Y = 3.7 + 1.07x r^2 = 0.998	Y = 9.8 – 0.092x r^2 = 0.956
Soybean	Y = 10.2 - 0.272x r^2 = 0.953	Y = 5.3 + 0.82x r^2 = 0.992	Y = 5.6 – 0.032x r^2 = 0.870
Corn	Y = 12.2 - 0.271x r^2 = 0.976	Y = 3.1 + 0.73x r^2 = 0.998	Y = 5.6 – 0.020x r^2 = 0.910
Olive (pomace)	Y = 29.5 - 0.586x r^2 = 0.981	Y = 3.2 + 0.34x r^2 = 0.960	Y = 0.8 – 0.007x r^2 = 0.996

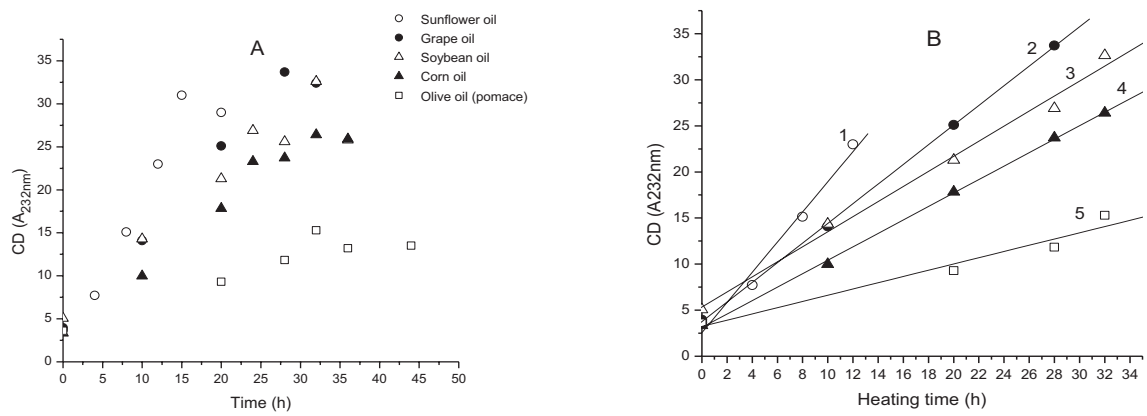

Fig. 4. Dependence of the content of conjugated dienes (A_{232nm}) on the heating times (h) of the oils: 1 – sunflower oil; 2 – grape seed oil; 3 – soybean oil; 4 – corn oil; 5 – olive (pomace) oil.

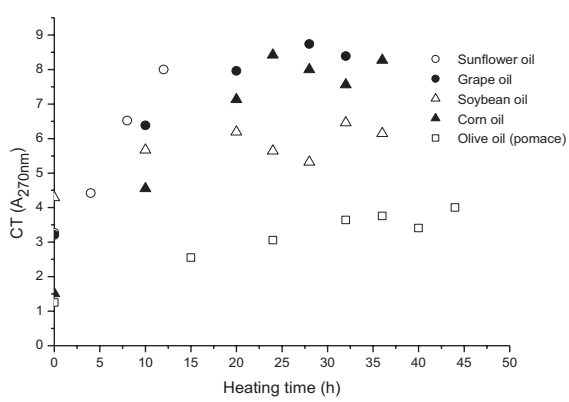

Fig. 5. Dependence of the content of conjugated trienes (A_{270nm}) on the heating times (h) of the oils.

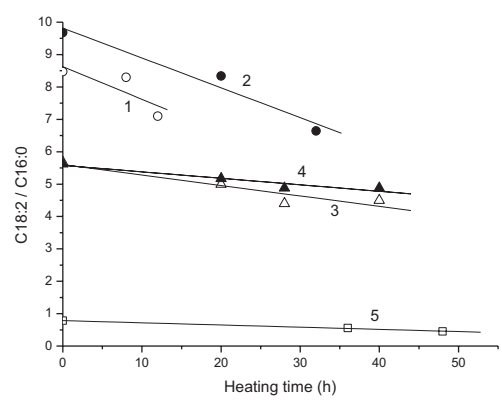

Fig. 6. Dependence of the changes in C18:2/C16:0 ratio on the heating times (h) of the oils: 1 – sunflower oil; 2 – grape seed oil; 3 – soybean oil; 4 – corn oil; 5 – olive (pomace) oil.

Content of conjugated trienes (A_{270nm})

Conjugated trienes absorbing at 270 nm are produced by linolenate oxidation products or by dehydration of hydroxylinoleate [13]. The results presented on Fig.5 show, that there was a trend of increasing triene content with the increase in heating time. This process is less pronounced in olive oil. In soybean oil conjugated trienes decompose more rapidly than in other oils.

Change in C18:2 C16:0 ratio

Monitoring of fatty acid changes in oils during deep fat frying is an effective method to assess thermal oxidative changes in the oils [15]. Linoleic acid content is frequently used as an indicator of the degree of oil degradation, since the polyunsaturated linoleyl chain is highly susceptible to oxidation. [16] found that changes in C18:2/C16:0 ratio was an effective parameter for assessing oxidation of oils. From Fig. 6, it can be seen that the C18:2/C16:0 ratio declined as time of heating is increased. From the values of the regression line slopes the rates of decrease in C18:2/C16:0 ratio (RD 18:2/16:0) were determined (Table 2). The results showed that this parameter decreased in the same order as RCDA: sunflower > grape seed > soybean > corn >olive oil.

Total polar components (TPC)

The content of total polar components (TPC) in used deep frying fats is until today an important criterion for assessing the decrease of fat quality [17]. TPC are considered to be nonvolatile compounds having a higher polarity than triacylglycerols, resulting from thermal, hydrolytic and oxidative alteration [18]. In several European

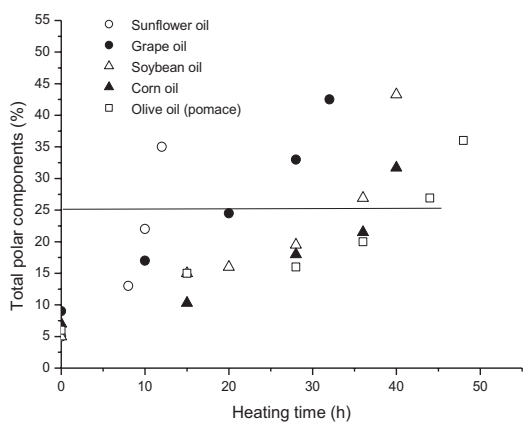

Fig. 7. Changes in total polar components (TPC) on the heating times (h) of the oils.

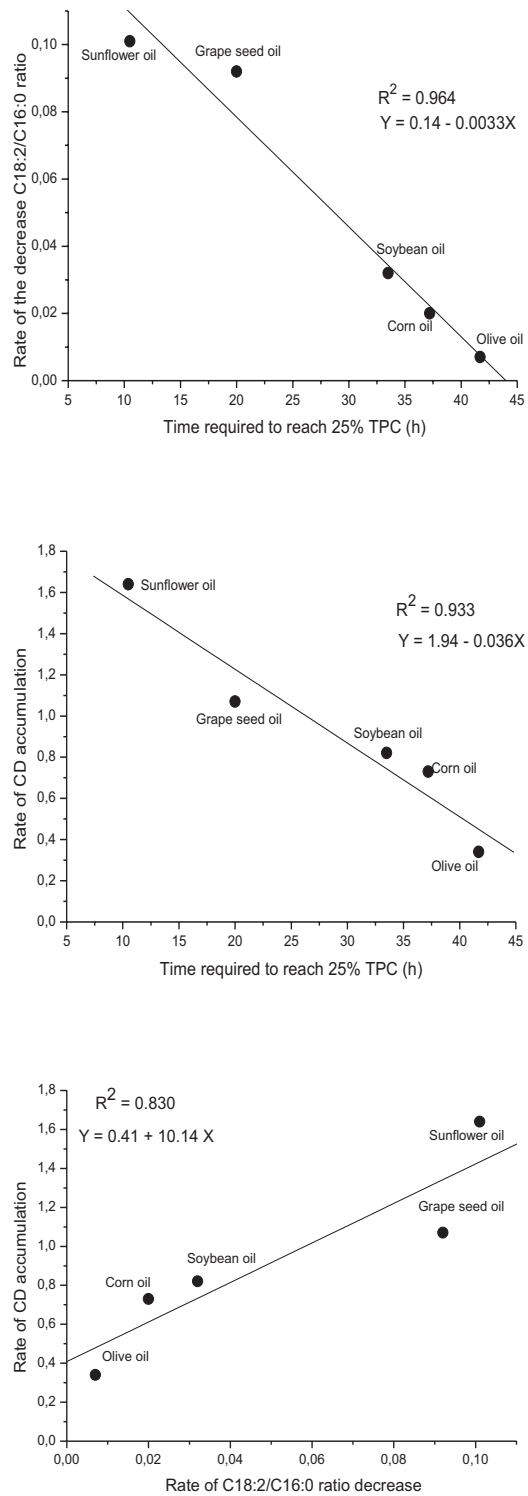

Fig. 8. Correlation between some parameters characterizing changes in the vegetable oils during heating at 180°C.

countries the maximum value for TPC is between 24 and 27% for commercial frying oils [19-21]. Research has shown that the fraction of polar components isolated from oxidized oils is the most toxic to laboratory animals [22]. In all oils, examined in this study, TPC content increased throughout the heating period. The results are presented on Fig. 7. Assuming that the limit of acceptance for the TPC is 25%, the time required to reach this limit differed for the oils examined and were: olive oil (41.7 h) > corn oil > (37.2 h) > soybean oil (33.5 h) > grape seed oil (20.0 h) > sunflower oil (10.5 h).

Some correlations between monitored parameters are presented on Fig. 8. The best one was observed between the rates of decrease in C18:2 / C16:0 ratio and total polar components.

CONCLUSIONS

The results revealed that olive oil has better stability against thermal oxidation when compared to polyunsaturated oils, which is due to fatty acid composition. On the other hand, corn and soybean oils (among unsaturated oils) are most resistant to oxidation at frying temperature.

Acknowledgments: *The authors are grateful to the National Council for Scientific Research in Bulgaria for the partial financial support under contract TK-X-1610.*

REFERENCES

1. C. Dobarganes, G. Marquez-Ruiz, *Current Opinion in Clinical Nutrition* & Metabolic *Care,* **6**, 157 (2003).
2. F.A. Aladedunye, R., Przybylski, *J. Am. Oil Chem. Soc.*, **86**, 149 (2009).
3. G. Marquez-Ruiz, M. C. Dobarganes, Nutritional and physiological effects of used frying oil and fats. In: Deep frying; chemistry, nutrition and practical application. M. D. Erickson (ed), AOCS, Urbana, IL, 2007, pp.173-203.
4. E. Choe, D. B. Min, *J. Food Sci.*, **72**, R77 (2007).
5. E. Tabee, S. Azadmard-Dimirchi, M. Jagerstad, P.C. Dutta, *J. Am. Oil Chem. Soc.*, **85**, 857 (2008).
6. E. De Marco, M. Savarese, C. Parisini, I. Battimo, S. Falko, R. Sacchi, *Eur. J. Lipid Sci. Techn.,* **109**, 237 (2007).
7. C. Gertz, S. Klostermann, S.P. Kochhar, *Eur. J. Lipid Sci. Techn.,* **102,** 543 (2000).
8. C.V. Fritsch, *J. Am. Oil Chem. Soc.*, **58**, 272 (1981).
9. W.W. Christie, Lipid Analysis: Isolation, Separation, Identification and Structural Analysis of Lipids, The Oily Press, Bridgwater, England, 2003, p.208.
10. N. Yanishlieva, A. Popov, E. Marinova, *Comptes rendus Acad. Bulg. Sci.,* **31**, 869 (1978).
11. N.Yanishlieva, E.Marinova, *Riv. Ital.Sost. Grasse*, **61**, 17 (1984).
12. M. H. Gordon, L. Kourimska, *J. Sci. Food Agric.*, **68**, 347 (1995).
13. E.N. Frankel, *Lipid Oxidation*. Dundee, Scotland: The Oily Press, 1998.
14. A. Gliszczynska-Swiglo, E. Sikorska, *J. Chromatogr. A*, **1048**, 195 (2004).
15. I. Jaswir, D. D. Kitts, Y. B. Che Man, T. H. Hassan, *J. Oleo Sci.*, **53**, 581 (2004).
16. K.A. Augustin, T. Asao, L.K. Heng, *J. Am. Oil Chem. Soc.*, **64**, 1670 (1987).
17. D. Firestone, Regulation of frying fats and oils. In: Deep frying, nutrition, and practical applications, Perkins, M. D. Erickson (Eds), Champaign: AOCS Press, 1996, pp.323-334.
18. M.C. Dobarganes,. G. Marquez-Ruiz, G., *Grasas y Aceites*, **49**, 331 (1998).
19. D. Firestone, R. F. Stier, M. Blumenthal, *Food Technol.,* **45**, 90 (1991).
20. F. J. Sanchez-Muniz, S. Bastida, S., *Forum of Nutrition*, **56**, 345 (2003).
21. A. Mariod, B. Matthäus, K. Eichner, I. H. Hussein, *J. Am. Oil Chem. Soc.*, **83**, 529 (2006).
22. T. P. Pantzaris, *Grasas y Aceites*, **49**, 319 (1998).

ОКИСЛИТЕЛНИ ПРОМЕНИ В РАСТИТЕЛНИ МАСЛА, НАГРЯВАНИ ПРИ ТЕМПЕРАТУРА НА ПЪРЖЕНЕ

Е.М. Маринова*, К.А. Сеизова, И.Р. Тоцева, Св.С. Панайотова, И.Н. Мареков, Св.М. Момчилова

Институт по органична химия с Център по фитохимия – БАН

Постъпила на 15 февруари, 2011 г.; коригирана на 29 март, 2011 г.

(Резюме)

Изследвани са окислителните промени в рафинирани слънчогледово, гроздово, соево, царевично и маслиново масла при 180°C (условия на пържене). Определени са следните параметри: пероксидно число (ПОЧ), окислителна стабилност (ИП), съдържание на спрегнати диени като абсорбция при 232 нм ($A_{232нм}$), съдържание на спрегнати триени като абсорбция при 270 нм ($A_{270нм}$), промени в мастнокиселинния състав (съотношение C18:2/C16:0) и съдържание на тотални полярни компоненти (ТПК). Резултатите показаха, че маслиновото масло е с най-висока стабилност при термично третиране. Сред полиненаситените растителни масла с най-висока стабилност се характеризират царевичното и соевото масла. Най-добра корелация е регистрирана между скоростта на намаление на съотношението C18:2/C16:0 и тоталните полярни компоненти.

Bulgarian Chemical Communications, Volume 44, Number 1 (pp. 64– 69) 2012

Mass transfer kinetics of biologically active compounds from Propolis

I. H. Tsibranska[1], B. Tylkowski[1], G.A. Peev[1], M. Giamberini[2], R. Garcia-Valls[2],

[1] *University of Chemical Technology and Metallurgy, Department of Chemical Engineering, 8 Kliment Ohridski blvd, 1756 Sofia – Bulgaria*

[2] *University Rovira i Virgili, Department of Chemical Engineering, Av. Països Catalans, 26, 43007 Tarragona – Spain*

Received March 28, 2011; Revised May 16, 2011

The present investigation is provoked by the increasing interest in propolis as a source of biologically active compounds (BAC) and the great differences in contact times, reported in literature, for their extraction by an ethanolic solvent. Two sets of kinetic investigations are performed:

- Liquid phase kinetic curves are obtained by spectrophotometric analysis of the extract (total polyphenols, flavones and flavonols, flavanones and dihydroflavonols). The total yield is determined gravimetrically.
- Size evolution of the propolis particles during extraction is continuously monitored by microscopy connected with a photo camera.

The effect of the liquid/solid ratio and the stirring intensity is studied. The results confirm that BAC release proceeds faster than usual solid-liquid extraction, because of the partial dissolution of the solid matrix, as well as the destruction to smaller particles, due to the particulate character of the propolis material. The effective mass transfer coefficient is of the order of 10^{-6} m/s. Favourable conditions for process performance are found.

Keywords: propolis, mass transfer, kinetics, biologically active compounds

INTRODUCTION

Propolis-containing products have been intensely marketed by pharmaceutical industry and health-food stores. Propolis is composed of 45% resins, 30% waxes and fatty acids, 10% essential oils, 5% pollens and 10% organic compounds and minerals [1, 2]. More than 300 compounds, among which terpenoids, steroids, sugars and aminoacids have been detected in raw propolis. Important bioactive compounds in propolis are flavonoids and phenolic acids, as well as their derivatives, because of their antibacterial, antifungal, antiprotozoan, antiviral, antitumoral, immunomodulatory, anti-inflammatory and antioxidant activity [3–8]. The most common process for propolis extraction uses ethanol as solvent. There are very few investigations concerning the mass transfer of propolis constituents and the reported contact times vary in a wide range, as can be seen from Table 1. It is also seen from Table 1 that two concentrations of the ethanolic solvent are mainly used for extraction. As the extraction of biologically active compounds (BAC) in aqueous solutions is much lower [16], ethanolic solvents with higher water content are not in common use.

Table 1. Experimental conditions for extraction of BAC from propolis

Time of extraction (days)	Origin of propolis/Reference	Pre-treatment	Solvent EtOH, %	Analytical control
90	Southeastern Brazil [9]	Powdered	96	TP* by Folin-Denis colorimetric method
14	European-Siberian and Irano-Turanian [10]	Grained	96	GC-MS analysis
7	Bulgaria and Brazil [11]	Ground	70	bactericidal activity
7	Beekeeping section of Lageado Farm (UNESP, Botucatu) [12]	Ground	70	immunomodulatory action
3	Greece, Aegean Sea islands and Cyprus [13]	Ground	70	TP by Folin-Ciocalteu colorimetric method
2	Turkey [14]	Grated	70	TP (Folin-Ciocalteu)
1	China [15]	–	96	TP (Folin-Ciocalteu)
7	Brazil [16]	In bench blender	EtOH or H_2O	TP (Folin-Ciocalteu) total flavonoids by HPLC

* TP – total phenolics

* To whom all correspondence should be sent:
E-mail: tsibranska@uctm.edu

© 2012 Bulgarian Academy of Sciences, Union of Chemists in Bulgaria

In [17] different diffusion models have been tested to describe the release kinetics of selected polyphenols from propolis incorporated into polylactic acid (PLA) film. With ethanol as a solvent a very fast release has been observed whatever the polyphenol.

The object of the present investigation is the mass transfer kinetics of BAC from propolis into ethanol-water solvent.

EXPERIMENTAL

Propolis was provided by the Centre of Phytochemistry of the Institute of Organic Chemistry, BAS, (Bulgaria); ethanol (99.9 %) and methanol (99.9%) were supplied by Valerus (Bulgaria); aluminium chloride anhydrous, potassium hydroxide (ISO), sodium carbonate anhydrous (ISO), sulfuric acid (96%), Folin-Ciocalteu's phenolic reagent and methanol Lichrosolv (99.8%), were supplied by Merck; pinocembrin was supplied by Extrasynthese (France); galangin was supplied by Fluka.

Before extraction the propolis material was cooled at 5°C and ground. The mean number-based diameter, obtained by ESEM micrographs and "Image-ProPlus 5" software, was 32 μm; 90% of the particles size was in the range of (15-52) ±2 μm [18]. Extraction was performed with 70% (v/v) EtOH-water solvent, as well as with pure ethanol at room temperature and different liquid/solid ratios (8 to 30 ml liquid/g solid). Contact times up to 2 days were used. Stirring (up to 300 rpm) was applied, using MM2A Lab. Pristroje Praha magnetic stirrer.

The decrease in the dimensions of propolis particles after contact with immobile liquid was continuously observed on an Axiovert 4OC microscope for transmitted-light brightfield and phase contrast with condenser 0.4, inclusive object traverser M, and optical micrographs from the particles taken by digital camera DeltaPix Invenio 3S, connected with the microscope. The undissolved solid collected after extract filtration, was determined gravimetrically.

UV-VIS analysis was performed on Hexiosy v 7.06 spectrophotometer:

- Flavones and flavonols were determined by aluminum chloride complex formation [19]. 20 ml methanol and 1 ml 5% $AlCl_3$ were added to 2 ml of the test solution and the volume was made up to 50 ml. After 30 min, the absorbance was measured at 425 nm. Blank: 2 ml methanol instead of test solution. Calibration with galangin was used in the concentration range 0.0052–0.052 mg/ml [18].

- Flavanones and dihydroflavonols were determined according to [20, 21]. 1 ml of the test solution and 2 ml of 2,4-dinitrophenylhydrazine (DNP) solution (1 g DNP in 2 ml 96% sulfuric acid, diluted to 100 ml with methanol) were heated at 50 °C for 50 min. After cooling to room temperature, the mixture was diluted to 10 ml with 10% (w/v) solution of KOH in methanol. 1 ml of the resulting solution was added to 10 ml methanol and diluted to 50 ml with methanol. Absorbance was measured at 486 nm. Blank: 1 ml methanol instead of the test solution. Calibration with pinocembrin was used in the concentration range 0.14–1.0 mg/ml [18].

- Total phenolics were quantified by the Folin–Ciocalteu's method [22]. 1 ml of the test solution was transferred into a 50 ml volumetric flask, containing 15 ml distilled water, and 4 ml of the Folin–Ciocalteu's reagent followed by 6 ml of a 20% sodium carbonate solution were added. The volume was made up to 50 ml with distilled water and kept for 2 h. Absorbance was measured at 760 nm. Blank solution: 1 ml methanol instead of test solution. Calibration with a 2:1 pinocembrin–galangin mixture was used in the concentration range 0.025–0.3 mg/ml [18].

RESULTS AND DISCUSSION

The ground propolis is characterized by a pronounced particle size distribution, shown in Fig.1.

By continuous observation of the particles in contact with the solvent (Fig. 2a), the time evolution of the particle size is obtained (Fig.2b). The latter undergoes essential alteration during the process, the final distribution being shifted to the left, corresponding to a decrease of the mean number-based particle diameter from 32 to 13 μm.

A certain correspondence is observed between the kinetic curves for polyphenolics release and the evolution of the mean particle size, as shown in Fig. 3. For comparison, the final concentration of polyphenols after 48 h is also given.

These results suggest a process involving BAC release, as well as partial dissolution of the solid matrix, as gravimetrically proven. The total solid content in the liquid phase after 15 min is 27 mg/ml and remains constant upon prolonging the time of extraction. The corresponding total phenolic concentration is 18.2 mg/ml, which constitutes about 67.6% of the dissolved solid substances

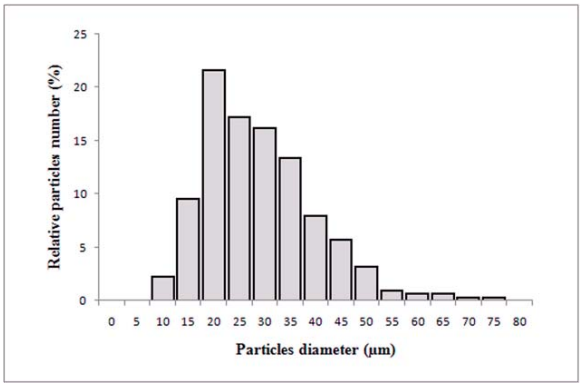

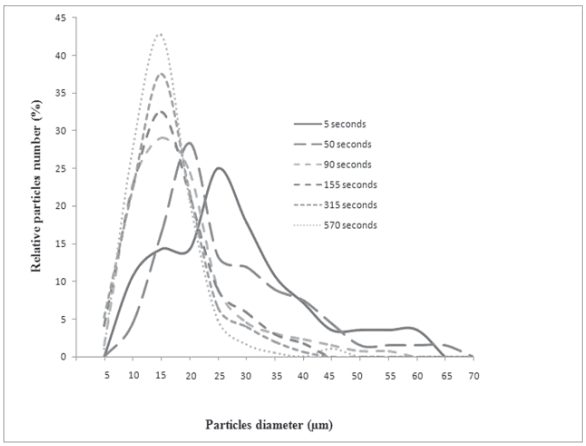

Fig.1 Initial particle size distribution

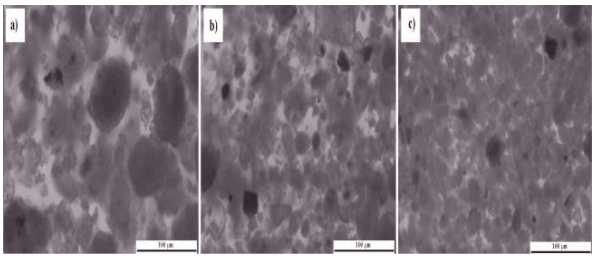

Fig.2. Optical micrographs for different time of extraction: a) 5s; b) 2 min; c) 15 min. Time evolution of the particle size distribution (70% ethanol, no mixing).

and 91.6% of the phenolics concentration after 48 h of contact. The use of pure ethanol slightly increases the total solid content (to 29 mg/ml after 15 min). Longer times of contact lead to a slight increase in the concentration of polyphenols - after 30 min the BAC are practically completely recovered (19.5 mg/ml).

As the mass transfer process is fast, no effect of stirring is observed, as shown in Fig.4. Few minutes are enough to reach the equilibrium concentration of the respective groups of extracted compounds,

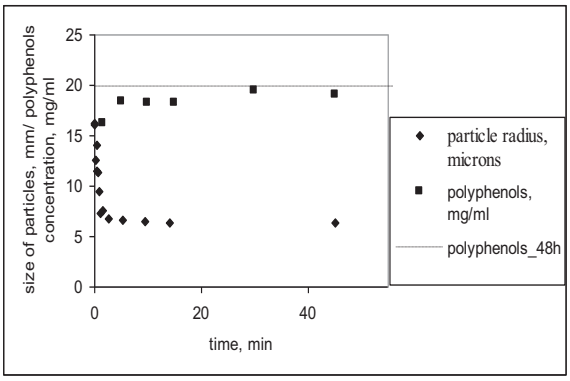

Fig. 3 Time evolution of the mean particle radius (μm) and the total phenolics concentration (mg/ml) at a liquid/solid ratio of 20.

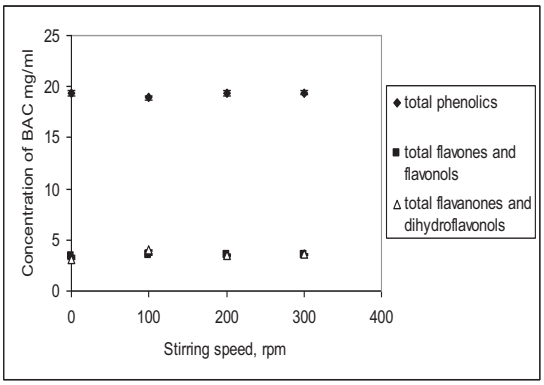

Fig. 4. Effect of the stirring speed on the extraction of BAC from propolis at a time of15 min and liquid/solid ratio of 20.

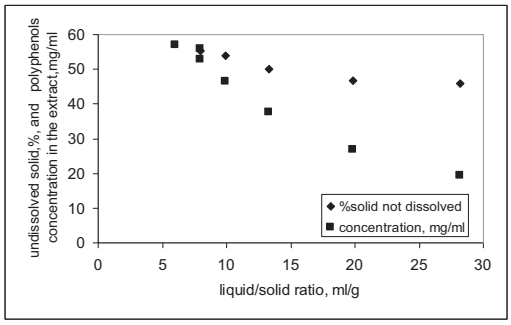

Fig.5. Undissolved propolis part and liquid phase concentration of total phenolics for different liquid/solid ratios.

which are (in mg/g propolis): total phenolics 386.4;flavones and flavonols 68.5; flavanones and dihydroflavonols 63.1.

Fig.5 shows the undissolved part (% of the solid mass) together with the liquid phase concentration (mg/ml) for increasing liquid/solid ratios. With liquid/solid ratios exceeding 20 ml/g the amount of undissolved solid remains practically constant (Fig.5). The insoluble part is about 46% of the initial mass of the propolis.

If we consider the BAC as diffusing species and the other propolis constituents as particle matrix, the above results show that part of the matrix also dissolves. In this way the mass transfer surface is renewed and the BAC extraction is accelerated.

The change in the particle mass is related to the mass balance of the extraction process:

$$\frac{dM_s}{dt} = \rho_s 4\pi R^2 N \frac{dR}{dt} = -\frac{dM_l}{dt} = -\frac{d\overline{C}_l}{dt} V_l \quad (1)$$

Here '*s*' and '*l*' denote the solid and liquid phase; *dR/dt* is known from Fig.3, the initial solid mass, particle radius and solid density are M_{so} = 1g, R_o= 16μm and ρ_s=1180kg/m^3 [22-23]; *N* is the number of particles, considered constant during extraction. The slope of the initial linear part of the *R(t)* curve in Fig.3 (the first 1.5 min) gives dR/dt=1.09·10^{-7}m/s. Hence the average liquid phase concentration is evaluated to $\overline{C}_l$=20.69 mg/ml, i.e., about 77% of the final measured total concentration in the extract, which is a reasonable result.

Eq.(1) can be written with respect to the mass transfer from the particle surface (with concentration C_R) into the surrounding liquid, accounting for the mass transfer coefficient *k* [m/s].

$$\frac{dM_s}{dt} = -\frac{dM_l}{dt} = -ka\left(C_R - \overline{C}_l\right)V_l \quad (2)$$

The average liquid phase concentration $C_l = \left(M_s(t=0) - M_s(t)\right)/V_l$ is experimentally calculated (here V_l is the liquid volume). The specific interface $a=6\varepsilon_s/(2R)=4\pi R^2 N/V_l$ decreases proportionally to the square of the particle radius, the initial value of ε_s being $\varepsilon_s=V_{s0}/V_l$=0.044 and the volume of the solid – $V_{s0}=M_{s0}/\rho_s=(4/3)\,\pi R_0^3 N$.

Eq.(2) supposes a linear plot of dM_s/dt vs $a\left(C_R - \overline{C}_l\right)V_l$, which is confirmed by the results in Fig.6. The slope gives k=1·10^{-6}m/s, which is about one order lower than the usually observed values for dissolution processes. The latter can be easily checked, using the well known relation:

$$Sh = \frac{k2R}{D_m} = \left(4 + 1.2Pe^{2/3}\right)^{1/2} \quad ,(3)$$

which tends to the limiting value of $Sh = 2$ in case of stagnant fluid [25].

The main components in the extract have molecular mass between 180 and 410 [15, 24]. Hence, the coefficients of molecular diffusion, estimated by Wilke-Chang equation, are of the order of 10^{-10} m^2/s. For instance, with $D_{m,pinobanksin}$= 3.4·10^{-10}m^2/s we obtain k=1.9·10^{-5}m/s. This coefficient is time dependent and increases with decreasing particle size. The deviation from the origin of the coordinate system in Fig.6 can be due to errors either in the value of the saturation concentration, or in the number of particles. A short discussion of the latter is given below.

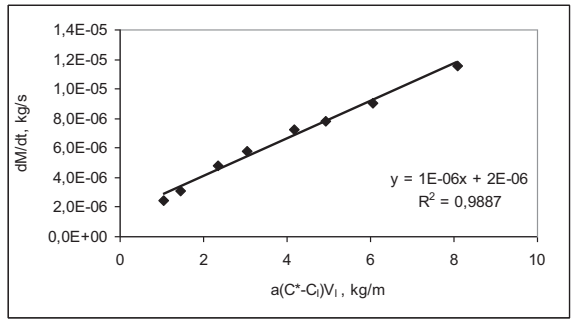

Fig.6. Determination of the effective mass transfer coefficient

From the analysis of the kinetic data (concentrations and particle size) the following question arises: is the particle size evolution due uniquely to mass transfer? For a positive answer the global balance with a constant number of particles should hold:

$$\Delta M = \rho_s N \frac{4\pi}{3}\left(R_0^3 - R_f^3\right) = V_l \overline{C}_l \quad (4)$$

Here '*0*' and '*f*' denote the initial and final volume averaged size of the particles (2*R*= 36 μm and 15 μm respectively). The initial number of particles (N_0) is:

$$N_0 = \frac{3M_{s0}}{\pi 4 R_0^3 \rho_s} \quad , \quad (5)$$

Combining eqs.(4) and (5) for $N=N_0$, the final liquid phase concentration is obtained:

$$\overline{C}_{l,f} = \frac{\left(R_0^3 - R_f^3\right)}{R_0^3 x} \quad (6)$$

where *x* stands for the initial liquid/solid ratio (V_l/M_{s0}=20).

Calculation by eq.(6) gives $\overline{C}_{l,f}$ =46.6 mg/ml, which is much higher than the experimentally obtained value $\overline{C}_l$=27 mg/ml and needs explanation. According to eq.(5) N_0 =3.55·10^7. As the final mass is M_{sf} = 0.46M_{s0} and 2R_f = 15 μm, then the final number of particles is N_f =23.9·10^7. A very probable reason for this difference lies in the destruction of mechanically unstable bigger

agglomerates of particles in contact with the solvent, which takes place in parallel to the dissolution process. This explanation is based on the particulate nature of the material, due to the way in which propolis is produced by the bees. The microscopic data, illustrated in Fig. 2, give some visual evidence for the increasing number of particles.

CONCLUSIONS

The results, obtained from the measured particle size and BAC concentrations during extraction, prove that the release is a fast process and the preparation of ethanolic extracts from propolis might be essentially rationalized by decreasing the speed of rotation and the time of contact.

If we consider the BAC as diffusing species and the other propolis constituents as particle matrix, the above results show that part of this matrix also dissolves. The insoluble part is about 46% of the initial mass of the propolis. At a liquid-solid ratio of 20 (ml/g) practically all the soluble part of the solid is dissolved.

The kinetics of BAC release lies somewhat between dissolution and the usual liquid-solid extraction with internal diffusion control, the effective mass transfer coefficient being of the order of 10^{-6}m/s. The partial dissolution of the solid phase leads to continuous renewal of the liquid-solid interface and to lower diffusion time in the particle, both resulting in an essential acceleration of the BAC extraction.

Acknowledgements: *The research leading to these results has received funding from the European Community's Seventh Framework Programme (FP/2007-2013) under grant agreement No PIAP-GA-2008-218068.*

REFERENCES:

1 E.L. Ghisalberti, P.R. Jefferies, R. Lanteri, J. Matisons, *Cellular and Molecular Life Sciences*, **34** (2), 157 (1978).
2 Ch. R. Chen, Ch. T. Shen, J.J. Wu, H.L. Yang, S. L. Hsu, Ch.M. J. Chang, 2009. *J. Supercrit. Fluids*, **50**, 176 (2009).
3 A.H. Banskota, Y. Tezuka, I. K. Adnyana, E. Ishii, K. Midorikawa, K. Matsushige, S. Kadota, *Phytomedicine*, **8** (1) 16 (2001)
4 A.H. Banskota, Y. Tezuka, S. Kadota, *Phytother. Res*., **15** (7), 561 (2001).
5 Z.S. Talas, M.F. Gulhan, *Ecotoxicol. Environ. Safety*, **72** (7), 1994 (2009).
6 A.E. Tosi, E. Re, M. E. Ortega, A. F. Cazzoli, *Food Chem.*, **104**, 1025 (2007).
7 J. M. Sforcin, *J. Ethnopharmacol*., **113** (1), 1 (2007)
8 G. Girgin, T. Baydar, M. Ledochowski, H. Schennach, D. N. Bolukbasi, K. Sorkun, B. Salih, G. Sahin, D. Fuchs, *Immunobiology*, **214** (2), 129 (2009).
9 C.S. de Funari, V. de Oliveira Ferro, B. M. Mathor, *J. Ethnopharmacol.*, **111** (2), 206 (2007).
10 A. Uzel, K. Sorkun, O. Oncag, D. Cogulu, O. Gencay, B. Salih, B., *Microbiol. Res.*, **160** (2), 189 (2005)
11 R.O. Orsi, J.M. Sforcin, S.R.C. Funari, V. Bankova, *Int. Immunopharmacol*., **5** (2), 359 (2005)
12 J.M. Sforcin, R.O. Orsi, V. Bankova, *J. Ethnopharmacol*., **98** (3), 301 (2005).
13 N. Kalogeropoulos, S.J. Konteles, E. Troullidou, I. Mourtzinos, V. T. Karathanos, *Food Chem.*, **116** (2), 452 (2009).
14 M. Popova, S. Silici, O. Kaftanoglu, V. Bankova, *Phytomedicine*, **12** (3), 221 (2005)
15 M.-R. Ahn, S. Kumazawa, Y. Usui, J. Nakamura, M. Matsuka, F. Zhu, T. Nakayama, *Food Chem.*, **101** (4), 1383 (2007).
16 B.C.B.S. Mello, J.C.C. Petrus, M.D. Hubinger, *J. Food Eng.*, **96,** 533 (2010)
17 E. Mascheroni, V. Guillard, F. Nalin, L. Mora, L. Piergiovanni, *J. Food Eng.*, **98** (3), 294 (2010)
18 B. Tylkowski, B. Trusheva, V. Bankova, M. Giamberini, G. Peev, A. Nikolova, *J. Membrane Sci.*, **348** (1-2), 124 (2010)
19 J. S. Bonvehi, F.V. Coll, *Z. Naturforschung*, **49**c, 712 (1994)
20 M. Popova, V. Bankova, D. Butovska, V. Petkov, B. Damyanova, A.G. Sabatini, G.L. Marcazzan, S. Bogdanov, 2003. *Honeybee Sci.-Tamagawa Univ.* **24** (2), 61 (2003)
21 M. Nagy, D. Grancai, *Pharmazie*, **51** (2), 100 (1996).
22 P.G. Waterman, S. Mole, Analysis of Phenolic Plant Metabolites, Blackwell Sci. Publ., Cambridge, 1994.
23 D. Biscaia, S.R.S., Ferreira, *J. Supercrit. Fluids*, **51** (1), 17 (2009)
24 C. Gardana, M. Scaglianti, P. Pietta, P. Simonetti, *J. Pharm. Biom. Anal.*, **45** (3), 390 (2007)
25 T. K. Sherwood, R.L. Pigford, Ch.R. Wilke, Mass Transfer, McGraw-Hill, New York, 1975.

КИНЕТИКА НА МАСОПРЕНАСЯНЕТО НА БИОЛОГИЧНО-АКТИВНИ ВЕЩЕСТВА ОТ ПРОПОЛИС

И.Х. Цибранска[1], Б. Тилковски[1], Г.А. Пеев[1], М. Джамберини[2], Р. Гарсиа-Валс[2],

[1]*Химико-технологичен и металургичен университет, Департамент по инженерна химия, бул. Климент Охридски 8, 1756 София*

[2]*Университет Ровира и Вирджили, Департамент по инженерна химия, Тарагона,Ииспания*

Постъпила на 28 март, 2011 г.; Коригирана на 16 май, 2011 г.

(Резюме)

Настоящето изследване бе провокирано от нарастналия интерес към прополиса като източник на биологично-активни вещества (БАВ), както и голямата разлика в публикуваните времена на контакт при тяхната екстракция с етанол-съдържащ разтворител. Бяха проведени два типа кинетични изследвания:

- Кинетичните криви в течна фаза бяха получени чрез спектрофотометричен анализ на екстракта (относно общи полифеноли, флавони и флавоноли, флаванони и дихридрофлавоноли). Общият извлек бе определян тегловно.
- Изменението на размера на частичките прополис във времето на екстракция беше непрекъснато следено микроскопски чрез свързана фотокамера.

Изследвано бе влиянието на хидромодула и скоростта на разбъркване. Получените резултати потвърждават, че извличането на БАВ протича по-бързо от обикновеното за екстракция твърдо-течност поради частично разтваряне на твърдата матрица, както и раздробяване на по-дребни частици поради зърнестия характер на изходния материал. Ефективният коефициент на масообмен е от порядъка на 10^{-6} m/s. Определени са благоприятните условия за провеждане на процеса.

Bulgarian Chemical Communications, Volume 44, Number 1 (70 – 73) 2012

Studies of tautomerism in the azonaphthol derivatives of benzimidazoles

S. Dincer

Department of Chemistry, Ankara University, 06100 Ankara, Turkey

Received January 11, 2011; Accepted December 6, 2011

The tautomeric behaviour of three azonaphthol derivatives of benzimidazoles, 1-[(6-nitro-1*H*-benzimidazol-5-yl)diazenyl]naphthalen-2-ol, 1-[1*H*-benzimidazol-5-yldiazenyl]naphthalen-2-ol and 1-[(1-methyl-1*H*-benzimi- dazol-5-yl)diazenyl]naphthalen-2-ol, were studied in solution, in solid state and in gas phase using spectroscopic techniques. The results show that the ketohydrazone tautomeric form is predominant in solution and in solid state while in gas phase the tautomeric equilibrium is on the azoenol side.

Keywords: Benzimidazole, azonaphthol, tautomerism, mass spectroscopy

INTRODUCTION

Heterocycles have been extensively used as diazo or coupling components in the synthesis of azo dyes [1–3] and many of these compounds display tautomerism depending on the intramolecular proton transfer which also determines their optical and physical characteristics. Their application as disperse dyes or photosensitive and photoconductive materials provokes a considerable interest in the technology of these compounds [4]. Owing to the properties of azo dyes, such as volatility, thermal lability, *etc.*, the tautomerism of these compounds has been widely studied by various techniques [5–9] including NMR, UV-vis, IR spectroscopy, X-ray crystallography and limited mass spectrometry analysis [10–12].

This paper reports the study of the azoenol-ketohydrazone tautomerization of the benzimidazole derivatives, namely, 1-[(6-nitro-1*H*-benzimidazol-5-yl) diazenyl]naphthalen-2-ol **1**, 1-[1*H*-benzimidazol-5-yl diazenyl]naphthalen-2-ol **2**, and 1-[(1-methyl-1*H*-benzimidazol-5-yl)diazenyl] naphthalen-2-ol **3**, using ^{1}H NMR, UV-vis, IR and mass spectroscopy (Scheme I).

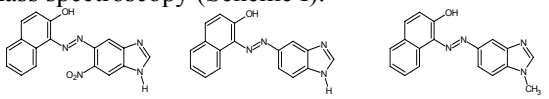

1 2 3

Scheme I. Structures of the reported compounds

MATERIALS AND METHODS

5-Nitro-1*H*-benzimidazole, naphthalen-2-ol, nitric acid, sulfuric acid, dimethyl sulfate and the solvents were purchased from Merck. Melting points were measured on a Gallenkamp apparatus. NMR measurements were carried out on a Bruker 500 MHz spectrometer. FTIR and UV-vis spectra were recorded on a Mattson 1000 FTIR spectrometer (in KBr discs) and on a UNICAM UV2–100 series spectrometer, respectively. Mass spectra were recorded on the AGILENT 1100 MSD spectrometer. Elemental analysis performed on the LECO 932 CHNS agreed with the calculated values.

EXPERIMENTAL

The synthesis of 5(6)-amino-6(5)-nitrobenzimidazole and its azonaphthol derivative – [(6-nitro-1H-benzimidazol-5-diazenyl] naphthalen-2–ol 1 was reported in a previous paper of the author [13]. The compound 2 was prepared according to ref. [13] and the compound 3 was synthesized in the same way using 5-amino-1-methyl-1H-benzimidazole as starting material.

Synthesis of 1-[(1-methyl-1H-benzimidazol-5-yl)diazenyl]naphthalen-2-ol

5-Amino-1-methyl-1H-benzimidazole: A mixture of 5-nitro-1*H*-benzimidazole (10 mmol), $(CH_3)_2SO_4$ (5.0 mL) and 1.5 mL 1.0 N NaOH was refluxed for 30 min. After cooling, the crude product was filtered and recrystallized from water. 1-Methyl-5-nitro-1*H*-benzimidazole was obtained as a brown solid, m.p. 203°C, yield 1.5 g (82%). This nitro compound was reduced using Sn/HCl by a standard

* To whom all correspondence should be sent.
E-mail: sdincer@science.ankara.edu.tr

© 2012 Bulgarian Academy of Sciences, Union of Chemists in Bulgaria

procedure; 5-amino-1-methyl-1*H*-benzimidazole was obtained as a yellow solid after recrystallization from ethanol, m.p. 158–159ºC, yield 0.98 g (67 %).

1-[(1-Methyl-1H-benzimidazol-5-yl)diazenyl]naphthalen-2-ol ***3***

5-Amino-1-methyl-1*H*-benzimidazole (10 mmol) was stirred at 0-5 °C into nitrosyl sulfuric acid prepared from sodium nitrite (0.7 g) and concentrated H_2SO_4 (10 mL). After diazotizing, a 5% solution of naphthalen-2-ol in 2 N NaOH was added. By adjusting the pH to 6.0–6.5, the crude product was precipitated, filtered and recrystallized from ethanol. The compound **3** was obtained as a dark-red solid, decomp. > 340 ºC, yield 2.5 g (79 %) (scheme II).

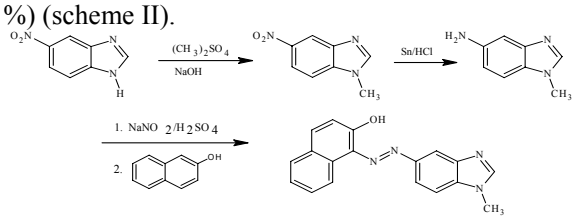

Scheme II. Synthesis of 5-amino-1-methyl-1*H*-benzimidazole and 1-[(1-methyl- 1*H*-benzimidazol-5-yl)diazenyl]naphthalen-2-ol

RESULTS AND DISCUSSION

The ^{1}H NMR, UV-vis and IR spectra of the azonaphthol derivatives were interpreted in respect of their azoenol-ketohydrazone tautomeric behavior in solution and in solid state. The mass spectra helped to throw light on these structures in gas phase, excluding external factors like solvents and intermolecular interactions.

^{1}H NMR spectra

The basic structure required for tautomerism is the existence of a labile proton in the molecule. This attitude is observed as azoenol ketohydrazone tautomerization in azonaphthol compounds containing hydroxy group conjugated with azo group as shown below.

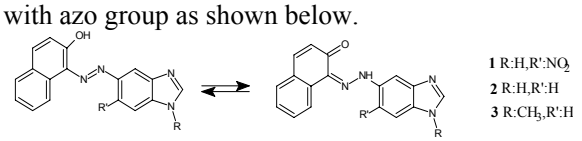

Tautomerisation of the azonaphthol derivatives of benzimidazole

The equilibrium between azoenol and ketohydrazone tautomers changed rapidly and the nature of the substituents in the phenyl ring affected the position of the equilibrium. Using ^{1}H NMR spectroscopy it was possible to decide the position of the labile hydrogen atom in the molecule and determine the ratio of tautomers present at the equilibrium depending on the intensity of the signals which are proportional to the molar amounts of the compounds.

The examination of the ^{1}H NMR spectra of the three azonaphthol compounds, measured in d_6-DMSO shows that the equilibrium between azoenol and ketohydrazone tautomers is predominantly shifted to the ketohydrazone form. The analysis also revealed that the nitro group attached to C(6) in the benzimidazole ring slightly shifted the tautomeric equilibrium towards the azoenol form because of the change in π electron configuration depending on the resonance in the benzimidazole ring.

The enumeration of atoms is shown below and the chemical shifts and coupling constants are presented in Table I. Multiplicity of signals is presented as: (s) singlet, (d) doublet, (t) triplet, (m) multiplet, (b) broad.

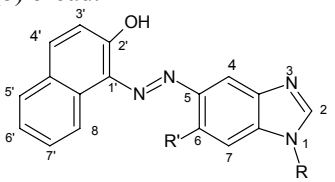

The enumeration of atoms

Table I. ^{1}H chemical shifts δ/ppm, and coupling constants J/Hz of azonaphthols

Compound	δ/ppm, J/Hz
	16.36, s; 12.60, b; 9.70, b; 8.57, s; 8.49, s; 8.29, s; 7.95, d, 8 Hz; 7.75, d, 9 Hz; 7.60-7.00, m; 6.79, d, 8 Hz
	15.35, s; 12.80, b; 12.20, b; 8.53, d, 3 Hz; 8.45, s; 8.00, d, 9 Hz; 7.98, d, 9 Hz; 7.85, d, 9 Hz; 7.66, t, 7 Hz; 7.60-7.90, m; 7.47, t, 7 Hz; 6.85, d, 9 Hz
	15.32, s; 13.20, b; 8.73, d, 7 Hz; 8.18, s; 7.12, d, 9 Hz; 7.99, d, 9 Hz; 7.76, d, 9 Hz; 7.70-7.90, m; 7.68, t, 8 Hz; 7.49, t, 8 Hz; 3.92

In all cases, in the spectra there is a signal in the range of 15.32–16.36 ppm corresponding tothe –N<u>H</u>-N= hydrazone protons. The broad peaks appearing at 12.60–13.20 ppm indicate –O<u>H</u> protons. The peaks observed between ca. 6.79 and 9.70 ppm are related to aromatic protons and their integration agrees with the number of protons for each compound.

UV-vis spectra

The UV spectra of the azonaphtol derivatives **1**, **2** and **3** show that ketohydrazone tautomers

predominantly exist in methanol solution. The strong band appearing at 480–500 nm indicates the presence of the ketohydrazone form while the band related to the azoenol form apparently disappeared. Using dichloromethane as a solvent with corresponding decrease in polarity, no absorption band about 400 nm was observed which proves that these compounds exist in azoenol form in non-polar solvents. It is suggested that the tautomerism strongly depends on solvent polarity causing intermolecular or intramolecular hydrogen bonding. Therefore, the ketohydrazone form can be stabilized by hydrogen bonding with polar solvents and when hydrogen bonding is not possible, the azoenol form is stabilized by intramolecular hydrogen bonding as shown below.

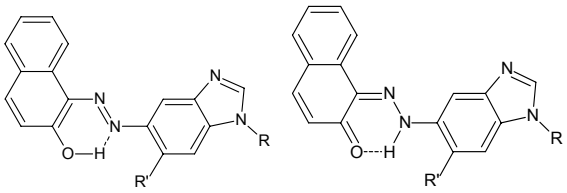

Intramolecular hydrogen bond in O–H.....N and N–H.....O forms

IR spectra

In all cases, the $\nu_{O\text{-}H}$ absorption bands observed around 3200-3000 cm^{-1}, are shifted to lower values as a result of the intramolecular hydrogen bond in the O-H.N form. This bonding favors the shift of the tautomeric equilibrium on the ketohydrazone side. The observation of $\nu_{C\text{-}O}$ phenolic absorption bands at 1320, 1300 and 1342 cm^{-1} for the compounds **1**, **2** and **3**, respectively, supported the existence of a ketohydrazone tautomer including an intra- molecular hydrogen bond in the N..O in the solid state. $\nu_{C=O}$ absorption bands confirming this structure are not distinguishable because of the overlapping with $\nu_{C=N}$ imine absorption band of the benzimidazole ring.

Mass spectra

Mass spectra of the azonaphthol derivatives of benzimidazoles were also interpreted in respect of their tautomeric behavior. The spectra resemble each other revealing the preference of the azoenol tautomeric form in the equilibrium. The formation of a ketohydrazone tautomer by the hydroxy group in *ortho* position affected the fragmentation pathways in mass spectrometry [14–17]. The ketohydrazone tautomer shows a cleavage of the single HN-N= bond, whereas the =N-C(napht) bond in the azoenol form should be preferably broken. The proposed fragmentation pathways are given in schemes III, IV and V.

Electron-impact (EI) fragmentation of this azonaphthol derivatives gives rise to the major ions $M^{+\cdot}\rightarrow(m/z\ 190)^{+}\rightarrow(m/z\ 163)^{+}\rightarrow(m/z\ 144)^{+}\rightarrow(m/z\ 115)^{+}$ for the compound **1** (scheme III) and $M^{+\cdot}\rightarrow(m/z\ 145)^{+}\rightarrow(m/z\ 115)^{+}$ for **2** (scheme IV) which corresponds to cleavage of the =N-C(napht) single bond.

The existence of the azoenol form of **1** was particularly supported by the $(M\text{-}190)^{+}$ ion of the major decomposition. The cleavage of the (benz) –N=N-C(napht) bonds occurred as indicated above depending on the electron donating power of the naphthalene ring [18–21]. On the other hand, the ion peaks $(m/z\ 178)^{+}\rightarrow(m/z\ 132)^{+}$ and $(m/z\ 157)^{+}$ in the mass spectra of **1** point to a minor fragmentation process of the ketohydrazone form due to the nitro group at *ortho* position.

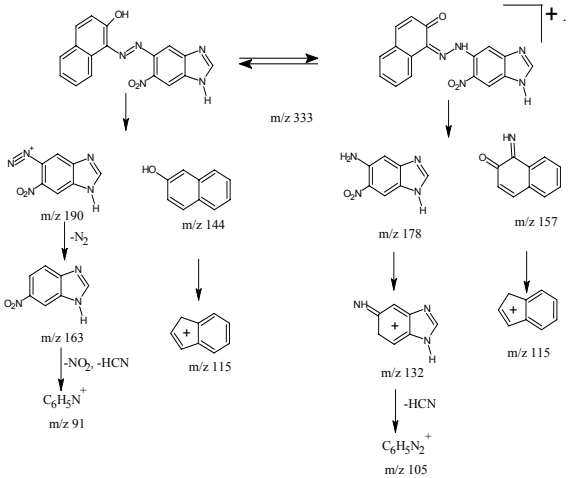

Scheme III. Proposed fragmentation pathway for compound **1**

In addition, the comparison of the abundances of the ion $(m/z\ 144)^{+}$ in the spectra of these compounds suggested that the azoenol tautomer dominates in the gas phase for **2** rather than for **1,** probably due to the resonance effect.

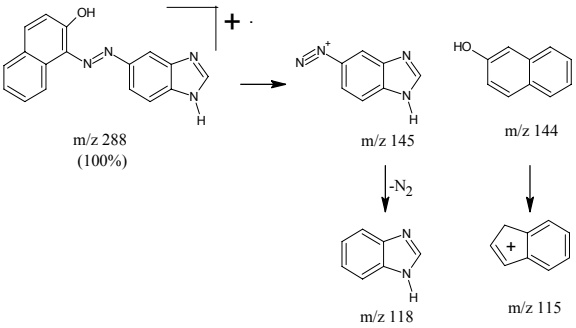

Scheme IV. Proposed fragmentation pathway for compound **2**

The main reaction observed in the mass spectra of the compound **3** is $(M+23)^{+\cdot} \rightarrow$ (m/z 288)$^{+}\rightarrow$(m/z 260)$^{+}\rightarrow$(m/z 144)$^{+}\rightarrow$(m/z 115)$^{+}$. The major ion at (m/z 288) corresponds to the loss of Na and -CH_3. The ion peak at (m/z 260) may be attributed to the proposed azoenol type fragmentation including N_2 loss. The ion peak (m/z 115) dominates in the spectrum and the ion peak observed at (m/z 144) confirms the cleavage of the azoenol tautomeric form (scheme V).

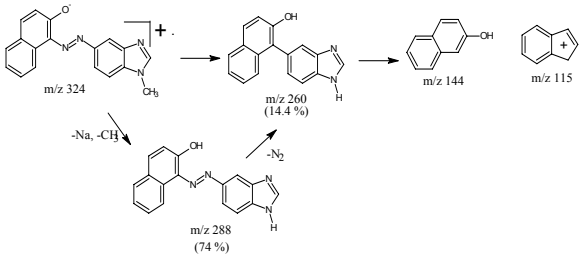

Scheme V. Proposed fragmentation pathway for compound **3.**

CONCLUSION

Three azonaphthol derivatives of benzimidazole were studied in respect of azoenol ⇄ ketohydrazone tautomerism using ^{1}H NMR, UV-vis, IR and mass spectroscopy. The results show that the ketohydrazone tautomeric form is predominant in solution and in solid state while the tautomeric equilibrium is on the azoenol side in gas phase.

REFERENCES

1. A. D. Towns, *Dyes and Pigments,* **42**, 3 (1999).
2. H. Zollinger, *Color Chemistry, VCH:New York,* 1987.
3. P. Gordon and P.Gregory, *Organic Chemistry in Color,* Springer-Verlag, Berlin, 1983.
4. H. Durr and H. Bouas-Laurenet, *Photochromism*: Molecules and Systems, Elsevier, Amsterdam, 1990.
5. A. Lyca, *Dyes and Pigments,* **43**, 27 (1999).
6. T. D. Klots, P. Devlin, W. B. Collier, *Spectrochim. Acta A,* **53,** 2445 (1997).
7. N. Sundaraganesan, S. Ilkiamani, P. Subramani and B. D. Joshua, *Spectrochim. Acta A***, 67**, 628 (2007).
8. K. Yamamoto, K. Nakai, T. Kawaguchi, *Dyes & Pigments,* **11,** 173 (1989).
9. R. M. Claramunt, C. Lopez, M. D. Santa Maria, D. Sanz, J. Elguero, *Progress in Nuclear Magnetic Resonance Spectroscopy,* **49**, 169 (2006).
10. K. Kobayashi, K. Kurihara, K. Hirose, *Bull. Chem. Soc. Jap.,* **45,** 3551 (1972).
11. T. Nishiwaki, *J. Chem. Soc. (C),* 428 (1968).
12. P. E. Allegretti, M. Schiavoni, E. A. Castro and J. J. P. Furlong, *World J. Chem.* **2**, 25 (2007).
13. S. Dincer, *Dyes and Pigments,* **53**, 263 (2002).
14. D. Nedeltcheva, B. Damyanova, S. Popov, *J. Mol. Struct.***, 749**, 36 (2005).
15. S.O. Lawesson, G. Schroll, H.J. Bowie, *Tetrahedron,* **24**, 1875 (1968).
16. A.G. Sullivan, R. Garner, S.J. Gaskell, *Rapid Commun. Mass Spectrom.,* 12, 1207 (1998).
17. H. C. Joshi, F. S. Kamounah, G. van der Zwan, C. Gooijer, L. Antonov, *J. Chem. Soc. Perkin Trans,* **12**, 2303 (2001).
18. H. C. Joshi, F. S. Kamounah, G. van der Zwan, C. Gooijer, L. Antonov, *J. Photochem. Photobiol.,* **152,** 183 (2002).
19. L. Antonov, S. Kawauchi, M. Satoh, J. Komiyama, *Dyes and Pigments,* **38**, 157 (1998).
20. L. Antonov, S. Kawauchi, M. Satoh, J. Komiyama, *Dyes and Pigments,* **40**, 163 (1999).
21. A. J. Borgerding, R. A. Hites, *J. Amer. Soc. Mass Spectrom.,* **5**, 1994, 407.

ИЗСЛЕДВАНЕ НА ТАВТОМЕРИЯТА ПРИ АЗОНАФТОЛОВИТЕ ПРОИЗВОДНИ НА БЕНЗИМИДАЗОЛИТЕ

С. Динджер

Департамент по химия, Университет в Анкара,Турция

Постъпила на 11 януари, 2011 г.; приета на 6 декември, 2011 г.

(Резюме)

Тавтомерното поведение на три азонафтолови производни на бензимидазолите (1-[(6-нитро-1*H*-бензимидазол-5-ил)диазенил]нафтален-2-ол, 1-[1*H*- бензимидазол -5-илдиазенил]нафтален-2-ол и 1-[(1-метил-1*H*-бензимидазол-5-ил)диазенил]нафтален-2-ол, е изследвано в разтвор, в твърдо състояние и в газова фаза с помощта на спектроскопски методи. Резултатите показват, че кетохидразонът преобладава в разтовора и в твърд състояние, докато в газова фаза равновесието е изтеглено към азоенолната форма.

Bulgarian Chemical Communications, Volume 44, Number 1 (pp. 74 – 82) 2012

Spectroscopic and thermal studies of perylene charge-transfer complexes

M.S. Refat[a,b*], H.M.A. Killa[c], A. El-Maghraby [b], M.Y. El-Sayed[c]

[a] *Department of Chemistry, Faculty of Science, Port Said University, Egypt*
[b] *Department of Chemistry, Faculty of Science, Taif University, 888 Taif, Kingdom Saudi Arabia*
[c] *Department of Chemistry, Faculty of Science, Zagazig, Zagazig University, Egypt*

Received January 14, 2011; revised April 21, 2011

Charge-transfer (CT) complexes formed between perylene (Pery) as donor with iodine (I_2), piciric acid (PA) and chloranilic acid (CLA) as acceptors were studied spectrophotometrically. The synthesis and characterization of perylene CT complexes of iodine, $[(Pery)_2]I^+.I_3^-$, picric acid, [(Pery)(PA)] and chloranilic acid, [(Pery)(CLA)] were described. These complexes were readily prepared by the reaction of Pery with I_2, PA and CLA using $CHCl_3$ as a solvent. The IR, UV-Vis and ^{1}HNMR spectral techniques, as well as elemental analysis (carbon, hydrogen and nitrogen contents) and thermal analysis were used to characterize the three perylene charge-transfer complexes. Benesi-Hildebrand method and its modification were applied to the determination of association constant (K) and molar absorption coefficient (ε).

Keywords: Perylene, charge-transfer complexes, picric acid, chloranilic acid, iodine, thermal studies.

1. INTRODUCTION

Charge-transfer materials have attracted broad interest in the recent years due to their efficiency in the field of magnetic, electrical conductivity and optical properties [1, 2]. Generally, charge-transfer complexes play an important role in biological systems as well as in the field of drug receptor binding mechanisms [3, 4]. The solid charge-transfer complexes formed between iodine and several types of electron donors such as aromatic hydrocarbons, polycyclic amines, mixed oxygen/nitrogen cyclic bases, aromatic/aliphatic amines have been studied and categorized [5–13]. The tri-iodide ion I_3^-, penta-iodide ion I_5^-, and ennea-iodide ion I_9^- were formed through the reaction of iodine with various donors like metal acetylacetonates [14–16], polyazacyclic [17–19], and crown ethers [20–23]. Some charge-transfer complexes show very interesting applications in the analysis of drugs in pure form or in pharmaceutical preparations [24, 25]. The charge-transfer (CT) in fullerene-based [26, 27] compounds is currently of great interest since these materials can be utilized as superconductors [28] and to produce non-linear optical activity [29]. In this paper the charge-transfer complexes obtained by the interactions of perylene (Pery) as a donor with σ-acceptors, like iodine and π-acceptors such as picric acid (PA) and chloranilic acid (CLA) were studied spectrophotometrically. The obtained data point to the formation of new and interesting CT complexes of the general formula $[(Pery)_2]I^+.I_3^-$ and [(Pery)(π-acceptor)].

2. MATERIALS AND METHODS

The general chemical structures of donor and acceptors are given in Fig. 1.

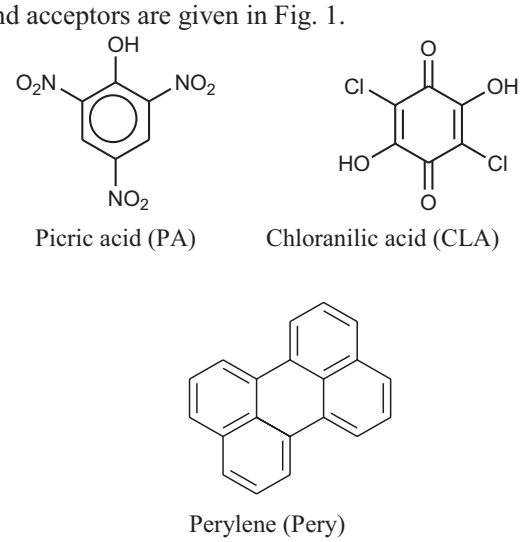

Fig. 1. General chemical structure of donors and acceptors

2.1. Perylene charge-transfer complexes

The solid CT complexes of Pery with π-acceptors like CLA and PA and σ-acceptors like I_2 were prepared by mixing 1 mmol of the donor in chloroform (10 ml) with 1 mmol of each acceptor

* To whom all correspondence should be sent:
E-mail: msrefat@yahoo.com

© 2012 Bulgarian Academy of Sciences, Union of Chemists in Bulgaria

in the same solvent with constant stirring for about 15 min. The solutions were allowed to evaporate slowly at room temperature; the resulting solid complexes were filtered and washed several times with little amount of solvent and dried under vacuum over anhydrous calcium chloride. The CT complexes: [(Pery)/(CLA)] (orange) with empirical formula $C_{26}H_{14}O_4Cl_2$; [(Pery)/(PA)] (yellow-green) with empirical formula $C_{26}H_{15}O_7N_3$ and [(Pery)/(I_2)] (yellow) were formed.

2.2. Electronic Spectra

The electronic spectra of the donors, acceptors and the resulting CT complexes were recorded in the region of (200–800 nm) using a Jenway 6405 spectrophotometer with quartz cells of 1.0 cm pathlength. The electronic (UV/vis) absorption spectrum of the iodine complex was measured in chloroform. The complex was formed by adding X ml of 5.0×10^{-4} M I_2 (X = 0.25, 0.50, 0.75, 1.00, 1.50, 2.00, 2.50 and 3.00 ml) to 1.00 ml of 5.0×10^{-4} M Pery. The volume of the mixture in each case was completed to 10 ml with the used solvent. The concentration of Pery in the reaction mixture was kept fixed at 0.5×10^{-4} M while the concentration of iodine was varied over the range from 0.125×10^{-4} M to 1.50×10^{-4} M. These concentrations produced donor:I_2 ratios in the range from 1:0.25 to 1:3.00.

Photometric titrations were performed [30] at 25ºC for the reactions of Pery with σ- or π-acceptor in methanol and/or chloroform as follow:

The concentration of the donor in the reaction mixtures was kept fixed at 1.0×10^{-4} M, while the concentration of acceptors (I_2, PA or CLA) were changed over a wide range from 0.25×10^{-4} to 4.00×10^{-4} M, which produced solutions with donor:acceptor molar ratios varying from 1: 0.25 to 1: 4.00.

2.3. Infrared Spectra

The infrared spectra of the reactants and the resulting CT complexes were recorded in KBr discs on a Bruker IFS 113V FT–IR spectrometer, in the wavenumber range (4000–400 cm^{-1}).

2.4. ^{1}H-NMR spectra

^{1}H-NMR spectra were obtained on a Varian spectrometer Gemini 200 MHz using d_6–DMSO as a solvent.

2.5. Thermal analysis

Thermogravimetric analysis (TGA) was performed on a Shimadzu TGA 50H instrument., 2-5 mg samples were heated in standard platinum TGA pans from 25°C to 600°C at a rate of 10°C/ min under nitrogen flow rate of 30 ml/min. The amount and weight change of each obtained compound were recorded as a function of temperature to determine thermal stability.

3. RESULTS AND DISCUSSION

Elemental analysis data of all perylene charge-transfer complexes are listed in Table 1. From this table, it can be seen that the data are in a good agreement with the calculated ones, and the composition of the CT complexes matched the molar ratios deduced from the photometric titration of Pery and the acceptors (σ- and π- acceptor).

Table 1: Elemental analysis CHN and physical parameters of the CT complexes formed in the reaction of Pery with iodine, CLA, and PA.

Complexes (FW)	M.wt	C%		H%		N%		Physical data	
		Found	Calc.	Found	Calc.	Found	Calc.	Color	Λm ($\Omega^{-1}cm^{-1}$ mol^{-1})
$[(Pery)_2]I^+.I_3^-$ ($C_{40}H_{242}I_4$)	1012	47.12	47.43	2.29	2.37	-	-	Violet red	49
[(Pery)(CLA)] ($C_{26}H_{14}Cl_2O_4$)	460	67.48	67.83	2.98	3.04	-	-	Red	10
[(Pery)(PA)] ($C_{26}H_{15}N_3O_7$)	481	64.59	64.86	3.08	3.12	7.92	8.73	Red	16

Table 2 Spectrophotometric data for the Pery-iodine CT-complex

Complex	λ_{max} nm	E_{CT}	K $l.mol^{-1}$	ε_{max} $l.mol^{-1}.cm^{-1}$	$f \times 10^2$	M (Debyes)	I_p (eV)
(Pery)2]I+.I_3^-	350	3.55	2.63×104	6.29×104	0.80	77.1	7.65

3.1. Iodine/Pery charge-transfer complex

The conductivity data confirm that this complex has a positive (I^+) and negative (I_3^-) charge resulting from the associated triiodide ion in accordance with the CT transition. The electronic absorption spectra of the 1:1 ratio in $CHCl_3$ together with those of the reactants I_2 and Pery are shown in Fig. 2. The spectra show two absorption bands which are not present in the spectra of the free reactants iodine and Pery. These bands at 350 and 293 nm are assigned to the CT complex formed by the reaction of Pery with I_2 in chloroform solvent. Photometric titration curves based on these two absorption bands are given in Fig. 3.

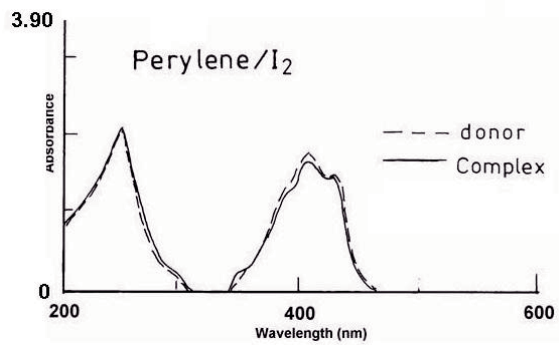

Fig. 2. Electronic absorption spectra of Pery/iodine reaction in $CHCl_3$.

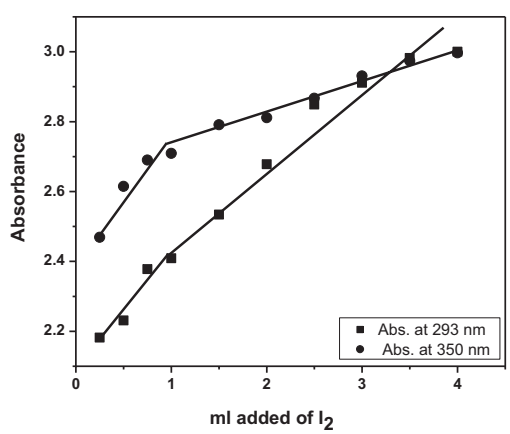

Fig. 3. Photometric titration curves for Pery/iodine system in $CHCl_3$ at 293 and 350 nm.

These photometric titration curves were obtained according to known methods [30] by plotting absorbance against ml added acceptor. The equivalence points shown in these curves clearly indicate that the formed CT complex between Pery and iodine is 1:1. The formation of 1:1 complex was supported by both elemental analysis and thermal measurements. However, the two absorption bands around 360 and 290 nm are well known [31–33] to be characteristic for the formation of the triiodide ion (I_3^-). Accordingly, the formed complex was formulated as $[(Pery)]_2I^+.I_3^-$.

It was of interest to observe that the solvent has a pronounced effect on the spectral intensities of the formed $[(Pery)]_2I^+.I_3^-$ complex. To study the stability of the Pery/iodine complex, it was necessary to calculate the values of the association constant, K, the molar absorption coefficient ε, and the oscillator strength, f, of the iodine complex. The 1:1 modified Benesi-Hildebrand equation [34] was used in the calculations.

$$\frac{C_a^o C_d^o l}{A} = \frac{1}{K\varepsilon} + \frac{C_a^o + C_d^o}{\varepsilon} \qquad (1)$$

where C_a^o and C_d^o are the initial concentrations of the acceptor (I_2) and the donor (Pery), respectively, and A is the absorbance of the strong bands around 290 and 360 nm. When the $C_a^o . C_d^o/A$ values are plotted against the corresponding $C_a^o + C_d^o$ values, straight lines were obtained with a slope of 1/ε and intercept of 1/kε. The oscillator strength f was obtained from the approximate formula in the equation of Tsubomura and Lang [35]. The oscillator strength values together with the corresponding energy of charge-transfer interaction, E_{CT}, ionization potential, I_p and dipole moment, μ are given in Table 2. The trend of the values in this Table reveals several facts.

The $[(Pery)_2]I^+.I_3^-$ complex shows high values of both the association constant (K) and the molar absorption coefficient (ε). This high value of K reflects the high stability of the iodine complex as a result of the expected high donation ability of Pery (five aromatic rings).

The high value of K agrees quite well with the existence of the tri-iodide ion, I_3^-, which is known to have high absorptivity value [31–33].

Finally, a general mechanism for the formation of the $[(Pery)_2]I^+.I_3^-$ complex is proposed, as follows:

$$2[Pery]+I_2 \rightarrow [Pery]_2I^+.I^-$$

$$[Pery]_2I^+.\ I^- + I_2 \rightarrow [Pery]_2I^+.I_3^-$$

The mid infrared spectra of Pery and the formed CT-complex, $[Pery]_2I^+.I_3^-$ were recorded as KBr discs. The spectral bands, resolved and assigned into their vibrational modes are given in Table 3.

As expected, the bands characteristic for the Pery unit in $[Pery]_2I^+.I_3^-$ are shown with small changes in band intensities and frequency values of aromatic ring and phenyl groups. This proves that the charge-transfer transition occurs from the aromatic ring to iodine (π–σ*).

Table 3. Infrared frequencies[(a)] (cm^{-1}) and tentative assignments for the Pery donor and $[(Pery)_2]I^+.I_3^-$ complex.

Pery	$[(Pery)_2]I^+.I_3^-$	Assignments[(b)]
3431 s,br	3434 s,br	$\nu_{(OH)}$; H_2O of KBr
3045 s	3046 ms	$\nu_{(CH)}$; □aromatic
2929 ms	2922 mw	
1653 ms	1647 w	$\nu_{(C=C)}$; aromatic
1516 ms	1605 mw	
1491 m	1590 w	Phenyl
1374 m	1529 w	
1327 m	1493 s	
1282 m	1379 w	
1210 m	1320 w	
	1213 w	
796 vs	810 vs	Aromatic rings
765 vs	765 vs	

Table 4. Maximum temperature, T_{max}/°C, and weight loss values of the decomposition stages for the $[(Pery)_2]I^+.I_3^-$ complex.

Decomposition	T_{max}/°C	Lost species	%weight losse	
			Found	Calc.
First stage	92°C	I_2	24.67%	25.10%
Second stage	291°C	I_2 + 2Pery moieties	72.44%	74.90%
Total loss			97.11%	100%
Residue		residual carbon	2.89%	0.00%

The far infrared spectrum of $[Pery]_2I^+.I_3^-$ was recorded in Nujol mulls dispersed on polyethylene windows in the region 50–400 cm^{-1}. The spectrum associated with the $[Pery]_2I^+.I_3^-$complex shows the characteristic bands for the triiodide ion, I_3^- at 135, 100 and 67 cm^{-1}. These bands can be assigned to the ν_s(I–I), A_1, ν_{as}(I-I), B_2 and $\delta(I_3^-)$, A_1, respectively. These three absorptions do not exist in the spectrum of the donor, Pery. However, the I_3^- ion may be linear ($D_{\infty h}$) or non-linear (C_{2v}). Group theoretical analysis indicates that the I_3^- with C_{2v} symmetry displays three vibrations ν_s(I–I), A_1, ν_{as}(I-I), B_2 and $\delta(I_3^-)$, A_1, all infrared active in agreement [31, 36, 37] with the observed three infrared bands for $[Pery]_2I^+.I_3^-$. Accordingly, the formed iodine complex is formulated as $[Pery]_2I^+.I_3^-$. The conversion of iodine molecules into polyiodide units is well known in the literature [31, 36, 37].

To confirm the proposed formula and structure of the new $[Pery]_2I^+.I_3^-$ complex, thermogravimetric analysis (TG/DTG) was carried out for this complex under N_2 flow. TGA thermograms and DTG curves are shown in Fig. 4. Table 4 gives the maximum temperature values, T_{max}/°C, together with the corresponding weight loss for each step of the degradation reactions of this complex. The obtained data strongly support the structure proposed for the complex under investigation as follows. The thermal decomposition of the Pery-iodine CT complex in inert atmosphere proceeds approximately with two main degradation steps (Fig. 4).

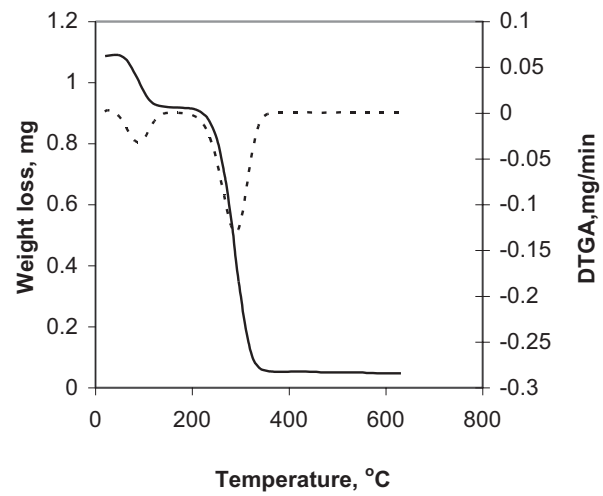

Fig. 4. TGA/DTG thermal diagram of $[(Pery)_2]I^+.I_3^-$ CT complex;(□) – TGA; (…) – DTGA.

The first stage of degradation at 92°C is accompanied by a weight loss of 24.67% corresponding to the loss of one iodine molecule. Theoretically, the loss of this molecule corresponds to a weight loss of 25.10%. The second decomposition stage occurs at a maximum temperature of 291°C. The weight loss associated with this step (72.44%), can be due to the loss of the second iodine molecule besides the organic moieties of two perylene molecules, in good agreement with the theoretical weight loss values of 74.90%. Accordingly, the mechanism for the thermal decomposition of the complex, $[Pery]_2I^+.I_3^-$ is proposed as follows:

$$[(Pery)_2]I^+.I_3^- \xrightarrow{92^oC} [(Pery)_2]I_2 + I_2$$

$$[(Pery)_2]I_2 \xrightarrow{291^oC} 2Pery + I_2$$

In recent years there has been increasing interest in determining the rate dependent parameters of solid-state non-isothermal decomposition reactions by analysis of the TG curves. Several equations [38–45] have been proposed as means of analyzing

a TG curve and obtaining values for kinetic parameters.

In the present investigation the general thermal behavior of the Pery/iodine CT complex in terms of stability ranges, peak temperatures and values of

Table 5. Kinetic and thermodynamic data of the $[(Pery)_2]I^+.I_3^-$ CT complex at the essential stage.

Complex	Parameters*	Coats-Redfern equation
$[(Pery)_2]I^+.I_3^-$	E	67.8
	A	$3.98x10^{+10}$
	ΔS	-23.1
	ΔH	56.8
	ΔG	49.8
	r	0.9954

*Units of parameters: E in $KJmole^{-1}$, A in s^{-1}, ΔS in $Jmole^{-1}K^{-1}$, ΔH and ΔG in $KJmole^{-1}$

kinetic parameters, is summarized in Table 5. The kinetic parameters E and Z were evaluated using Coats-Redfern equation. The kinetic parameters, ΔH, ΔS and ΔG are tabulated in Table 6. Taking the main decomposition steps as a criterion, the values of the activation entropies, (–ΔS) in this complex indicate that the activated complex has a more ordered structure than the reactants. ΔG is positive for a reaction for which ΔH is positive and ΔS is negative. The reactions for which ΔG is positive and ΔS is negative are considered as unfavorable or non-spontaneous. Reactions are classified as either exothermic (ΔH < 0) or endothermic (ΔH > 0) on the basis of whether they give off or absorb heat. Reactions can also be classified as exergonic (ΔG < 0) or endergonic (ΔG > 0) on the basis of whether the free energy of the system decreases or increases during the reaction. The correlation coefficients of the Arrhenius plots of the thermal decomposition steps were found to lie closer to the value 0.9954, showing a good fit with a linear function. It is clear that the thermal decomposition process of the iodine complex is non-spontaneous, i.e., the complex is thermally stable.

3.2. π–acceptors/Pery charge-transfer complexes

The electronic absorption spectra of the reactants, Pery (1.0×10^{-4} M) and the acceptors CLA and PA (1.0×10^{-4} M) in $CHCl_3$ along with those of the formed 1:1 CT complexes are shown in Fig. 5 (A and B). The spectra demonstrate that the formed CT complexes have absorption bands at 300 nm for [(Pery)(CLA)] and 348 nm for [(Pery)(PA)] complexes. These bands are located as hypsochromic behavior in the spectra of the CT products rather than reactants. The stoichiometry of the Pery-acceptor reactions was shown in all cases to be of ratio 1:1. The 1:1 stoichiometry was strongly supported by the photometric titration

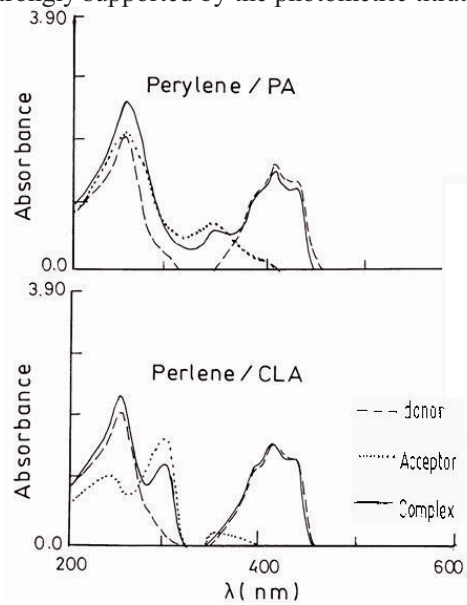

Fig. 5. Electronic absorption spectra of: (A): Pery/CLA and (B): Pery/PA reactions in $CHCl_3$

measurements as well. In these measurements, the concentration of Pery was kept fixed, while the concentration of the acceptors was varied over the range from 0.25×10^{-4} M to 3.00×10^{-4} M. Photometric titration curves based on these measurements are shown in Fig. 6 (A and B). The Pery-acceptors equivalence points indicate that the Pery: acceptor ratio in all cases is 1:1 and this result agrees quite well with the elemental analysis and infrared spectra of the solid CT complexes. Accordingly, the CT complexes formed upon reaction of Pery as a donor with the π-acceptors under investigation in chloroform have the general formula [(Pery)(acceptor)]. The 1:1 modified Benesi-Hildebrand method [34] was used in calculating the values of the association constant, K and the molar absorption coefficient, ε. The spectral data of the two Pery CT complexes are given in Table 6. These complexes show high values of both the association constant (K) and the molar absorption coefficients (ε). These high values of K confirm the expected high stability of the formed CT complexes as a result of the expected high donation power of Pery as a chromophore system containing a conjugated structure (C=C). The equilibrium constants are strongly dependent on the nature of the used acceptor including the type of electron withdrawing substituents, such as nitro and halo groups.

Table 6. Spectrophotometric results for the CT complexes of (A): [(Pery)(CLA)] and (B): [(Pery)(PA)].

Solvent	λ_{max} (nm)	E_{CT} (eV)	K ($l.mol^{-1}$)	ε_{max} ($l.mol^{-1}.cm^{-1}$)	f x 10^{+2}	M (Debyes)	I_p (eV)
A	300	4.14	117 x 10^{+2}	132 x 10^{+2}	0.142	30.10	8.01
B	348	3.57	117 x 10^{+2}	264 x 10^{+2}	0.246	42.40	7.61

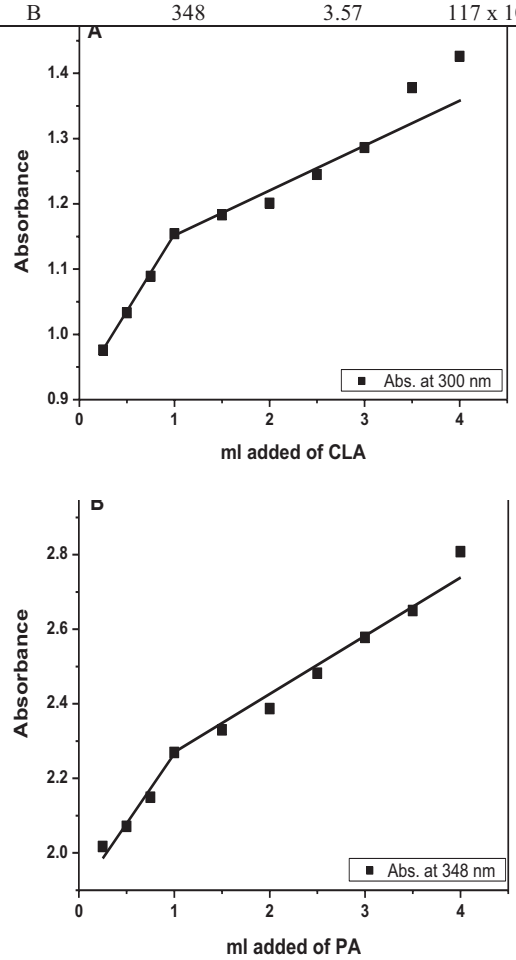

Fig. 6. Photometric titration curves for (A): Pery/CLA and (B): Pery/PA reactions in $CHCl_3$ at 300 and 348 nm, respectively.

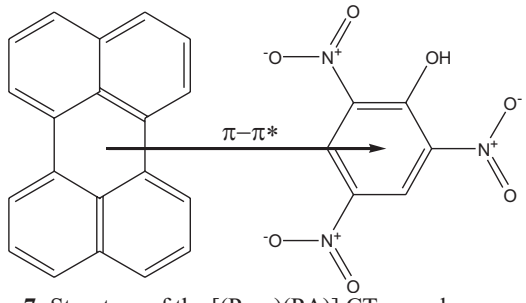

Fig. 7: Structure of the [(Pery)(PA)] CT complex

Full assignments for the infrared bands of [(Pery)(π-acceptor)] CT complexes are given in Table 7. A comparison of the relevant IR spectral bands of the free donor, Pery and acceptors (CLA and PA) with the corresponding ones appearing in the IR spectra of the isolated CT complexes clearly indicated that the characteristic bands of Pery show some shift in the frequencies, as well as some change in their band intensities. This could be

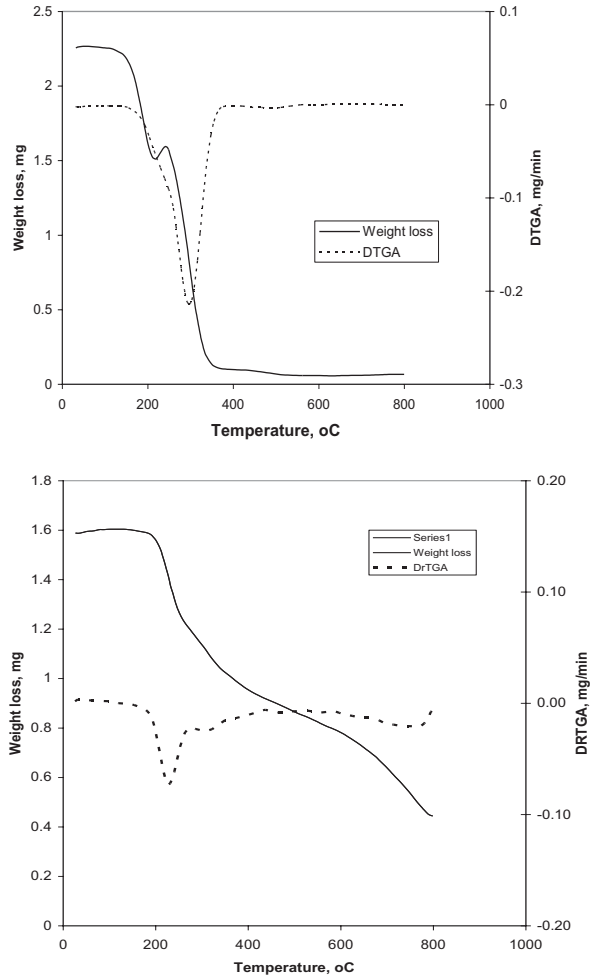

Fig. 8. TGA/DTG thermal diagrams of: (A): [(Pery)(CLA)] and (B): [(Pery)(PA)] CT complexes.

attributed to the expected symmetry and electronic structure changes upon formation of the CT complex. Moreover, the IR spectra of the molecular complexes of CLA and PA with Pery indicate that the ν(C-Cl) and ν(NO_2) of the free acceptors (CLA and PA) are generally shifted to lower wavenumber values upon complexation. Thus we can conclude that the molecular complexes are formed through π–π* charge migration from HOMO of the donor to the LUMO of the acceptor (Fig. 7).

The ^{1}HNMR spectrum of the [(Pery)(PA)] CT complex in d_6-DMSO displayed distinct signals with appropriate singlet and multiplets. The singlet accounting for the proton centered at δ 3.40 (1H; OH) is assigned to the proton of the phenolic group of picric acid; the other multiplet peaks at δ 7.30–8.40 ppm are due to protons of the aromatic groups of Pery and PA. The decrease in the intensities of hydrogen protons of Pery and PA proved that the CT interaction occurred.

Thermogravimetric analysis (TGA and DTG) was carried out in dynamic nitrogen atmosphere (30 ml/min) with a heating rate of 10 ºC/min using a Shimadzu TGA-50H thermal analyzer. CLA and PA complexes of Pery were studied by thermogravimetric analysis from ambient temperature to 800°C in nitrogen atmosphere. The TG curves were redrawn as % mass loss *vs.* temperature curves. Typical TG curves are presented in Fig. 8 (A and B), and the temperature ranges and percentage mass losses of the decomposition reaction are given in Table 8 together with evolved moiety and the theoretical percentage mass losses. The overall mass loss from the TG curves is 97.16% for Pery/CLA and 72.75% for Pery/PA complexes. All complexes show two peaks of mass loss. The first and the second peak are due to the decomposition of the acceptors and the Pery moieties. The final products were polluted with carbon.

Table 7. Infrared frequencies[(a)] (cm^{-1}) and tentative assignments for CLA, PA, [(Pery)(CLA)] and [(Pery)(PA)] compounds.

CLA	PA	Pery/CLA	Pery/PA	Assignments
3235 s, br	3416 br	3234 vs	3435 s,br	ν(O-H); H-bonded
	3103 ms	3046 m	3104 s	ν(C-H); aromatic
			3056 vw	
---	2980 sh	2924 vw	2920 vw	ν_s(C-H)
	2872 w			ν_{as}(C-H)
1664 ms	1861 ms	1866 vw	1613 s	ν(C=O); NO_2 of PA
1630 vs	1632 vs	1782 w	1605 vs	ν(C=C)
	1608 vs	1663 s	1590 w	Ring breathing bands
	1529 vs	1630 vs	1516 s	
		1542 vw		
---	1432 s	1491 s	1492 ms	C-H deformation
1368 s	1343 ms	1369 vs	1410 ms	ν(C-C)
1263 vs	1312 w	1265 vs	1378 s	ν(C-N)
1207 w	1263 w	1210 s	1365 w	ν(C-O)
1168 w	1150 ms	1184 w	1339 vs	Phenyl
	1086 s		1305 s	
			1277 s	
			1216 s	
			1184 w	
			1149 s	
			1078 s	
981 vs	917 vs	982 vs	938 ms	(C-H) bend
851 vs	829 w	851 s	914 vs	Aromatic rings
		809 vs	817 vs	
752 vs	781 s	763 vs	770 s	Skeletal vibrations
690 vs	732 s	692 s	729 s	
	703 s	570 s		
	652 sh			
569 vs	522 ms	541 w	544 ms	δ(ONO); PA
			419 w	CNC deformation

Thermal analysis curves of the Pery complexes show that decomposition takes place in two stages in the temperature range between 100–400 ºC for the Pery/CLA complex and between 150-800°C for the Pery/PA complex (Fig. 8 A and B). The two endothermic decomposition stages correspond to decomposition of the donor and acceptors. The TG curves of the two complexes show weight losses (Found 97.16, Calcd. 97.39%) for the Pery/CLA complex and (Found 72.75%, Calcd. 72.65%) for the Pery/PA complex corresponding to the loss of $C_{24}H_{14}O_4Cl_2$ organic moiety and $C_{15}H_{15}N_3O_7$ organic moiety for Pery/CLA and Pery/PA complexes, respectively. The final product formed at 800°C is residual carbon. Reported data on thermal analysis studies in nitrogen atmosphere indicate that the two Pery complexes decompose to give a number of remaining carbons according to the acceptor.

Table 8. Maximum temperature, T_{max}/ºC, and weight loss values of the decomposition stages for the [(Pery)(CLA)] and [(Pery)(PA)] compounds.

Decomposition of [(Pery)(CLA)]	T_{max}/ºC	Lost species	%weight losses	
			Found	Calc.
First stage	219ºC	$C_{24}H_{14}O_4Cl_2$	97.16%	97.39%
Second stage	299ºC			
Total loss			97.16%	97.39%
Residue		Carbon residual	2.84%	2.61%
Decomposition of [(Pery)(PA)]	**T_{max}/ºC**	**Lost species**	**%weight losses**	
			Found	Calc.
First stage	230ºC			
Second stage	325ºC	$C_{15}H_{15}N_3O_7$	72.75%	72.65%
Total loss			72.75%	72.65%
Residue		Carbon residual	27.25%	27.35%

The kinetic and thermodynamic parameters of the decomposition of the Pery complexes, namely, activation energy (*E*), enthalpy (Δ*H*), entropy (Δ*S*) and free energy of decomposition (Δ*G*) as well as the pre-exponential factors (*A*) were evaluated graphically using the Coats-Redfern relationship. A plot of $\ln\left[\frac{-\ln(1-\alpha)}{T^2}\right]$ against $1/T$ gives a slope

from which E was calculated and Z (Arrhenius constant) was determined from the intercept. The entropy of activation (ΔS), enthalpy of activation (ΔH*) and the free energy changes of activation (ΔG) were calculated using the following equations:

$$\Delta H = E - RT_m \; ; \Delta G = \Delta H - T_m \Delta S$$

The calculated values of E, Z, ΔS, ΔH and ΔG for the decomposition steps are given in Table 9. On comparing the activation energy of the first stage of decomposition for the two CT complexes, the order of the activation energy values of the different acceptors was PA>CLA. This difference may be due to the reactivity of the complexes and the electronic configuration of the acceptors attached to Pery. These results agree well with those of the TG analysis detailed above. The ΔS values of the main stage for all complexes were found to be negative, indicating that the activated complex was more ordered than the reactants.

Table 9. Kinetic and thermodynamic parameters data of (I): [(Pery)(CLA)] and (II): [(Pery)(PA)] compounds.

Compounds	Parameter					r
	E / $kJmol^{-1}$	Z / s^{-1}	ΔS / $Jmol^{-1}K^{-1}$	ΔH / $kJmol^{-1}$	ΔG / $kJmol^{-1}$	
I	101	4.53×10^{8}	–83.5	97.1	139	0.9940
II	48	2.89×10^{4}	–161	45.5	106	0.9887

CONCLUSION

Perylene, as a powerful laser dye, formed stable intermolecular CT complexes with the electron acceptors iodine (I_2), picric acid (PA) and chloranilic acid (CLA) in $CHCl_3$. The stoichiometry of the present CT complexation determined by the molar ratio method showed that association was in 1:1 molecular ratio. The equilibrium constants, K, and molar absorption coefficients, ε, of the complexes were determined by the Benesi-Hildebrand method. The increase in the K values reflected the high stability of the Pery charge-transfer complexes as a result of the expected high donation power of Pery (five aromatic rings). The activation of enthalpies and entropies of Pery complexes were calculated utilizing Coats-Redfern equation. The entropies were more negative, suggesting that the formation of Pery charge-transfer complexes is favored at low temperatures and the complexes are more ordered than the reactants.

REFERENCES

1. J. Ulanskki, *Synth. Met*., **39**, 13 (1990).
2. H.A. Hashem, M.S. Refat, *Surf. Rev. Lett*., **13**, 439 (2006).
3. R.S. Mandal, C.J. Lahiri, *Indian Chem. Soc.*, **76,** 347 (1999).
4. Feng, J., Zhong, H., Xuebau, B D., *Ziran Kexueban*, **27**, 691 (1999).
5. P. Pal, T.N. Misra, *J. Phys. D: Appl. Phys*., **23**, 218 (1990).
6. C.D. Bryan, A.W. Cordes, R.C. Haddon, R.G. Hicks, R.T. Oakley, T.T., Palstra, A.S. Perel, S.R. Scottla, *Chem. Mater*., **6**, 508 (1994).
7. G.G. Roberts, D. G. Thomas, *J. Phys. C: Solid State Phys*., **7,** 2312 (1974).
8. H. Kusama, H. Sugihara, *Solar Energy Mat. & Solar Cells*, **90**, 953 (2006).
9. H.M.A. Salman, M.R. Mahmoud, M.H.M. Abou-El-Wafa, U.M. Rabie, R.H. Crabtree, *Inorg. Chem. Comm*., **7**, 1209, (2004).
10. N.A. Al-Hashimi, *Spectrochim. Acta Part A*, **60**, 2181 (2004).
11. Kh.A. Hassan, *Spectrochim. Acta Part A*, **60**, 3059 (2004).
12. L.I. Bebawy, N. El-Kousy, J.K. Suddik, M. Shokry, *J. Pharm. Biomedical Ana*l., **21**, 133 (1999).
13. M.M. Ayad, *Spectrochim. Acta Part A*, **50**, 671 (1994).
14. S.M. Teleb, M.S. Refat, *Spectrochimica Acta Part A,* **60**, 1579 (2004).
15. N. Kulevsky, K.N. Butamina, *Spectrochim. Acta*., **46A**, 79 (1990).
16. E.M. Nour, S.M. Teleb, M.A.F. Elmosallamy, M.S. Refat, *S. Afr. J. Chem.,* **56**, 10 (2003).
17. E.M. Nour, L. Shahada, *Spectrochim. Acta Part A*, **44**, 1277 (1988).
18. L. Shahada, S. Alkaabi, E.M. Nour, *Acta Chim. Hung*., **127**, 297 (1990).
19. E.M. Nour, S.M. Metwally, M.A.F. El-Mosallamy, Y. Gameel, *Spectrosc. Lett*., **30**, 1109 (1997).
20. S.R. Salman, S.M. Al-Marsumi, *Spectrochim. Acta Part A*, **49**, 435 (1993).
21. M. Shamsipur, M.H. Mashhadizadeh, *J. Incl. Phenom.*, **38**, 277 (2000).
22. A. Semmani, M. Shamsipur, *J. Chem. Soc., Dalton Trans.*, 2215 (1996).
23. W. Hirsch, J. Greenman, R. Pizer,. *Can. J. Chem*., **71**, 2171 (1993).
24. G.A. Saleh, H.F. Askal, M.F. Radwan, M.A. Omar, *Talanta*, **54**, 1205 (2001).
25. H. Salem, *J. Pharm. Biomedical Anal.*, **29**, 527 (2002).
26. H.W. Kroto, J.R. Heath, S.C. O'Brien, R.F. Smalley, *Nature*, **318**, 162 (1985).
27. E. Rohlfing, A. Kaldor, A. *J. Chem. Phys*., **8**, 13322 (1984).
28. M. Ricco, M. Bissbiglia, R. Derenzi, R., F. Bolzoni, *Solid State Comm*., **101**, 413 (1997).

29. F. Kajzar, Y. Okada-Shudo, C. Meritt, Z. Kafafi, *Synth. Methods*, **94**, 91 (1998).
30. D.A. Skoog, "Principle of Instrumental Analysis", 3rd ed., Saunder College Publishing, New York, (Chapter 7) (1985).
31. W. Kiefer, H.J. Bernstein, *Chem. Phys. Lett*., **16**, 5 (1972).
32. J. Andrews, E.S. Prochaska, A. Loewenschuss, *Inorg. Chem*., **19**, 463 (1980).
33. K. Kaya, N. Mikami, Y. Udagawa, M. Ito, *Chem. Phys. Lett*., **16**, 151 (1972).
34. R. Abu-Eittah, F. Al-Sugeir, *Can. J. Chem*., **54**, 3705 (1976).
35. H. Tsubomura, R. Lang, *J. Am. Chem. So*c., **86**, 3930 (1964).
36. A.G. Maki, R. Forneris, *Spectrochim. Acta*, **23A**, 867 (1967).
37. F.W. Parrett, N.J. Taylor, *J. Inorg. Nucl. Chem.*, **32**, 2458 (1970).
38. E.S. Freeman, B. Carroll, *J. Phys. Chem*., **62,** 394 (1958).
39. J. Sestak, V. Satava, W.W. Wendlandt, *Thermochim. Acta*, **7**, 333 (1973).
40. W. Coats, W., J.P. Redfern,. *Nature*, **201**, 68 (1964).
41. T. Ozawa, *Bull. Chem. Soc. Jpn*., **38**, 1881 (1965).
42. W.W. Wendlant, "Thermal Methods of Analysis", Wiley, New York, (1974).
43. H.W. Horowitz, G. Metzger, *Anal. Chem*., **35**, 1464 (1963).
44. J.H. Flynn, L.A. Wall, *Polym. Lett*., **4**, 323 (1966).
45. P. Kofstad, *Nature*, **179**, 1362 (1957).

СПЕКТРОСКОПСКИ И ТЕРМИЧНИ ИЗСЛЕДВАНИЯ НА ПЕРИЛЕНОВИ КОМПЛЕКСИ С ПРЕНОС НА ЗАРЯД

М.С. Рефат [a, b], Х.М.А. Кила[c], А. Ел-Маграби[b], М.И. Ел-Сайед[c]

[a)] *Департамент по химия, Факултет за наука, Университет в Порт-Саид, Египет*

[b] *Департамент по химия, Факултет за наука, Университет в Таиф, Кралство Саудитска Арабия*
[c] *Департамент по химия, Факултет за наука, Университет в Загозиг, Египет*

Постъпила на 14 януари,.2011 г.; коригирана на 21 април, 2011 г.

Изследвани са спектроскопски комплексите с пренос на заряд, образувани между перилен като донор с йод, пикринова киселина и хлоранилова киселина. Описани са синтезите и охарактеризирането на тези комплекси. Те се приготвят лесно, като за разтворител се използва хлороформ. Използвани са инфра-червена, UV-Vis and ^{1}H-ядрено-магнитно-резонансна спектроскопия, елементен анализ (за въглерод, водород и азот) както и термогравиметричен анализ за охарактеризиране на трите комплекса. Приложен е методът на Benesi-Hildebrand и негова модификация за определянето на асоциационната константа (K) и моларния абсорбционен коефициент (ε).

Bulgarian Chemical Communications, Volume 44, Number 1 (pp. 83 – 86) 2012

A facile synthesis of an indol-dihydrotestosterone succinate derivative

Lauro Figueroa-Valverde[1], Francisco Díaz-Cedillo[2], Elodia García-Cervera[1]

[1]*Lab. Farmacoquímica, Facultad de Ciencias Químico-Biológicas, Universidad Autónoma de Campeche, Av. Agustín Melgar, Col Buenavista C.P.24039 Campeche Cam., México.*
[2]*Esc. Nal. de Ciencias Biológicas del Instituto Politécnico Nacional. Prol. Carpio y Plan de Ayala s/n Col. Santo Tomas, México, D.F. C.P. 11340.*

Received March 4, 2011; Accepted June 20, 2011

In this study, an indol-dihydrotestosterone succinate derivative (**4**) was synthesized. The first stage, involved the preparation of an indol-dihydrotestosterone derivative (**3**) by the reaction of dihydrotestosterone (**1**) with phenylhydrazine using hydrochloric acid as catalyst. The second stage was achieved by reacting **3** with anhydride succinic or succinic acid to form an indol-dihydrotestosterone succinate derivative (**4**).

Keywords: dihydrotestosterone, phenylhydrazine, succinate.

INTRODUCTION

There are several methods for the synthesis de indoles; for example, the preparation of 2-Substituted Indoles by Photostimulated Reactions of *o*-Iodoanilines with Carbanions[1]. Other reports show the preparation of a series of benzonitrile derivatives on position 6 or 4 of indole ring via a Leimgruber-Batcho reaction[2]. In addition, other studies showed that ruthenium catalyzed synthesis of indoles from N-substituted anilines and alkanolamines[3]. Other data show the synthesis of 2-substituted indoles from 2-ethynylanilines with tetrabutylammonium fluoride[4]. It is important to mention, that has been development several indoles steroid derivatives, for example, the synthesis of 17-indazole androstene derivatives[5] using dehydroepiandrosterone acetate as substrate. Other data showed the procedure for synthesis of 1'-Methylindolo (3',2':2, 3)2(5a)-androsten-17-one which was prepared by the Fischer indole synthesis[6]. Additionally, other studies show the synthesis of 1′*H*-5α-Cholest-2-eno[3,2–*b*]indoles using the Fisher reaction[7]. All these works show several procedures are available for synthesis of several indol-compounds derivatives; nevertheless, expensive reagents and special conditions are required. In this study, an indol-dihydrotestosterone succinate derivative (**4**) was synthetized; the first stage was achieved by reacting dihydrotestosterone (**1**) with phenylhydrazine (**2**) in presence of hydrochloric acid to form 3-indole-dihydrotestosterone derivative (**3**); the second stage was achieved by reacting **3** with anhydride succinic or succinic acid to form **4**.

EXPERIMENTAL

General methods

Dihydrotestosterone and the other compounds evaluated in this study were purchased from Sigma-Aldrich Co., Ltd. The melting points for the different compounds were determined on an Electrothermal (900 model). Infrared spectra (IR) were recorded using KBr pellets on a Perkin Elmer Lambda 40 spectrometer. ^{1}H and ^{13}C NMR spectra were recorded on a Varian VXR–300/5 FT NMR spectrometer at 300 and 75.4 MHz in $CDCl_3$ using TMS as internal standard. EIMS spectra were obtained with a Finnigan Trace GCPolaris Q. spectrometer. Elementary analysis data were acquired from a Perkin Elmer Ser. II CHNS/0 2400 elemental analyzer.

10,13-Dimethyl-4,5,6,7,8,9,10,11,12,13,14,15,16,17-tetradecahydro-1H-8-aza-inden [2,3,b]cyclo-penta[a]phenanthren-17-ol (3).

A solution of 100 mg dihydrotestosterone (0.34 mmol), 60 mg phenylhydrazine (0.55 mmol) in 10 mL of ethanol was stirred for 10 min at room temperature. Then 0.5 mL of hydrochloric acid was added and the mixture was stirred for 48 h at room temperature. The reaction mixture was evaporated to a smaller volume, diluted with water, and extracted with chloroform. The organic phase was evaporated to dryness under reduced pressure, the residue was purified by crystallization from methanol-water (3:1) yielding 75% of product;

* To whom all correspondence should be sent:
E-mail: lauro_1999@yahoo.com

© 2012 Bulgarian Academy of Sciences, Union of Chemists in Bulgaria

m.p.: 192-194 ºC; IR: V_{max} = 3,330, 3119 cm^{-1}; ^1H NMR (300 MHz, $CDCl_3$) δ_H; 0.76 (s, 3H), 0.78 (s, 3H), 0.98–1.13 (m, 4H), 1.30–1.46 (m, 6H), 1.55-1.93 (m, 7H), 2.23–2.61 (m, 4H), 4.01 (m, 1H), 7.09 (m, 1H), 7.18 (m, 1H), 7.36 (m, 1H), 7.42 (m, 2H), 7.49 (broad, 2H) ppm. ^{13} C NMR (75.4 Hz, $CDCl_3$) δ_C; 11.12 (**C**–26), 12.40 (**C**–25), 20.60 (**C**–16), 23.83 (**C**–20), 24.05 (**C**–24), 29.48 (**C**–12), 31.02 (**C**–21), 31.96 (**C**–13), 33.68 (**C**-9), 35.60 (**C**–14), 37.03 (**C**–17), 37.79 (**C**–10), 40.55 (**C**–11), 43.93 (**C**-18), 51.44 (**C**–19), 54.76 (**C**–15), 76.86 (**C**–22), 105.72 (**C**–3), 110.56 (**C**–8), 117.63 (**C**-6), 118.21 (**C**–5), 120.79 (**C**–4), 126.65 (**C**–7), 133.72 (**C**–23), 135.33 (**C**–2) ppm. EI-MS *m/z:* 363.16 (M^+ 13), 237.34, 129.16. Anal. Calcd for $C_{25}H_{33}NO$: C, 82.60; H, 9.15, N, 3.85; O, 4.44. Found: C, 82.60; H, 9.12

Succinic acid mono-(10, 13-Dimethyl-4,5,6,7,8,9,10,11,12,13,14,15,16,17-tetradeca-hydro-1H-8-aza-inden[2,3,b]cyclopenta[a]phenanthren-17-yl)ester (4).

Method A

The compound **3** (100 mg, 0.27 mmol) was added to a solution of 54 mg anhydride succinic (0.54 mmol), 3 mL of pyridine in 10 mL of toluene was gently refluxed for 8 h, and then cooled to room temperature. The reaction mixture was evaporated to a smaller volume, diluted with water, and extracted with chloroform. The organic phase was evaporated to dryness under reduced pressure. The residue was purified by crystallization from hexane:methanol:water (1:2:1) yielding 78% of product **4**. m.p.: 158–160 ºC; IR: V_{max} = 3,326, 1,615, 1,712 cm-1; ^1H NMR (300 MHz, $CDCl_3$) δ_H; 0.78 (s, 3H), 0.80 (s, 3H), 1.01–1.14 (m, 4H), 1.30-1.46 (m, 3H), 1.51–1.64 (m, 5H), 1.70–1.93 (m, 3H), 2.23–2.48 (m, 4H), 2.52 (t, 2H, J = 6.0 Mhz) 2.54 (t, 2H, J = 6.0 Mhz), 2.66 (m, 1H), 4.68 (m, 1H), 7.09 (m, 1H), 7.18 (m, 1H), 7.36 (m, 1H), 7.42 (m, 2H), 9.40 (broad, 2H) ppm. ^{13}C NMR (75.4 Hz, $CDCl_3$) δ_C; 12.08 (**C**-25), 12.10 (**C**–26), 20.60 (**C**-16), 23.83 (**C**–20), 24.05 (**C**–24), 27.60 (**C**–21), 29.20 (**C**-12), 29.48 (**C**-30, **C**–31), 31.96 (**C**–13), 33.68 (**C**–9), 35.60 (**C**–14), 37.03 (**C**–17), 37.79 (**C**–10), 40.55 (**C**–11), 43.93 (**C**–18), 51.44 (**C**–19), 54.76 (**C**–15), 79.80 (**C**–22), 105.72 (**C**–3), 110.56 (**C**–8), 117.63 (**C**–6), 118.21 (**C**–5), 120.79 (**C**–4), 126.65 (**C**–7), 133.72 (**C**–23), 135.33 (**C**–2), 171.80 (**C**–32), 173.60 (**C**–28) ppm. EI-MS *m/z:* 463.20 (M^+ 13). Anal. Calcd. for $C_{29}H_{37}NO_4$: C, 75.13; H, 8.04, N, 3.02; O, 13.80. Found: C, 75.10; H, 8.00

Method B

The compound **3** (100 mg, 0.27 mmol) was added to a solution of 65 mg succinic acid (0.55 mmol) and 100 mg 1,3-dicyclohexylcarbodiimide (0.48 mmol) in 15 cm3 acetonitrile-water (3:1) and 69 mg *p*-toluenesulfonic acid monohydrate (0.36 mmol) was added and the mixture was stirred at room temperature for 72 h. The solvent was then removed under vacuum and the crude product was purified by crystallization from methanol-hexane-water (3:2:1) yielding 78% of product. Similar ^1H NMR and ^{13}C NMR data were obtained compared with method A product.

RESULTS AND DISCUSSION

In this study, an indol-dihydrotestosterone succinate derivative (**4**) was synthetized; the first stage involves the synthesis of an indol-dihydrotestosterone derivative (**3**). It is important to mention that several protocols have been development for preparation of indol derivatives, nevertheless different protocols suffers from several drawbacks; 1) The products of reaction have limited stability and 2) the need to use hazardous reagents for their preparation[8,12]. In this study, the compound **3** was synthetized by reacting dihydrotestosterone (**1**) with phenylhydrazine (**2**) in presence of hydrochloric acid to form 3-indole-dihydrotestosterone derivative; (Figure 1, see). ^1H NMR spectra of **3** showed chemical shifts at 0.76 and 0.78 ppm for methyls present in the steroid nucleus. In addition, other signals at 0.98-4.01 ppm for hydrogens involved in the steroid nucleus were found. Other signals at 7.09-7.42 ppm for methylenes involved in the phenyl group were display. Finally, a signal at 7.49 ppm for protons involved in both amine and hydroxyl groups were found. The ^{13}C NMR spectra display chemical shifts at 11.12 and 12.40 ppm for the carbons of methyls presents in the steroid nucleus of **3**. Another chemical shifts at 20.60-76.86 ppm for carbons of methylenes involved in the steroid nucleus were exhibited. Finally, several signals at 105.72-135.33 ppm for carbons corresponding to methylenes involved in the indol group were found. The presence of **3** was further confirmed from mass spectrum which showed a molecular ion at *m/z* 363.16.

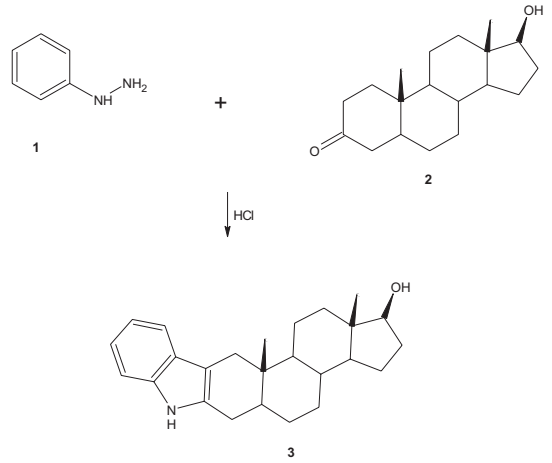

Fig. 1. Synthesis of an indol-dihydrotestosterone derivative (**3**). Reaction of dihydrotestosterone (**2**) with phenylhydrazine (**1**) using hydrochloric acid as catalyst to form of **3**.

On the other hand, the second stage was achieved by the synthesis of **4** which contains in the D-ring of the steroid nucleus an arm with ester functional group coupled to the steroid nucleus of **4**. It is important to mention, that there are diverse reagents to produce esters derivatives, nevertheless; most of the conventional methods have found only a limited use for this purpose[13,14]. In this study, two different methods were used; in the first step the technique reported by Figueroa and coworkers[15] for esterification of steroids using the compound **3**, succinic anhydride and pyridine (method A) for ester bond formation en the new arm bound to nucleus steroid in the compound **4** (Figure 2, see)

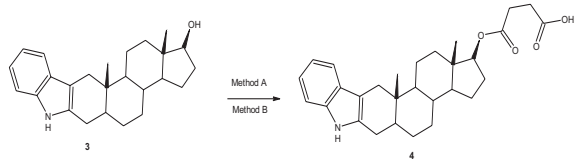

Fig. 2. Synthesis of an indol-dihydrotestosterone succinate derivative (**4**). Method A. Reaction of **3** with anhydride succinic using as catalyst pyridine to form **4**; Method B. Reaction of **3** with succinic anhydride using as catalyst 1,3-dicyclohexylcarbodiimide in presence of *p*-toluenesulfonic acid monohydrate to form **4**.

was used; in the second step was achieved by the reaction of **3** with succinic acid in presence of 1,3-dicyclohexylcarbodiimide to form **4** (method B). It is important to mention that during recent years, some carbodiimides derivatives such as the dicyclohexylcarbodiimide (DCC) have attracted increasing attention as condensing agents in ester synthesis[16,17]. Nevertheless, it is important to mention that when dicyclohexylcarbodiimide is used as condensing agent in esters synthesis, yields of the esters are often unsatisfactory because of formation of the N-acylurea derivative as by-product. Some reports reveal that addition of a catalytic amount of a strong acid to the esterification reaction in the presence of dicyclohexylcarbodiimide considerably increases the yield of esters and reduces the formation of the N-acylurea compound[18]. For this reason, esterification of the hydroxyl group of **3** with succinic acid in the presence of dicyclohexylcarbodiimide and *p*-toluenesulfonic acid (Scheme 2) was used to increase the yield of **4**. It was found that the use of carbodiimide derivative results in higher yields compared to the ester bond formed with method A.

The results indicate that ^{1}H NMR spectrum of **4** showed signals at 0.78 and 0.80 ppm for methyls present in the steroid nucleus. Additionally, other signals at 1.01–2.48, 2.66 and 4.68 ppm for hydrogens involved in the steroid nucleus were found. Other signals at 2.52–2.54 ppm for methylenes involved in arm bound to steroid nucleus of **4**; at 7.09–7.42 ppm for phenyl group were display. Finally, a signal at 9.40 ppm for both amine and hydroxyl groups were found. The ^{13}C NMR spectra display chemical shifts at 12.08 and 12.10 ppm for the carbons of methyls presents in the steroid nucleus of **4**. Other chemical shifts at 20.60–29.20 and 31.96–79.80 ppm for carbons of methylenes involved steroid nucleus; at 29.48 ppm for methylenes involved in arm bound to steroid nucleus were exhibited. Finally, other signals at 105.72–135.33 ppm for indol group; at 171.80 ppm for carboxyl group and at 173.80 ppm for ester group were exhibited. The presence of **4** was further confirmed from mass spectrum which showed a molecular ion at *m/z* 463.20.

CONCLUSIONS

In this work, we report an easy methodology to synthesize indol-dihydrotestosterone succinate derivative.

REFERENCES

1. S. Barolo, A. Lukach, R. Rossi. *J. Org. Chem.*, **68,** 2807 (2003).
2. 2M. Lézé, A. Palusczak, R. Hartmann, M. Borgne. *Bioorg. Med. Chem.. Lett.*, **18**, 4713 (2008).
3. D. Lee, C. Cho, J. Kim, Y. Youn, S. Shim, H. Song H. *Bull. Korean Chem. Soc.*, **17**, 1132 (1996).
4. A.Yasuhara, Y. Kanamori, M. Kaneko, A. Numata, Y. Kondo, T. Sakamoto. *J. Chem. Soc. Perkin Trans.,* **4**, 529 (1999).
5. M. Vania, T. Vasaitis, V. Njar, R. Salvador. *Steroids.*, **72**, 939 (2007).

6. R. Haugland, J. Yguerabide, L. Stryer. PNAS**, 63,** 23 (1969).
7. J. Samu, J. Botyánszki, H. Duddeck, G. Snatzke,, *Liebigs Ann. Chem*., **11**, 1225 (1993).
8. P. Kutschy, M. Dzurilla, M. Takasugi, A. Sabová, *Coll. Czech. Chem. Commun.*, **64**, 348 (1999).
9. H. Zhang, H. Ye, A. Moretto, K. Brumfield, B. Maryanoff., *Org. Lett.*, **2**, 89 (2000).
10. M. Chiara I. Candiani, G. Visentin, W. Cabri, F. Zarini, N. Mongelli, A. Bedeschi. *Tetraedron Lett*., **38**, 2307 (1997).
11. H. Kusama, J. Takaya, N. Iwasawa. *J. Am. Chem. Soc*., **124**, 11592 (2002).
12. G. Humphrey, J. Kuethe *J. Chem. Rev.*, **106**, 2875 (2006).
13. O. Yellin. J. *Lipid Reserch*., **13**, 554 (1972).
14. S. Bernês, H. Torrens, G. López, A. Buttenklepper. *Acta Cryst*., **E59,** 1372 (2003).
15. L. Figueroa-Valverde, F. Díaz-Cedillo, L. Tolosa, G. Maldonado, G. Ceballos G., *J. Mexican. Chem. Soc.*, **50**, 42 (2006).
16. H. Zhu, F. Yang, J. Tang, M. He. *Green Chem*., **5**, 38 (2003).
17. F. Kurzer, K. Douraghi-Zadeh., *Chem. Rev*., **67**, 107 (1967).
18. E. Felder, U. Tiepolo, A. Mengassini A. *J. Chromatogr*. **82**, 291 (1973).

ЛЕСНА СИНТЕЗА НА ПРОИЗВОДНО НА ИНДОЛ-ДИХИДРОТЕСТОСТЕРОН СУКЦИНАТА

Л. Фигероа-Валверде[1], Ф. Диас-Седильо[2], Е.Гарсиа-Сервера[1]

[1]*Лаборатория по фармацевтична химия, Факултет по химико-биологични науки, Автономен университет на Кампече, Мексико*
[2]*Висше училище по биологични науки, Национален политехнически институт, Санто Томас, Мексико*

Постъпила на 4 март, 2011 г.; приета на 20 юни, 2011 г.

Синтезирано е производно на индол-дихидротестостерон сукцината (**4**). В първия етап, свързан с приготвянето на производното на индол-дихидротестостерона (**3**) чрез реакцията с дихидротестостерон (**1**) с фенилхидразин с хлороводород като катализатор. Вторият етап се извършва, като **3** реагира с янтарен анхидрид или с янтарна киселина и се получава производното на индол-дихидротестостерон сукцината (**4**).

Bulgarian Chemical Communications, Volume 44, Number 1 (pp. 87 – 91) 2012

Novel catalyst of mixed SiO_2-TiO_2 supported tungsten for metathesis of ethene and 2-butene

S. Chaemchuen[1], W. Limsangkass[1], B. Netiworaraksa[1], S. Phatanasri[1*], N. Sae-Ma[1], K. Suriye[2]

[1]*Center of Excellence on Catalysis and Catalytic Reaction Engineering, Department of Chemical Engineering, Faculty of Engineering, Chulalongkorn University, Bangkok 10330, Thailand*
[2]*SCG Chemicals Co., Ltd. 1 Siam-cement Rd, Bang sue, Bangkok 10800, Thailand*

Received March 8, 2011; Revised May 9, 2011

Mixed SiO_2-TiO_2 supported tungsten catalysts containing 8 wt.% tungsten were prepared by incipient wetness impregnation. The catalyst with 10% TiO_2 addition, designated as WO_3/SiO_2-10Ti, displayed improved conversion and propylene selectivity, 72 % and 48 %, respectively, toward metathesis of ethylene and 2-butene compared with conventional silica supported tungsten without TiO_2 addition. The better dispersion of tungsten achieved by TiO_2 addition and the tetrahedral tungsten oxide species of relatively high surface were believed to be responsible for the good metathesis activity of the catalyst for propylene formation.

Keyword: Metathesis**,** Silica-Titania, Mixed support, Tungsten

1. INTRODUCTION

Recently, there has been an ever increasing demand of polypropylene owing to the considerable growth of propylene production [1–2]. One of the pathways for propylene production is the metathesis reaction of ethene and 2-butene using suitable catalysts [3-4]. Supported WO_3 catalysts are known from several patents and publications where well dispersed low-loaded WO_3/SiO_2 catalysts have been claimed to have activity equal to that of catalysts of appreciable higher tungsten content. This points to the importance of obtaining a well dispersed catalyst [5–7].

Verpoort *et al.* [8-12] have made extensive studies on olefin metathesis catalysts relating to the catalytic activity of supported tungsten phenoxide complexes, activation and characteristics of a 'molecular' tungsten unit on silica and have found that the catalytic activity was related to the structure of the molecular entities on the surface of the precursor. Many researchers have tried to improve the catalyst performance by using composite supports, such as Al_2O_3–SiO_2 [13], Al_2O_3–B_2O_3 [14–15], and Al_2O_3–P_2O_5 [16]. Recently, SiO_2-TiO_2 mixed oxides were used as the support material for Pt [17–19], Er [20], Au[21], Ni [22], Fe–Pt [23] and Mo [24] metals in many reactions. It was found that the presence of a mixed oxide support has great effect on the dispersion of the active components and their catalytic performances. Therefore, the objective of this work was to investigate the effect of mixed SiO_2–TiO_2 supported tungsten catalysts with 8 wt% metal loading on the catalytic performance in propylene production by metathesis.

2. EXPERIMENTAL

2.1 Catalysts Synthesis

SiO_2-TiO_2 mixed oxide supports were prepared by physical mixing of silica gel, Davisil grade 646 (pore volume: 1.15 cm^3/g, supplied by Aldrich) and titania (Degussa P25). The catalysts were impregnated with an aqueous solution of metatungstate hydrate (Aldrich, 99.9%), to yield an 8 wt% loading on the mixed oxide support, then dried at 110 ºC overnight. The catalysts were calcined at 550 ºC for 8 h with a heating rate of 10 ºC/min in an air atmosphere. These prepared catalysts are denoted as WO_3/ SiO_2–xTi, where x indicates the wt. % of TiO_2 (5, 10, 30) in the SiO_2–TiO_2 support.

2.2 Catalyst Characterization

Surface areas of the samples were determined using a multipoint BET method. The catalyst samples were degassed at 300ºC and 10^{-3} mm Hg for 3 h. Adsorption measurements were carried out using liquid nitrogen at –196ºC with a Micromeritics ASAP 2020 device. The Raman spectra of the samples were collected by projecting a continuous wave YAG laser of Nd (810 nm)

* To whom all correspondence should be sent:
E-mail: s_phatanasri@yahoo.com

© 2012 Bulgarian Academy of Sciences, Union of Chemists in Bulgaria

through the samples at room temperature. A scanning range of 200–1400 cm^{-1} with a resolution of 2 cm^{-1} was applied. Phase identification and investigation of the crystallite samples was performed by X-ray diffraction (Siemens D5000) using Ni filter Cu Kα radiation from 10º to 60º.

2.3 Reaction Studies

The catalyst sample was placed at the center of a reactor with inner diameter (ID) of 7.5 mm. The catalyst was pretreated at 500 ºC in nitrogen flow for 1 h before allowing the catalyst to cool down in an inert atmosphere to the reaction temperature 400 ºC. The reaction conditions were as follows: pressure=0.1MPa, C_2H_4/trans-2–C_4H_8=2. The sampling was made at 8 h on stream, and sample analysis was performed on a Shimadzu GC 2014 equipment with a column of packed 10% silicone SE–30 (3.02 m with 0.53 mm ID) and a FID detector using helium as the carrier gas (5 ml/min).

3. RESULTS AND DISCUSSION

The catalysts performance on the metathesis activity of ethene and trans-2-butene is shown in Table 1. and Fig. 1. It was found that both conversion of 2-butene and propylene selectivity increased with TiO_2 addition and as high as 72% of conversion of 2-butene and 48% of propylene selectivity were obtained on a 10% TiO_2-containing catalyst designated as WO_3/SiO_2-10Ti. However, the side reaction of isomerization to 1-butene, cis-2-butene and butadiene became more competitive with the 30% TiO_2-containing catalyst, and almost no propylene formation was observed on the silica-free TiO_2 supported tungsten catalyst. According to XRD patterns of the relevant catalysts shown in Fig. 2, peaks characteristic to tungsten crystallites at 2θ of 23.12, 23.60 and 24.38º were observed while silica is almost amorphous. It was noticed that lower peak intensities in this region corresponding to a lower amount of tungsten crystallites were discernible upon increasing the amount of TiO_2, and those peaks almost disappeared for the silica-free TiO_2 supported tungsten catalyst. This indicates the higher dispersion of tungsten species on the mixed SiO_2-TiO_2 support. Nevertheless, the intrinsic lower surface of TiO_2 seemed to result in a lower BET surface of the mixed SiO_2-TiO_2 supported tungsten catalysts with a high loading of TiO_2, as shown in Table 1. The marked increase in both conversion of 2-butene and propylene selectivity on WO_3/SiO_2–10Ti may be attributed to the higher dispersion of tungsten resulting from TiO_2 addition. However, the metathesis activity site for propylene formation on the 30% TiO_2-containing catalyst, WO_3/SiO_2–30Ti, tends to be overshadowed by the TiO_2-related secondary reaction sites for 1-butene, cis-2-butene and butadiene formation.

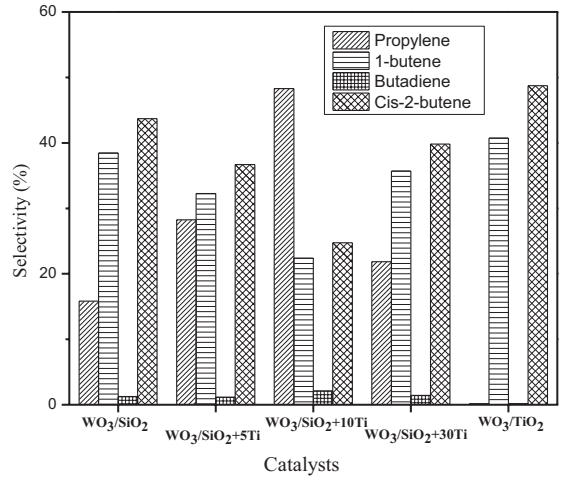

Fig.1. The product distribution of different catalysts after 8 h on stream.

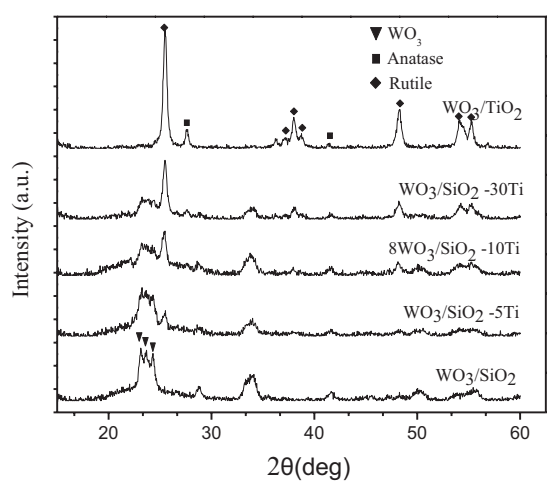

Fig.2. The XRD patterns of WO_3/SiO_2-xTi catalysts.

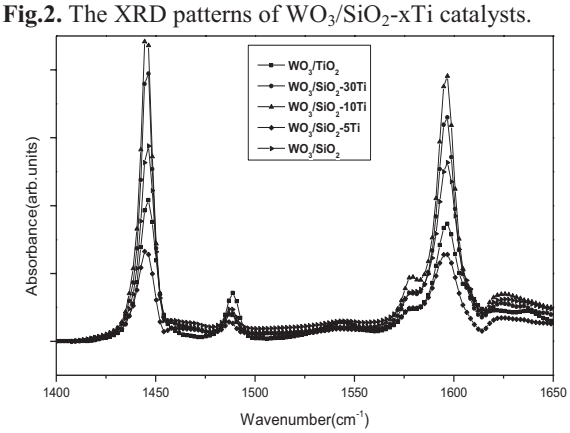

Fig3. The FT-IR spectra of pyridine adsorbed on various samples at 50°C.

Raman spectroscopy was adopted as a suitable tool for determination of the structure of tungsten

Table1. The property and activity of catalysts with different TiO_2 content on mixed SiO_2-TiO_2 supported tungsten catalysts

Catalysts	TiO_2content (% wt)	Conversion (%)	BET Surface area (m^2g^{-1})	Raman ratio I_{970}/I_{805}
WO_3/SiO_2	0	63	257	0.64
WO_3/SiO_2-5Ti	5	65	250	0.88
WO_3/SiO_2-10Ti	10	72	240	1.11
WO_3/SiO_2-30Ti	30	63	194	0.89
WO_3/TiO_2	100	57	50	0.66

species present in supported catalysts. Huang *et al.* [25] proposed that the band at 970 cm^{-1} was assigned to the surface tetrahedral tungsten oxide species which are the active species for metathesis reaction to propylene. According to the literature, the ratio of the relative intensities of Raman bands between 970 and 805 cm^{-1} (I_{970}/I_{805}) was used to reflect the relative content of active sites for propylene formation. As shown in Table 1, the maximum ratio of I_{970}/I_{805} was achieved for WO_3/SiO_2–10Ti (10 wt% TiO_2 content).

The Lewis and Brønsted acidities were assessed by adopting the FT-IR technique for the desorption of pre-adsorbed pyridine at 50ºC. As shown in Fig.3, the sharp peaks around 1595 and 1445 cm^{-1} were assigned to Lewis acid sites and the less intense one around 1488 cm^{-1} to the Brønsted acid site [26]. It was found that WO_3/SiO_2-10Ti displayed the highest number of total acid sites compared to the titania-free sample; however, the number of acid sites decreased with further addition of TiO_2 above 10%. Kim *et al.* [27] reported that the number of surface acid sites linearly increases with tungsten oxide surface density below tungsten oxide monolayer surface coverage. However, the number of exposed surface acid sites continuously decreases with tungsten oxide density at the above monolayer surface coverage because of the presence of WO_3 crystallites. The highest amount of acid sites found for WO_3/SiO_2–10Ti in this work should be attributed to the better dispersion of tungsten species to obtain tungsten oxide monolayer surface coverage. Nonetheless, with TiO_2 addition higher than 10%, the smaller support surface area influenced by the intrinsic low surface area of TiO_2 compared with SiO_2 may be not enough to obtain tungsten oxide monolayer surface coverage. As a consequence, the state of the above-monolayer surface coverage may be obtained for the catalysts with TiO_2 addition higher than 10%, causing a decrease in the number of acid sites. The H_2–TPR technique was used to investigate the interaction between tungsten species and the SiO_2-TiO_2 support. The H_2 uptake and the temperatures corresponding to the lower and higher reduction are summarized in Table 2. Ramirez *et al.* [28] ascribed the reduction peak at higher temperatures to the reduction of well-dispersed tungsten species rich in tetrahedral coordination. The variation in H_2 uptake as well as the shift of the reduction peak to higher temperature established for the samples with TiO_2 addition reflects the modification of surface tungsten oxide species as well as the stronger interaction between tungsten and the SiO_2-TiO_2 support. WO_3/SiO_2–10Ti should be a sample rich in surface tetrahedral tungsten oxide species, which contribute to the improvement in metathesis activity.

Table 2. The relative amount of H_2 uptake and reduction temperature of catalysts with different TiO_2 content in mixed SiO_2-TiO_2 supported tungsten catalysts.

Catalysts	H_2 uptake (a.u.)	Reduction Temperature (ºC)
WO_3/SiO_2	4.74	531, 800
WO_3/SiO_2-5TiO_2	3.94	531, 807
WO_3/SiO_2–10TiO_2	3.78	537,817
WO_3/SiO_2-30TiO_2	3.08	537,824
WO_3/TiO_2	1.80	601,810

4. CONCLUSION

The improvement in catalytic performance by using a mixed support is a cheaper and more convenient approach, compared with changing the process conditions or the process system. The mixed SiO_2-TiO_2 supported tungsten catalyst containing 10% TiO_2 markedly improved both conversion of 2-butene and propylene selectivity for metathesis of ethene and trans-2-butene. Though the detailed mechanism is subject to further investigation, the preliminary characterization reveals that less tungsten crystallites are formed, which reflects the

better dispersion of tungsten as well as the achievement of relatively high surface tetrahedral tungsten oxide species, widely accepted as the metathesis active site for propylene formation. While TiO_2 addition seems to contribute to the better dispersion of tungsten, TiO_2 itself favors the secondary reaction of 1-butene, cis-2-butene and butadiene formation. WO_3/SiO_2–10Ti (10% TiO_2 content) represents a novel metathesis catalyst which displays good propylene selectivity not overshadowed by TiO_2-related secondary reaction sites.

Acknowledgements: The authors would like to express their deep appreciation to the Thailand Research Fund (TRF) and SCG Chemical Co., Ltd. for their financial support. Special thanks also go to the Office of Higher Education Commission for its support of the National Research University Program (CC557A).

REFERENCES

1. P.K. Ludwig, J.E. Asplin, G.F. Stuntz , W.A. Wachter, B.E. Henry , US Patent 6,069,287 (2000) (to Exxon Research and Engineering Corporation)
2. J.P. Dath, W. Vermeiren, K. Herrenbout, WO00/78894 (2000) (to Fina Oil and Chemical Corporation)
3. J.C. Mol, *J. Mol. Catal*. A**.,** **213**, 39 (2004).
4. R.M. Venner, S.I. Kantorowicz. *Technol. Q. Summer* 141 (2001).
5. D. Davazoglou, A. Moutsakis, V. Valamontes, V. Psycharis, *J. Electrochem. Soc.*, **144** (2), 595 (1997).
6. J. Hietala, EP Patent 0,524,522 A1 (1993), to Neste Oy.
7. J. Hietala, P. Knuuttila, A. Kytökivi, US Patent 5,372,982 (1994), to Neste Oy.
8. F. Verpoort, A.R. Bossuyt, B. Coussens, L. Verdonck, *J. Mol. Catal*. A, **115**, 207 (1997).
9. F. Verpoort, A.R. Bossuyt, B., L. Verdonck, *J. Electron Spectrosc. Relat. Phenom*., **82**, 151 (1996)
10. F. Verpoort, A. Bossuyt, L. Verdonck, *J. Chem. Soc., Chem. Commun.,* 417 (1996).
11. F.Verpoort, A.R. Bossuyt, L. Verdonck, *J. Mol. Catal*. **95**, 75 (1995).
12. F.Verpoort, L.Fiermans, A.R. Bossuyt, L.Verdonck, *J. Mol. Catal*. **90**, 43 (1994).
13. M. Sibeijn, J.C. Mol, *Appl. Catal.*, **67**, 279 (1991).
14. X. Xu, C. Boelhouwer, J.I. Benecke, D. Vonk, J.C. Mol, *J. Chem. Soc. Faraday Trans.,* **82**, 1945 (1986).
15. F.C. Sheu, C.T. Hong, W.L. Hwang, C.J. Shih, J.C. Wu, C.T. Yeh, *Catal. Lett*. **14**, 297 (1992).
16. M. Sibeijn, R. Spronk, J.A.R. van Veen, J.C. Mol, *Catal. Lett*., **8**, 201 (1991).
17. H.S. Hoffmann, P.B. Staudt, T.M.H. Costa, C.C. Moro, E.V. Benvenutti, *Surf. Interface Anal.*, **33**, 631 (2002).
18. B.K. Min, W.T. Wallace, D.W. Goodman, *J. Phys. Chem.* B., **108**, 14609 (2004).
19. X. Zhang, H. Yang, F. Zhang, K.Y. Chan, *Mater. Lett*., **61**, 2231 (2007).
20. Q. Fang, M. Meier, J.J. Yu, Z.M. Wang, J.Y. Zhang, J.X. Wu, A. Kenyon, P. Hoffmann, I.W. Boyd, *Mater. Sci. Eng.* B., **105**, 209 (2003).
21. A.M. Venezia, F.L. Liotta, G. Pantaleo, A. Beck, A. Horváth, O. Geszti, A. Kocsonya, L. Guczi, *Appl. Catal*. A., **310**, 114 (2006).
22. J.R. Grzechowiak, I. Szyszka , A. Masalska, *Catal. Today*, **137**, 433 (2008).
23. H. Tang, C.H. Yu, W. Oduoro, H. He, S.C. Tsang, *Langmuir*, **24**, 1587 (2008).
24. X. Gao, I.E. Wachs, *Catal. Today,* **5**, 233 (1999).
25. S. Huang, F. Chen, S. Liu, Q. Zhu, X. Zhu, W. Xin, Z. Feng, C. Li, Q.X. Wang, L. Xu, *J. Mol. Catal*: A., **267**, 224 (2007).
26. X.L Yang, R. Gao, *J. Phys. Chem*. C., **112**, 3819 (2008).
27. T. Kim, A. Burrows, *J. Catal.*, **246**, 370 (2007).
28. J. Ramirez, A.G. Alejandre, *J. Catal*., **170**, 108 (1997).

НОВ КАТАЛИЗАТОР ОТ ВОЛФРАМ ВЪРХУ SIO_2-TIO_2 ЗА МЕТАТЕЗА НА ЕТЕН И 2-БУТЕН

С. Чемчуен[1], У. Лимсангкас[1], В. Нетовораракса[1], С. Фатанасри[1] , Н. Сае-Ма[1], К. Сурие[2]

[1]Център за върхови постижения по катализ и инженерство на каталитичните реакции, Департамент по инженерна химия, Инженерен факултет, Университет Чулалонгкорн, Бангкок 10330, Тайланд
[2]SCG Кемимълс Co., лимитед, 1 Сиам-цемент роуд, Банг сю, Бангкок 10800, Тайланд

Постъпила на 8 март, 2011 г.; коригирана на 9 май, 2011 г.

(Резюме)

Приготвени са волфрамови катализатори, нанесени върху смес от SiO2-TiO2, съдържаща 8 % тегл. волфрам чрез мокро импрегниране. Катализаторът с добавка от 10% TiO2, определен като WO3/SiO2-10Ti, показва подобрена конверсия (72 %) и селективност спрямо пропилена (48 %) и съответно по отношение метатезата на етена и 2-бутена спрямо конвенционален катализатор от волфрам върху силициев диоксид без добавка на титанов диоксид. Предполага се, че добрата активност на катализатора спрямо образуването на пропилен се дължи на по-добрата дисперсия на волфрама при добавянето на титановия диоксид и на тетраедричния волфрамов оксид с голяма повърхност.

Bulgarian Chemical Communications, Volume 44, Number 1 (pp. 92 – 98) 2012

Electroless deposition of nanodisperse metal coatings on fabrics

M. Petrova*[1], M. Georgieva[1], Ek. Dobreva[2], G. Avdeev[1]

[1]*Rostislaw Kaischew Institute of Physical Chemistry, Bulgarian Academy of Sciences, Acad. G. Bonchev St., bl. 11, Sofia 1113, Bulgaria*
[2]*Technical University of Sofia, 8, Kliment Ohridski Blvd., Sofia 1000, Bulgaria*

Received March 7, 2011; revised June 16, 2011

Metal plated fabrics are modern composite materials characterized by a combination of the beneficial physiological and ergonomic properties of the textile substrate with those of the deposited metal coating.

A technology was developed for deposition, by chemical methods, of nanodisperse copper coatings with various types of dispersoids (graphite, SiO_2, Al_2O_3 and TiO_2) onto two types of polyethyleneterephtalate (PET) polyester fabrics: woven and non-woven. The influence of the deposition conditions of the coatings on their thickness, electroconductivity, elemental composition and morphology was studied.

Key words: Electroless copper plating, Nanodisperse metal coatings, Woven fabric, Non-woven fabric, Specific electrical resistance, Electromagnetic interference shielding.

1. INTRODUCTION

Metal plated fabrics have valuable properties which make them suitable for various applications in everyday life and in engineering technologies.

Metal plated fabrics are electroconductive and are employed in electrical engineering and electronics as electric heating components. These materials are used for production of highly efficient plastic screens [1, 2] for protection against electromagnetic emissions within the radio wavelength range. The good heat reflecting properties of metallized fabrics make them perspective materials for green house construction elements, for manufacture of cold/heat-resistant clothing for protecting people exposed to extremely low or high temperatures for many hours.

All known methods for metal plating of dielectrics are employed in the process of metallization of fibres and textile materials of various chemical nature. The electroless deposition via reduction of metal ions in aqueous solutions has proved to be the most readily available, convenient and highly effective technique for deposition of metal coatings onto dielectric substrate. Various methods for metal plating of fibres and fabrics have been described in a number of articles and patents [1–6].

Reference [3] treats the two-step activation of a cotton fabric, whereby the object is first immersed in a solution containing Sn^{2+} or Ti^{3+}, and then in a noble metal solution, preferably of $PdCl_2$. Then the object is chemically plated with copper or other metal coating. Most often fibres or fabrics of PET are metal plated, which is the reason why their behaviour in alkaline medium has been investigated by many authors [4–7].

A detailed study into the pre-treatment of polyester fibres with potassium or sodium hydroxide has been described in reference [4]. The authors have established that as a result of the above pre-treatment the mass of the PET fibres is reduced by about 10%, the surface is roughened and its area increased. Moreover, etching leads to formation of caverns on the polymer surface thus increasing the thickness of the metal deposit and improving its adhesion to the substrate. The authors state that the reason for these changes is not clear.

The research reported in reference [5] has established that PET + $2OH^-$ → disodium terepthalate + ethylene glycol.

The rate of polymer dissolution increases with time, temperature and area of the processed surface. The alkali concentration and the presence of a cationic surface active substance (SAS) also have an impact on the process rate.

The thickness of electroless nickel or copper coatings deposited on a textile made of polyethyleneterephtalate, as well as their adhesion and specific electrical resistance have been investigated with regard to their dependence on the etching conditions in alkaline medium and on the duration of the electroless metallization process [6].

* To whom all correspondence should be sent:
E-mail: mpetrova@ ipc.bas.bg

© 2012 Bulgarian Academy of Sciences, Union of Chemists in Bulgaria

It has been found that with increase of NaOH concentration in the etching solution up to 250 g/L the thickness of the deposited nickel coating grows to 0.80 μm, the adhesion determined by the metal loss in dry friction being relatively low (1.0 mg/dm). At higher alkali concentrations the investigated parameters substantially decline. The thickness, adhesion and specific electrical resistance of the coating are most significantly affected by the duration of the electroless metallization process. With an increase of the nickel layer thickness up to 3.2 μm the metal loss rises up to 18.4 mg/dm, the specific resistance being 0.69×10^{-2} Ωm.

Lately, the so called disperse coatings have been used in engineering technology. A basic characteristic of these coatings is that solid dispersoids are incorporated into the base deposition material (called matrix), thus forming a second phase. The preferred metals for matrix deposition are nickel, cobalt, copper, etc. The physical and chemical properties of dispersoids affect the properties of the deposited disperse coating. Possible dispersoids may be micropowders of nanoparticles of high-melting-point oxides, carbides, silicides, borides, nitrides, diamonds, etc.

The influence of the particle size of diamond and tungsten carbide (150, 1000, 2000 nm) dispersed in cobalt and nickel coatings on their adhesion, hardness and tribological behavior is discussed in ref. [8, 9]. It has been established that these coatings could be an alternative to chromium coatings obtained via reduction of hexavalent chromium.

The literature survey evidences that nanodisperse coatings are mostly deposited on solid metal or dielectric substrates.

The aim of the present work is to produce nanodisperse coatings on textile materials (fabrics), which can find wide application in engineering technology (industry).

2. EXPERIMENTAL

Electroless deposition of disperse copper coatings on substrates of woven and non-woven textile ("Yambolen", Bulgaria) was carried out employing the following technological scheme: degreasing in alkaline solution for 15 min at 65ºC; activation in colloidal activator A–75–12 (product of the Technical University–Sofia) for 5 min; alkaline treatment by a commercial X–75-4 accelerator (product of the Technical University-Sofia) for 5 min; chemical plating in copper containing electrolyte.

The basic components of the base electrolyte (BE) (working electrolyte, WE) were copper sulfate, formaldehyde, Na_2-EDTA complexing agent and stabilizer2 (a commercial product of the Technical University–Sofia). The working electrolyte had a pH within the range 12.5÷12.8.

It is a must to use non-stationary electrolytes for the deposition of disperse coatings in order to avoid sedimentation of the dispersoid. That is why air agitation was employed in the present experiments. The dispersoids used were graphite, TiO_2, Al_2O_3, SiO_2 in the form of powders with particle size between 30 and 60 nm for TiO_2, Al_2O_3, SiO_2, and between 7 – 10 μm for graphite particles (Institut für Baustoff- und Umweltschutz-Technologie GmbH Weimar, Germany).

The deposition rate was determined by gravimetric analysis. The obtained thickness was called by us "conditional thickness of the coating".

Energy dispersive X-ray microanalysis (EDX) was used to determine the content of the dispersion particles in the coating. The coating morphology and the particle size distribution on its surface were examined by scanning electron microscopy (SEM) on the JEOL JSM 733 (Japan) microscope.

The electric conductivity of the metallized specimens was measured on a stand specially designed to that end, using a method similar to the four-point probe for measuring the conductivity of semiconductor materials.

The phases contained in the deposits were identified by X-ray diffraction analysis (XRD). An automated vertical powder diffractometer Philips PW 1050 equipped with a secondary monochromator (Cu Kα radiation) was used for the purpose. The XRD patterns were recorded within the angle range from 10 to 80 degrees 2θ at an angle step of 0.04º and 1s exposition time.

Adhesion tests of the coatings were carried out at the Technical University-Sofia and the samples were subjected to burnishing in dry and wet conditions (according to Bulgarian Standard 4680-87).

3. RESULTS AND DISCUSSION

3.1. Influence of dispersoid concentration on the conditional thickness of the coating and on its incorporation in the coating

It was established in our previous investigations [10] that the conditional thickness of the coatings increases with increasing deposition time and temperature. The best incorporation in the chemically obtained disperse coatings was observed

for TiO_2 as compared with the other dispersoids. Therefore, TiO_2 was selected for the present experiments aimed at determining the optimum dispersoid concentration in the electrolytic bath for deposition of composite copper coatings onto textile fabrics.

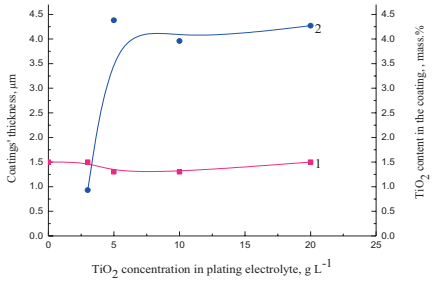

(a)

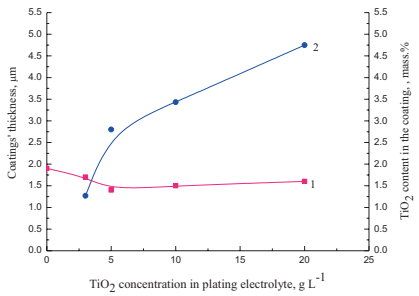

(b)

Fig. 1: Influence of TiO_2 concentration in the plating electrolyte on the conditional thickness of the coating (curve 1) and on dispersoid incorporation in the coating (curve 2) deposited on: (a) woven fabric; (b) non-woven fabric. Deposition time 30 min at 30ºC.

The experiments were conducted with TiO_2 concentrations in the plating electrolyte of 3, 5, 10 and 20 g/L. As is evident from the data in Fig. 1a, at TiO_2 concentrations from 0 to 5 g/L, a certain degree of dispersoid incorporation into the coating deposited onto a woven substrate is reached, after which the percent incorporation does not substantially change with further increase in dispersoid concentration (curve 2). At plating on a non-woven substrate, the increase in TiO_2 concentration (from 3 to 20 g/L) in the working electrolyte leads to a proportional increase in the percent content of TiO_2 in the coating (Fig. 1b, curve 2). The conditional thickness of the coating remains almost the same at different TiO_2 concentrations (curve 1). The composite copper coating with dispersed TiO_2 is a high quality coating with good adhesion and high percentage of dispersoid incorporation.

The surface structure of the disperse coatings prepared at 3, 5, 10 and 20 g/L concentrations of TiO_2 in the plating electrolyte was studied. It was established that with increase in TiO_2 concentration in the plating electrolyte (up to 10 g/L), thickening of the individual fibres was observed, leading to a denser structure of the deposit.

3.2. Influence of the nature of various dispersoids on the properties of the obtained disperse coatings

These investigations were performed using a base electrolyte containing various dispersoids (graphite, SiO_2, Al_2O_3, TiO_2) at a concentration of 5 g/L, 30ºC and 30 min deposition time. The obtained experimental results summarized in Table 1 evidence that, on both types of fabrics, coatings with the highest conditional thickness and degree of dispersoid incorporation are obtained from solutions containing graphite. Some adhesion problems of this coating to the substrate were, however, noticed.

Table 1

Type of disperse particles	Woven textile substrate		Non-woven textile substrate	
	Conditional coating thickness, μm	Dispersoid content in coating, wt.%	Conditional coating thickness, μm	Dispersoid content in coating, wt.%
Base electrolyte (BE)	1.5	-	1.9	-
BE + 5 g/L graphite	1.8	18.7	2.5	28.3
BE + 5 g/L SiO_2	1.5	1.7	1.8	1.4
BE + 5 g/L Al_2O_3	1.5	1.4	1.8	1.2
BE + 5 g/L TiO_2	1.3	4.4	1.4	2.8

The difference in the percentage of included TiO_2 in the coating (4.4% in the woven fabrics and 2.8% in the non-woven fabrics), is probably due to the fact that the non-woven one consists of pressed polymer fabrics which hamper the diffusion of the electrolyte in the depth of the sample, while the woven fabrics are of porous structure.

No substantial difference in the deposition kinetics of the other dispersoids (SiO_2, Al_2O_3, TiO_2) was observed, and the highest degree of incorporation was registered for TiO_2.

In an attempt to resolve the adhesion problem with graphite disperse coatings we used two types of surface active substances (SAS): Veranol (nonylphenol polyglycol ether), which is a non-ionogenic surfactant, and sodium lauryl sulfate, an anionic surfactant. The following disperse coatings were deposited on the woven fabric: BE + 5 g/L graphite + SAS Veranol (0.5 g/L), and BE + 5 g/L graphite + SAS sodium lauryl sulfate (0.5 g/L). First, a pure copper coating was deposited onto the fabric for 5 min under air agitation and then

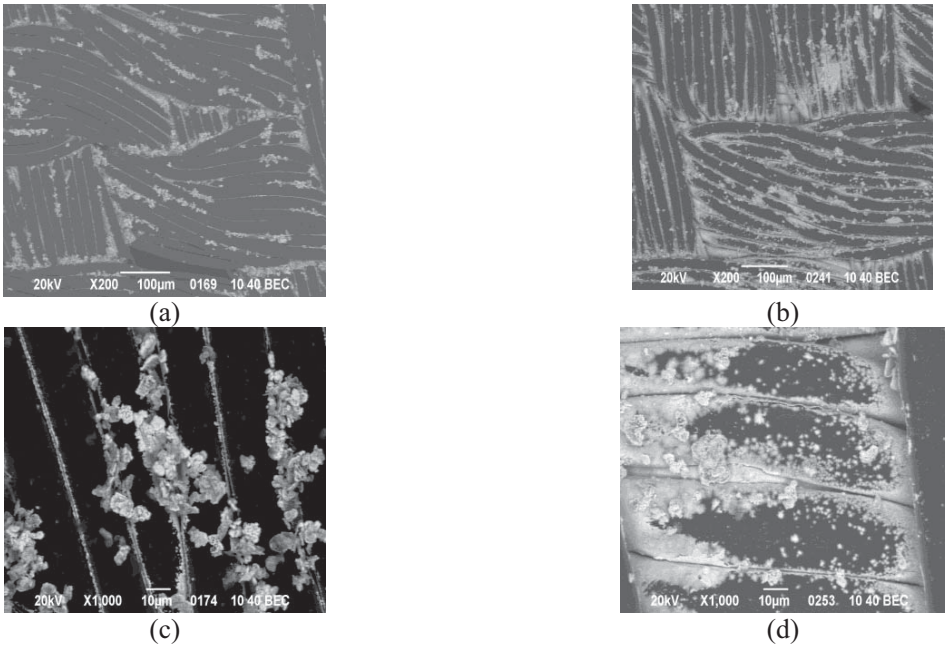

Fig. 2: SEM images of woven fabric: (a) and (c) with 2.5 g/L graphite; (b) and (d) with 10 g/L graphite. Deposition time 30 min at 30ºC.

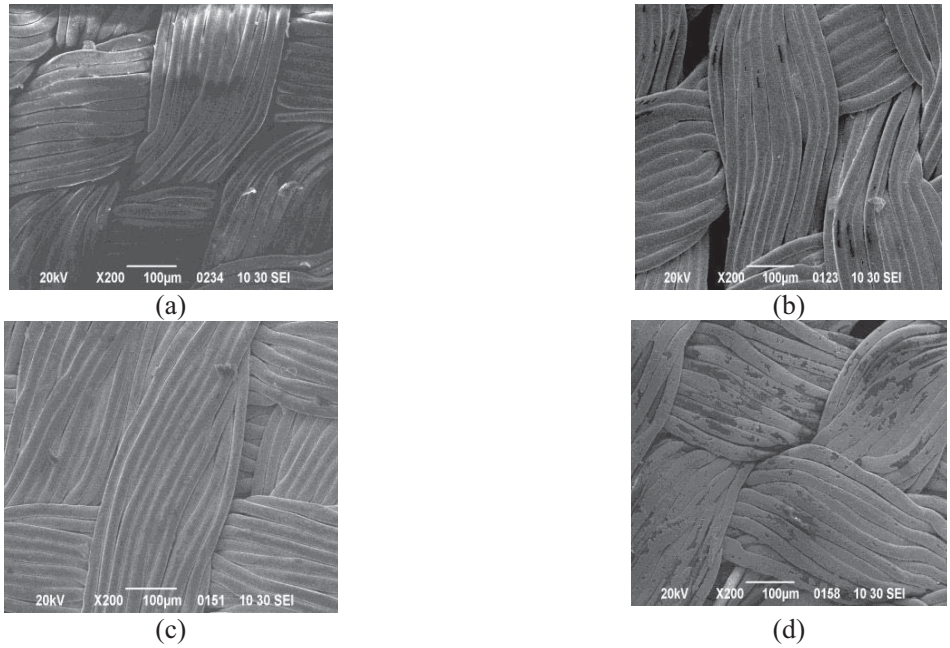

Fig. 3: SEM images of disperse coatings on woven fabric deposited from electrolytes containing various dispersoids: (a) non-treated woven fabric; (b) copper coating; (c) with 5 g/L Al_2O_3; (d) with 5 g/L SiO_2; (e) with 5 g/L graphite; (f) with 5 g/L TiO_2. Deposition time 30 min at 30ºC.

graphite was added to the bath. Both surface active substances proved equally effective in solving the adhesion problem. The influence of graphite concentration in the deposition electrolyte on the degree of incorporation in the disperse coating was investigated by conducting deposition experiments with 1 h deposition time and 2.5, 5 or 10 g/L graphite concentration using Veranol (0.5 ml/L) as SAS. The SEM images of the obtained coatings (Fig. 2) clearly indicate that the increased graphite concentration in the electrolyte leads to an increase in the percent incorporation in the coating.

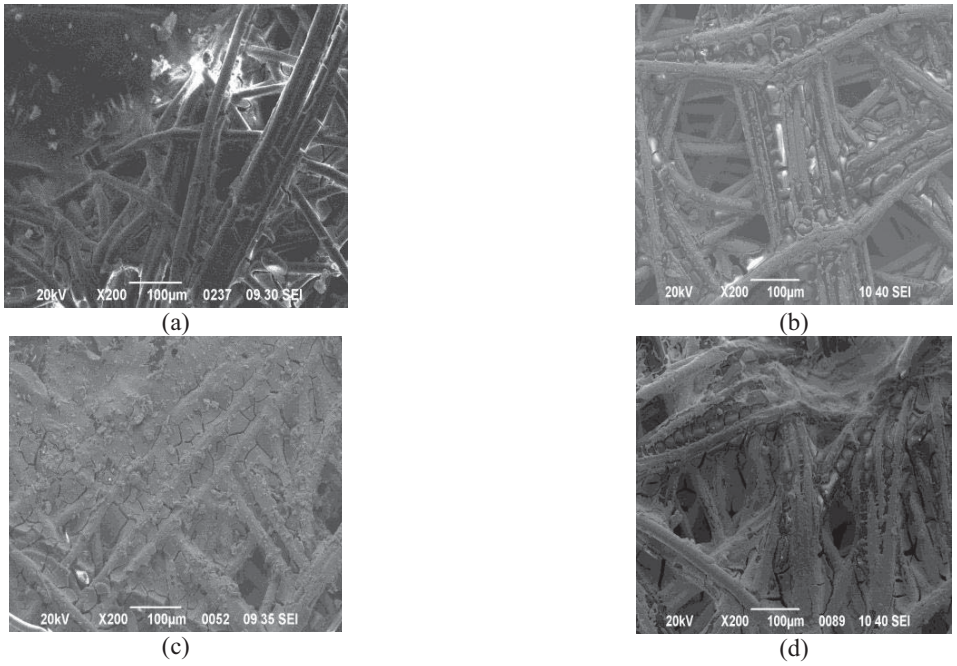

Fig. 4. SEM images of disperse coatings on non-woven fabric deposited from electrolytes containing various dispersoids: (a) non-treated non-woven fabric; (b) copper coating; (c) with 5 g/L graphite; (d) with 5 g/L TiO_2. Deposition time 30 min at 30ºC.

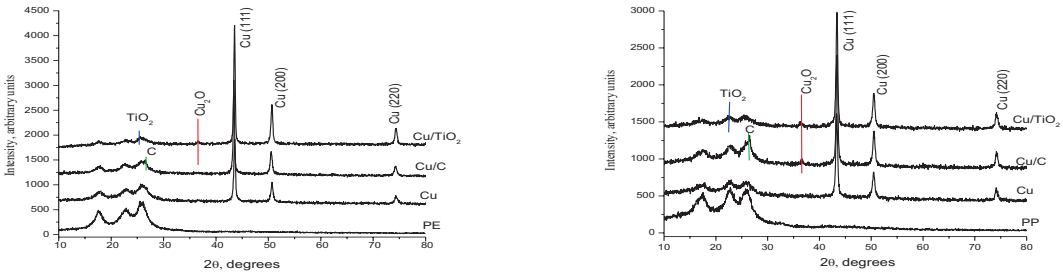

Fig. 5. XRD patterns of disperse copper coating deposited from electrolyte containing 5 g/L TiO_2 (a) of woven fabric and (b) of non-woven fabric. Deposition time 30 min at 30ºC.

The conditional thickness of the disperse coatings in the presence of nanoparticles remains almost unchanged upon varying the graphite concentration, except for the graphite containing disperse coating as compared to the one obtained from base electrolyte. Analogous results were obtained in previous experiments with ABS substrates [11].

The morphology of the obtained disperse coatings was examined by scanning electron microscopy (SEM). The SEM pictures are presented in Figs. 3 and 4. The SEM images in Figs. 3e and 4c support the data in Table 1 evidencing higher percent incorporation of graphite in the coatings as compared to other dispersoids. The most compact structure is observed when TiO_2 is present in the electrolyte (Figs. 3f and 4d). It can be presumed that the coating is initially deposited in the caverns formed on the polymer surface as a result of etching [3], and then grows to cover the whole fibre surface.

Table 2.

Type of disperse particles	Specific electrical resistance, Ωm	
	Woven textile (as substrate)	Non-woven textile (as substrate)
Base electrolyte(BE)	6.0×10^{-3}	7.2×10^{-3}
BE + 5g/l graphite	6.1×10^{-3}	7.4×10^{-3}
BE + 5g/l SiO_2	6.5×10^{-3}	7.6×10^{-3}
BE + 5g/l Al_2O_3	6.5×10^{-3}	7.6×10^{-3}
BE + 5g/l TiO_2	6.8×10^{-3}	8.1×10^{-3}

For better characterization of the disperse coatings under investigation their specific resistance was determined (Table 2). The obtained experimental data evidence that the specific

electrical resistance of disperse copper coatings is of the same order (a little higher) as that of pure copper deposits.

The phases contained in the deposits were identified by X-ray diffraction analysis (Figs. 5a and 5b). For the purpose, first the diffractograms of the primary substrates were recorded and the characteristic peaks for woven and for non-woven textile were identified. This approach allowed for better distinction between the substrate peaks and the peaks identifying the different phases in the thin layers deposited onto it. The obtained diffractograms feature well pronounced peaks of Cu identified using the PDF #04–0836 entry of the database provided by the International Centre for Diffraction Data (ICDD). These experimental data indicate that the obtained coatings are of desired thickness and of adequate crystallinity. The intensity distribution is typical for randomly oriented powder samples and indicates that there are no visible texture effects in the deposits.

No signs of same influence of the dispersoids on the deposition of Cu were observed (*e.g.*, changes in parameters, crystallinity size or texture).

For the coatings containing disperse particles, only the strongest peaks of TiO_2 (anatase) or C (graphite) could be identified on the diffractograms due to their small amount. Their strongest peaks overlay the strongest peaks of the woven and non-woven textile phases, but still the changes in curve profile and in peak position can be distinguished fairly well to confirm the presence of minimum quantities of C (PDF #75–2078) and TiO_2 (PDF #89–4203) in the coatings.

As a result of Cu reactivity, slight oxidation of the sample surface is observed, which exhibits a minimum content of a Cu_2O phase (PDF #65-3288).

4. CONCLUSIONS

The optimum conditions of a previously developed technology for electroless metallization of fabrics were determined. Pure copper, as well as dispersed copper coatings containing various types of dispersoids (graphite, SiO_2, Al_2O_3 and TiO_2) were chemically deposited onto two types of polyester fabrics: woven textile and non-woven textile. Semi-bright coatings of uniform thickness were obtained which give the textiles aesthetic appearance. The specific electrical resistance of the coatings was determined.

The obtained experimental data indicate that these coatings can be used as protective screens against electromagnetic interference (i.e. for EMI shielding) and find application in industry, agriculture and everyday life.

Acknowledgement: *The authors gratefully acknowledge the financial support of the National Foundation "Scientific Research" (Bulgaria) under Contract No. DID02/28.*

REFERENCES

1. BG Patent № 40243/02.02 (1994)
2. Al. Lirkov, H. Petrov, Ek. Dobreva, D. Dimitrov, Intern. Conf. on Processing and Fabrication of Advanced Materials VI, Singapore, 1997
3. US Patent № 4681591/21.07 (1987)
4. US Patent № 5871816/16.02 (1999)
5. A.M. Grancariec, N. Kallay, *J. Applied Polymer Science,* **49**, 175 (1993)
6. E. Dobreva, Al.Lirkov, Chr.Petrov, First Intern. Congress on Adhesion Sci. & Techn., The Netherlands, p. 110. (1995)
7. Eun Gyeong Han, Eun Ae Kim, Kyung Wha Oh, *Synthetic Metals,* **123**, 469 (2001)
8. M. Klingenberg, E.W. Brooman, T.A. Naduy, *Plating and Surface Finishing*, 4, 42 (2005)
9. R.H.Guo, S.Q.Jiang, C.W.M.Yuen, M.C.F.Ng, *J. Appl. Electrochem.,* **39**, 907 (2009).
10. M. Petrova, *Trans. Inst. Metal Finishing,* **82,** 43 (2004)
11. M. Petrova, *Galvanotechnik***, 5**, 1103 (2003)

БЕЗ-ЕЛЕКТРОДНО ОТЛАГАНЕ НА НАНОДИСПЕРСНИ МЕТАЛНИ ПОКРИТИЯ ВЪРХУ ТЪКАНИ

М. Петрова[1], М. Георгиева[1], Ек. Добрева[2], Г. Авдеев[1]

[1]*Институт по физикохимия "Акад. Ростислав Каишев", Българска академия на науките,ул. Акад. Г. Бончев, бл. 11, София 1113,България*

[2]*Технически университет, София, бул. Климент Охридски 8, София 1000, България*

Постъпила на 7 март, 2011 г.; коригирана на 16 юни, .2011 г.

Метализираните тъкани са съвременни композитни материали, характеризиращи се с съчетаването на благоприятни физиологични и ергономични свойства на текстилния носител и металното покритие.
Разработена е технология за химическо отлагане на нанодисперсно медно покритие с различни диспергиращи агенти (графит, SiO_2, Al_2O_3 и TiO_2) върху два вида текстил от полиетилен-терефталат (PET): тъкан и нетъкан. Изследвано е влиянието на условията на отлагане върху дебелината на покритията, електропроводимостта, елементния състав и морфологията им.

Bulgarian Chemical Communications, Volume 44, Number 1 (pp. 99 – 100) 2012

ACADEMICIAN ROSTISLAV KAISHEV – A LIFE DEDICATED TO SCIENCE

The book contains the reminiscences of Acad. Rostislav Kaishev – the founder, together with Professor Ivan N. Stranski of the modern physical chemistry in Bulgaria and a creator of the worldwide recognised Bulgarian school of nucleation and crystal growth. It is based on the story told by Acad. R.Kaishev and recorded by Prof. A.Milchev and Prof. S.Stoyanov between October 2001 and April 2002. The second supplemented edition of this book consists of three parts.

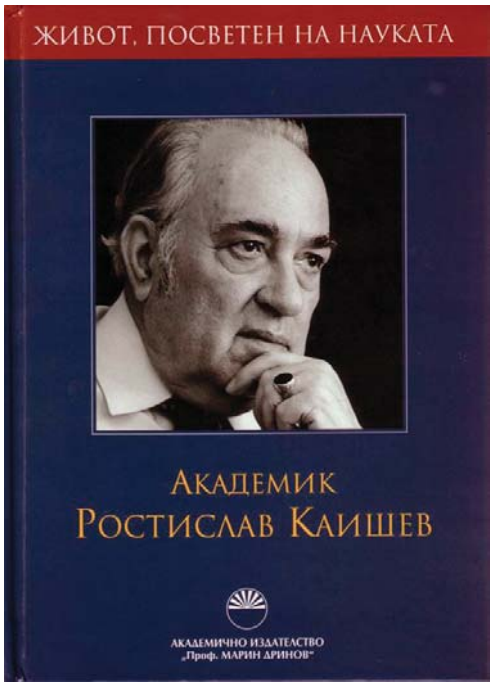

The first part contains the reminiscences of Acad. R.Kaishev, which refer to the period 1908-1960 and cover his childhood, youth, university studies, the work on his PhD thesis in Germany (1930-1932), his scientific research work with Prof. I.N.Stranski on the modern theory of crystal growth, the founding of the Chair of Physical Chemistry at the University of Sofia and the Institute of Physical Chemistry at the Bulgarian Academy of Sciences (BAS), etc. The contacts of Acad. R.Kaishev with famous foreign scientists, among them the professors F.Simon, M.Volmer and H.Betge (Germany), the academicians A.N.Frumkin, Ya.B.Zeldovich and P.Rebinder (Russia) and others are described, as well.

The second part contains brief recollections of Acad. R.Kaishev, written by his daughter Prof. Anastasia Kaisheva from the Institute of Electrochemistry and Energy Systems, BAS, and 16 of his closer students and co-workers: Acad. G.Bliznakov, Acad. P.Bonchev, Acad. I.Gutzov, Acad. D.Exerowa, Acad. A.Popov (Vice President of BAS), Prof. A.Milchev, Prof. Chr.Nanev, Prof. D.Nenov and Prof. S.Stoyanov from the Institute of Physical Chemistry "Acad.

Rostislav Kaishev", BAS, Prof. V.Platikanova from the Institute of Optical Materials and Technologies "Acad. J.Maliniovski", BAS, Prof. D.Platikanov and Prof. B.Toshev from the Physical Chemistry department at the Chemical Faculty of Sofia University "St. Kliment Ohridski", Prof. A.Gittis (USA), Prof. A.Chernov (Russia), Prof. B.Mutafchiev (France) and Prof. G.Staikov (Germany). These recollections shed additional light on the remarkable personality of the outstanding scientist Rostislav Kaishev.

The third part contains some pieces of writting, selected by the compilers A.Milchev and S.Stoyanov to give the readers an idea of the spirit of the Institute of Physical Chemistry beyond the sphere of pure science. The purpose of this part is to show that people involved in scientific research are ordinary people, who, apart from their scientific work, know how to joke and entertain themselves as every ordinary person, as every Bulgarian. This part is also supplemented with some jocular readings.

The book is illustrated with numerous unique photographs from the personal archives of Acad. Rostislav Kaishev. It is in Bulgarian and can be found in the bookstore of Marin Drinov Academic Publishing House, Acad. G.Bonchev Str. block 6, 1113 Sofia and in the bookstore "Academic Book" of the Headquarters of BAS, 15th November str. 1, 1040 Sofia.

.

Alexander Milchev
Stoyan Stoyanov

Bulgarian Chemical Communications, Volume 44, Number 1 (pp. 101 – 102) 2012

АКАДЕМИК РОСТИСЛАВ КАИШЕВ – ЖИВОТ, ПОСВЕТЕН НА НАУКАТА

Академик Ростислав Каишев, създателят на българска школа в областта на кристалния растеж и учител на няколко поколения български физикохимици, до края на дните си запази своята ясна мисъл и бистър ум. Читателят може да се убеди в това от автентичния разказ на този забележителен български учен, записан от проф. Александър Милчев и проф. Стоян Стоянов през периода октомври 2001 г. – април 2002 г. и включен в настоящето второ, допълнено издание на тази книга.

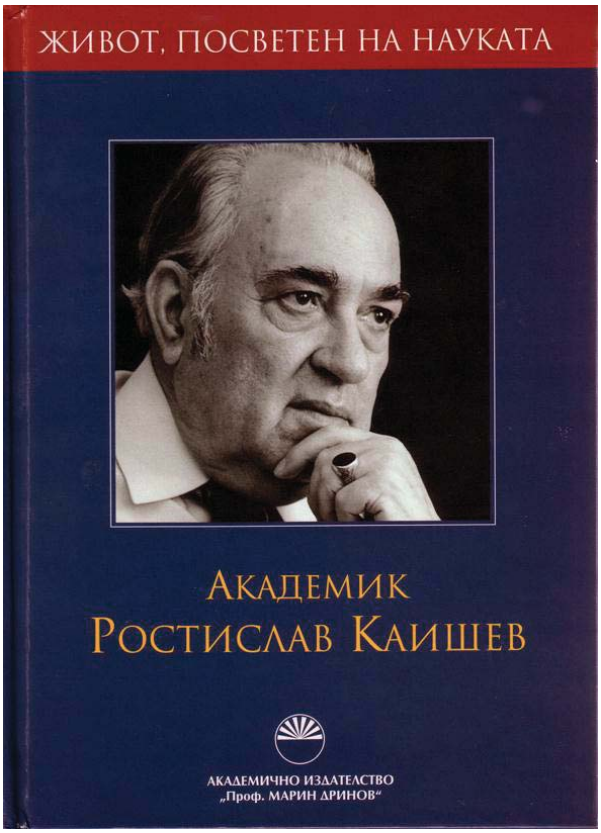

Първата част на книгата съдържа спомените на акад. Р. Каишев за неговите детски, юношески и студентски години, за работата върху докторската му дисертация в Германия под ръководството на известния немски физикохимик проф. Франц Симон, за изследванията му с проф. Иван Странски, посветени на съвременната теория на кристалния растеж, както и за основаването на Катедрата по физикохимия на Софийския Университет и на Института по физикохимия на БАН. Описани са и контактите на акад. Р. Каишев с видни чуждестранни учени, между които проф. М.Фолмер

(Германия), проф. Х.Бетге, председател на академия „Леополдина” (Германия), академиците А.Н.Фрумкин, Я.Б.Зелдович и П.Ребиндер (Русия) и др.

Втората част съдържа кратки спомени за акад. Р.Каишев споделени с читателя, от дъщеря му доцент Анастасия Каишева от Института по електрохимия и енергийни системи, БАН и от 16 негови близки ученици и сътрудници: академиците Г.Близнаков, П.Бончев, И.Гуцов, Д.Ексерова и А.Попов (зам.председател на БАН), проф. А.Милчев, проф. Х.Нанев, проф. Д.Ненов и проф. С.Стоянов от Института по физикохимия „Ростислав Каишев”, БАН, доц. В.Платиканова от Института по оптически материали и технологии “Акад. Й.Малиновски”, БАН, проф. Д.Платиканов и проф. Б.Тошев от Катедрата по физикохимия на СУ „Св.Климент Охридски”, проф. А.Гиттис (САЩ), проф. Б.Мутафчиев (Франция), проф. Г.Стайков (Германия) и проф. А.А.Чернов (Русия). Тази част на книгата хвърля допълнителна светлина върху личността на академик Ростислав Каишев, като един голям учен и изключителен човек.

Третата част включва материали, подбрани от съставителите, за да дадат представа за духа в Института по физикохимия на БАН, извън сферата на чистата наука. Целта на тази част е да покаже, че хората занимаващи се с наука са обикновени хора, които извън научните си занимания умеят да се шегуват и забавляват като всеки обикновен човек, като всеки българин. С няколко шеговити четива е допълнена и тази последна част на второто издание.

Книгата е илюстрирана с многобройни уникални фотографии от личния архив на академик Ростислав Каишев. Предлага се в книжарницата на Академичното издателство „Проф. Марин Дринов”, ул. Акад. Георги Бончев, блок 6, 1113 София, както и в книжарница „Академична книга” в сградата на Централно управление на БАН, ул. „15 Ноември” № 1, 1040 София.

Александър Милчев
Стоян Стоянов

BULGARIAN CHEMICAL COMMUNICATIONS

Instructions about Preparation of Manuscripts

General remarks: Manuscripts are submitted in English by e-mail or by mail (in duplicate). The text must be typed double-spaced, on A4 format paper using Times New Roman font size 12, normal character spacing. The manuscript should not exceed 15 pages (about 3500 words), including photographs, tables, drawings, formulae, etc. Authors are requested to use margins of 3 cm on all sides. For mail submission hard copies, made by a clearly legible duplication process, are requested. Manuscripts should be subdivided into labelled sections, e.g. **Introduction, Experimental, Results and Discussion**, *etc*.

The title page comprises headline, author's names and affiliations, abstract and key words.

Attention is drawn to the following:

a) **The title** of the manuscript should reflect concisely the purpose and findings of the work. Abbreviations, symbols, chemical formulas, references and footnotes should be avoided. If indispensable, abbreviations and formulas should be given in parentheses immediately after the respective full form.

b) **The author**'s first and middle name initials, and family name in full should be given, followed by the address (or addresses) of the contributing laboratory (laboratories). **The affiliation** of the author(s) should be listed in detail (no abbreviations!). The author to whom correspondence and/or inquiries should be sent should be indicated by asterisk (*).

The abstract should be self-explanatory and intelligible without any references to the text and containing not more than 250 words. It should be followed by key words (not more than six).

References should be numbered sequentially in the order, in which they are cited in the text. The numbers in the text should be enclosed in brackets [2], [5, 6], [9–12], etc., set on the text line. References, typed with double spacing, are to be listed in numerical order on a separate sheet. All references are to be given in Latin letters. The names of the authors are given without inversion. Titles of journals must be abbreviated according to Chemical Abstracts and given in italics, the volume is typed in bold, the initial page is given and the year in parentheses. Attention is drawn to the following conventions:

a) The names of all authors of a certain publications should be given. The use of "*et al*." in the list of references is not acceptable.

b) Only the initials of the first and middle names should be given.

In the manuscripts, the reference to author(s) of cited works should be made without giving initials, e.g. "Bush and Smith [7] pioneered...". If the reference carries the names of three or more authors it should be quoted as "Bush *et al*. [7]", if Bush is the first author, or as "Bush and co-workers [7]", if Bush is the senior author.

Footnotes should be reduced to a minimum. Each footnote should be typed double-spaced at the bottom of the page, on which its subject is first mentioned.

Tables are numbered with Arabic numerals on the left-hand top. Each table should be referred to in the text. Column headings should be as short as possible but they must define units unambiguously. The units are to be separated from the preceding symbols by a comma or brackets.

Note: The following format should be used when figures, equations, *etc*. are referred to the text (followed by the respective numbers): Fig., Eqns., Table, Scheme.

Schemes and figures. Each manuscript (hard copy) should contain or be accompanied by the respective illustrative material as well as by the respective figure captions in a separate file (sheet). As far as presentation of units is concerned, SI units are to be used. However, some non-SI units are also acceptable, such as °C, ml, l, etc.

The author(s) name(s), the title of the manuscript, the number of drawings, photographs, diagrams, etc., should be written in black pencil on the back of the illustrative material (hard copies) in accordance with the list enclosed. Avoid using more than 6 (12 for reviews, respectively) figures in the manuscript. Since most of the illustrative materials are to be presented as 8-cm wide pictures, attention should be paid that all axis titles, numerals, legend(s) and texts are legible.

The authors are asked to submit **the final text** (after the manuscript has been accepted for publication) in electronic form either by e-mail or mail on a 3.5'' diskette (CD) using a PC Word-

processor. The main text, list of references, tables and figure captions should be saved in separate files (as *.rtf or *.doc) with clearly identifiable file names. It is essential that the name and version of the word-processing program and the format of the text files is clearly indicated. It is recommended that the pictures are presented in *.tif, *.jpg, *.cdr or *.bmp format, the equations are written using "Equation Editor" and chemical reaction schemes are written using ISIS Draw or ChemDraw programme.

The authors are required to submit the final text with a list of three individuals and their e-mail addresses that can be considered by the Editors as potential reviewers. Please, note that the reviewers should be outside the authors' own institution or organization. The Editorial Board of the journal is not obliged to accept these proposals.

EXAMPLES FOR PRESENTATION OF REFERENCES

REFERENCES

1. D. S. Newsome, *Catal. Rev.–Sci. Eng*., **21**, 275 (1980).
2. C.-H. Lin, C.-Y. Hsu, *J. Chem. Soc. Chem. Commun*., 1479 (1992).
3. R. G. Parr, W. Yang, Density Functional Theory of Atoms and Molecules, Oxford Univ. Press, New York, 1989.
4. V. Ponec, G. C. Bond, Catalysis by Metals and Alloys (Stud. Surf. Sci. Catal., vol. 95), Elsevier, Amsterdam, 1995.
5. G. Kadinov, S. Todorova, A. Palazov, in: New Frontiers in Catalysis (Proc. 10th Int. Congr. Catal., Budapest, 1992), L. Guczi, F. Solymosi, P. Tetenyi (eds.), Akademiai Kiado, Budapest, 1993, Part C, p. 2817.
6. G. L. C. Maire, F. Garin, in: Catalysis. Science and Technology, J. R. Anderson, M. Boudart (eds), vol. 6, Springer-Verlag, Berlin, 1984, p. 161.
7. D. Pocknell, *GB Patent* 2 207 355 (1949).
8. G. Angelov, PhD Thesis, UCTM, Sofia, 2001.
9. JCPDS International Center for Diffraction Data, Power Diffraction File, Swarthmore, PA, 1991.
10. CA **127**, 184 762q (1998).
11. P. Hou, H. Wise, *J. Catal.*, in press.
12. M. Sinev, private communication.
13. http://www.chemweb.com/alchem/articles/1051611477211.html.

CONTENTS

СЪДЪРЖАНИЕ